Out-of-equilibrium dynamics and thermalization of isolated and driven Bose gases in low dimension

Clément Duval

SCIENCES SORBONNE UNIVERSITÉ

Laboratoire Kastler Brossel
Physique quantique et applications

THÈSE DE DOCTORAT DE SORBONNE UNIVERSITÉ

Spécialité : Physique

École doctorale nº 564 : Physique en Île-de-France

réalisée

au Laboratoire Kastler Brossel

sous la direction de Nicolas Cherroret

présentée par

Clément Duval

pour obtenir le grade de :

DOCTEUR DE SORBONNE UNIVERSITÉ

Sujet de la thèse :

Dynamique hors d'équilibre et thermalisation des gaz de Bose isolés et forcés en basse dimension

soutenue le 11 septembre 2023

devant le jury composé de :

M^me	Isabelle BOUCHOULE	Rapportrice
M^me	Léonie CANET	Examinatrice
M.	Nicolas CHERRORET	Directeur de thèse
M.	Nicolas DUPUIS	Président du jury
M.	Nicolas PAVLOFF	Examinateur
M.	Adam RANÇON	Rapporteur

Remerciements

Alors que mes années à Jussieu s'achèvent, je tiens à remercier ici tous ceux ayant contribué à la réalisation de cette thèse.

Tout d'abord, je souhaite remercier mon directeur de thèse Nicolas Cherroret. J'ai grandement bénéficié de sa rigueur d'analyse et de son attention portée à la bonne transmission du travail de recherche, qu'il soit écrit ou dit. Cette exigence scientifique aurait été un peu vaine si elle n'avait pas été doublée d'une profonde gentillesse, pour laquelle je lui suis sincèrement reconnaissant.

J'ai eu la chance d'être encadré par Dominique Delande à mon arrivée au LKB pour un stage d'avant-thèse dont le sujet a largement dévié de son intention première. Sa disponibilité pour répondre aux questions naïves, y compris sur des sujets souvent considérés comme ingrats, a été essentielle pour m'accrocher au wagon des gaz de Bose.

Je souhaite également adresser mes remerciements à tous les membres du jury, en particulier à Isabelle Bouchoule et à Adam Rançon pour avoir accepté le rôle de rapporteurs.

Enfin, ces années au LKB auraient été bien mornes sans la présence de Federico, Hugo et Élyse. L'émulation au Polygone, les déjeuners libanais pour « aller voir la mer », les vacances diverses et les tournées au Pantalon, ont éclairé mon quotidien. Mon entourage familial a eu le même effet : vous êtes ce qui compte pour moi.

Contents

Introduction

The broad success of statistical mechanics, covering both classical and quantum systems, low- and high-energy physics, should not obscure the fact that fundamental questions of the field remain unanswered or lack a unified description. At the core of these frontiers is the notion of *ergodicity*, which refers to the ability of a classical system to dynamically explore its configuration space in a uniform way. Classically, this property is a consequence of chaos, defined as the exponential sensitivity to initial conditions. Ergodicity, extended to the quantum realm, is a multifaceted concept that embraces two seemingly distant topics addressed in this thesis: relaxation of *isolated* systems (Chapters 1-3) and transport in *periodically driven* models (Chapters 4-5).

Isolated quantum systems A typical problem related to ergodicity is the relaxation of quantum systems that are not in contact with an environment. At late times, ergodic systems are expected to reach some stationary state of maximal Von Neumann entropy, where almost all the information about initial conditions is lost. This statement is non-trivial, because it seems to contradict the structure of unitary time evolution, that preserves the inner product between any two initial vectors. In the past decades, the eigenstate thermalization hypothesis (ETH) [1, 2] has emerged as the main paradigm to overcome this issue. The ETH is a conjecture on the matrix elements of *local* observables for "generic" Hamiltonians. Loosely speaking, it postulates that the eigenstates found within the bulk of the spectrum are *thermal*, in the sense that they can be described by a Gibbs ensemble [3, 4]. Due to the propagation of entanglement, it is consequently not possible to recover information about the initial conditions without a *global* measurement [5], generally beyond the reach of experiments. For a given small subregion that can be probed experimentally, the entire system acts like a bath, and therefore an external reservoir is not needed to define the intensive quantities (temperature, chemical potential, and so on) that characterize the Gibbs ensembles. It is worth highlighting that the ETH is believed to rely on random matrix theory (RMT) [6, 7], although this remains largely unproven [8]. More precisely, isolated quantum systems with *discrete* spectra are ergodic if their spectral properties (or their dynamical correlation functions) can be described by those of an ensemble of identical and fictitious systems (random matrices) that are equiprobable. These random matrices are generated by imposing the independence of their random coefficients, under the constraint of the system's

symmetries.

In parallel, systems escaping ergodicity, even slightly, are also of general interest, as they provide a way to protect information over time. A first class of such systems is composed of integrable models [9–19], that possess an extensive set of conserved quantities, preventing the loss of memory of the initial state. Importantly, the lack of thermalization of these systems is not incompatible with the concept of "equilibration" [20], in the sense that a relaxation towards a particular state is still possible. Indeed, local observables of integrable models can relax towards generalized Gibbs ensembles (GGE) [21, 22] that take into account the additional conserved quantities due to integrability. The case of near-integrable quantum models, as explored experimentally in the famous quantum Newton's cradle [23], provides an intermediate scenario where a long-lasting nonequilibrium state is first reached, a regime named "prethermalization" that can be characterized by the GGE, before the system eventually relaxes to the ordinary Gibbs ensemble, due to the small non-integrable part of the Hamiltonian. Another illustration of deviations from ergodicity is given by the many-body localized phase [5, 24, 25], which has been described as an Anderson-like insulator in the presence of interactions and strong disorder, and for which all the eigenstates are nonergodic. Finally, the study of so-called quantum many-body scars [26–29], recently triggered by an experiment on a chain of Rydberg atoms [30], represents a weak ergodicity breaking scenario. In this case, only a *few* eigenstates of the Hamiltonian are nonergodic, so that initial conditions chosen in the corresponding subspace can lead to nonthermal dynamics.

With regard to the relaxation of isolated quantum systems, ultracold atoms experiments [31, 32] serve as both a means and an end. Thanks to this platform, one-dimensional (1D) Hamiltonians, which had long been considered a purely academic pursuit despite the abundance of theoretical works on integrability and the wealth of numerical methods, could be probed experimentally [23, 33–35]. In higher dimensions, a new generation of experiments has also appeared, exploring, e.g., the relaxation dynamics of cold-atomic gases in the strong-interaction limit [36, 37] or the emergence of universal scaling laws for quenches in the vicinity of the condensation transition in three dimensions [38, 39]. Concomitantly, theoretical developments based on quantum kinetic approaches have been proposed to describe the nonequilibrium evolution of three-dimensional (3D) quantum gases toward thermalization [40–43]. In comparison, the case of two-dimensional (2D) nonequilibrium Bose gases has so far received less attention, although more and more accurate experiments of nonequilibrium physics have been performed with 2D quantum gases [44–46]. One of the aims of this thesis (Chapters 1-3) is precisely to fill this gap. Different from 3D Bose gases, only superfluid quasi-condensates with quasi-long-range order exist for ultracold bosons in two dimensions, which requires a special treatment of phase fluctuations [47–49]. 2D Bose gases also experience an interaction-driven Kosterlitz-Thouless transition, around which the dynamics exhibits specific temporal features [45, 50, 51], which will not be considered in this thesis.

Periodically driven problem As discussed in the previous case of autonomous Hamiltonians, quantum ergodicity is often tied to the ETH's validity, or to the onset of thermalization in a nonequilibrium situation. However, in a generic *periodically driven* problem, the energy is not conserved, and, consequently, neither the concept of thermalization nor the standard formulation of the ETH is applicable. For sufficiently simple periodically driven models, characterized by a *discrete* spectrum and a time-periodic Hamiltonian (i.e., Floquet systems), quantum ergodicity hinges on random matrix theory [52, 53]. On the other hand, for periodically driven interacting Bose gases that are the focus of Chapters 4-5, (i) the spectrum of excitations is *continuous*, (ii) the mean-field nonlinear self-interaction is typically aperiodic, so that the relevance of RMT in this context is not established.

On the other hand, ergodicity in periodically driven systems can also be approached from the point of view of *transport*. This connection has been extensively explored since the introduction of the celebrated standard map by Chirikov [54, 55], a paradigmatic model of classical chaos, which displays diffusive behavior in momentum space. In other words, the momentum variance of the standard map grows linearly in time, similarly to a random walk process [56]. The quantization of the standard map, known as the "quantum kicked rotor", has led to the discovery of dynamical localization [57–59], a spectacular consequence of quantum interferences that completely inhibit diffusion, resulting in a saturation of the momentum variance in time. From this perspective, transport properties can be used to distinguish between ergodic (e.g., diffusive) or non-ergodic (e.g., localized) behaviors of periodically driven systems. More recently, Bose gases with periodically kicked repulsive interactions, a system known as the Gross-Pitaevskii map, were shown to exhibit strong ergodic features characterized by an exponential increase of the momentum variance [60–62]. Even more surprisingly, in the case of attractive interactions, this model was also demonstrated to support solitonic solutions [63] for which the momentum variance remains equal to its initial value, a strongly non-ergodic behavior. A more thorough theoretical analysis of the Gross-Pitaevskii map is the second objective of this thesis. As was already mentioned, an important aspect of all these 1D models is their possible implementation in cold atoms setups [64, 65].

Outline of the thesis The goals of this thesis are (i) to develop the suitable framework for describing the process of thermalization in a 2D isolated Bose gas with weak repulsive interactions, (ii) to apply such framework to concrete experimental protocols, and (iii) to explore the mechanisms of transport in a realistic driven 1D Bose gas with kicked interactions.

In the first chapter, we give a concise overview of the existing research on 2D isolated Bose gases, with emphasis on their nonequilibrium dynamics. To illustrate this, we discuss a few quench experiments that serve as motivation for our work. Then, in Chapter 2, we construct a general Keldysh field theory allowing us to describe the nonequilibrium quench dynamics of uniform 2D Bose gases up to their final thermalization. In particular, this approach naturally reveals the separation

of time scales between fast coherent phenomena occurring at short times, such as prethermalization, and slow relaxation mechanisms driving the gas to its final thermal state. This formalism is then applied to a realistic quench scenario in the first part of Chapter 3, where the time-dependence of concrete observables (the spatial coherence function and the structure factor of the Bose gas) are computed. In the second part of this chapter, we also devise a self-consistent extension of our formalism in order to probe the deep infrared regime of 2D Bose gases where the perturbative approach could be insufficient (Sec. 3.2). This leads us to propose novel predictions for the phonon relaxation rates of 2D Bose gases.

In the second part of this thesis (Chapter 4), we discuss the case of a 1D Bose gas subjected to a periodic sequence of infinitely short "kicks" of the interaction strength, the so-called "Gross-Pitaevskii map" [62]. In this system, we recover and extend existing results on the exponential spreading of wave packets. Starting from these results, we then introduce in Chapter 5 a more realistic model where the interaction kicks are of finite width. By means of both numerical and theoretical arguments, we show that this apparently innocent modification significantly alters the transport properties of the Gross-Pitaevskii map by turning the exponential spreading into a sub-diffusive one, with a potentially substantial impact on experiments. The main results and perspectives of the thesis are finally discussed in the conclusion, and a few technical details are collected in five appendices.

Many of the results presented in this thesis have been published in the following papers:

- C. Duval, D. Delande, and N. Cherroret, "Subdiffusion in wave packets with periodically kicked interactions," *Phys. Rev. A*, vol. 105, p. 033309, 2022.
- C. Duval and N. Cherroret, "Quantum kinetics of quenched two-dimensional Bose superfluids," *Phys. Rev. A*, vol. 107, p. 043305, 2023.

Chapter 1

Isolated two-dimensional Bose gases: From equilibrium to nonequilibrium

In this chapter, we introduce the physical system that will be studied in the next two chapters, namely a uniform and isolated two-dimensional (2D) gas of bosons with repulsive interactions, and review some of its equilibrium properties. In particular, we introduce the two-point spatial correlation function G_1, and discuss how it scales across the Berezinskii-Kosterlitz-Thouless (BKT) transition [66, 67]. We also comment on the interest of using "hydrodynamic" variables to describe this system, at least at temperatures well below the critical temperature.

Next, we move into the realm of nonequilibrium 2D gases. To illustrate their physics, our goal is not to provide an exhaustive analysis but rather choose to describe a few recent "quench" experiments. The first one, carried in Cheng Chin group in 2013 [44], involves a 2D Bose superfluid exhibiting coherent oscillations of its time-dependent structure factor following an interaction quench. The second one, conducted within the group of Quentin Glorieux in Paris, investigates the paraxial propagation of a laser through a cavityless, nonlinear medium consisting of an atomic vapor heated to over $T \sim 400$ K [68]. In this context, a phenomenon called "pre-thermalization" was observed in the (time-dependent) coherence function G_1. Analogously to the Cheng Chin experiment, this "quantum fluids of light" platform effectively allows to study nonequilibrium 2D Bose gases at the mean-field level, despite the ten orders of magnitude in energy that separate the two setups.[1] The last experiment, finally, was performed in Jean Dalibard group in 2018 [69] and explores the propagation of density waves in a plane of rubidium atoms cooled down to the superfluid regime. By probing long enough times, this experiment showed evidence for a mechanism of phonon relaxation, eventually responsible for the thermalization of the Bose gas.

[1] Temperatures of the degenerate cesium gas used in Ref. [44] are of the order of $\sim$ 10 nK, to be compared with the $\sim$ 400 K of the rubidium vapor of Ref. [68].

At a theoretical level, an objective of this chapter is also to lay the foundations of a nonequilibrium field theory that can deal with generic dynamical quantum problems such as those mentioned above, and that will be detailed in the next chapter. As a first step in this direction, in the last part of the chapter we discuss a couple of methods used to tackle nonequilibrium problems with quantum gases. First, the "Fermi golden rule" (FGR), which can be combined with detailed balance arguments to derive the quantum analogue of a Boltzmann equation for superfluids. The FGR is a common way to implement perturbation theory to study the relaxation of degenerate quantum gases towards Gibbs ensembles [70–76], even though its scope is limited to small deviations from equilibrium; for some quantum quenches, the initial state might not fulfill the required conditions for its application. Alternatively, the direct use of Heisenberg equations of motion (cf. [77] and references therein) can be used to probe the short-time dynamics of a weakly interacting Bose gas. This technique can be employed far from equilibrium, but in general it is not suitable for describing later times where divergences occur, unless educated approximations are made [41].

1.1 2D Bose gases at equilibrium

1.1.1 Microscopic Hamiltonian

Our starting point is the many-body Hamiltonian of a uniform, low-temperature, 2D gas of bosons with repulsive contact interactions,

$$\hat{H} = \int d^2\boldsymbol{r}\Big(-\frac{1}{2m}\hat{\psi}^\dagger \Delta_{\boldsymbol{r}} \hat{\psi} + \frac{g}{2}\hat{\psi}^\dagger\hat{\psi}^\dagger\hat{\psi}\hat{\psi}\Big), \tag{1.1}$$

where the field $\hat{\psi}$ satisfies the bosonic canonical commutation rule $[\hat{\psi}(\boldsymbol{r}), \hat{\psi}^\dagger(\boldsymbol{r}')] = \delta(\boldsymbol{r}-\boldsymbol{r}')$ and we have set $\hbar = 1$. In Eq. (1.1), we have taken the thermodynamic limit, i.e., the number of particles and the size of the system are considered infinite, while the density of the gas ρ remains finite. The repulsive interaction strength $g > 0$ is linked to the 2D scattering length a_s by the relation [78–80]

$$g = \frac{4\pi}{m}\frac{1}{\log[1/(\rho_0 a_s^2)]}, \tag{1.2}$$

where ρ_0 is the mean density of particles.[2] Throughout this thesis, we consider the dilute gas limit for which $\rho_0 a_s^2 \ll 1$. In this regime, the coupling constant g is significantly smaller than $4\pi/m$. Alternatively, in terms of the healing length $\xi \equiv \sqrt{1/4g\rho_0 m}$, the dilute limit corresponds to $\rho_0\xi^2 \gg 1$.

In two dimensions, the Mermin-Wagner-Hohenberg theorem [83, 84] states the impossibility of continuous symmetry breaking at finite temperature for short-range

[2] In all rigor, the coupling constant g in Eq. (1.1) refers to the *bare* interaction, whereas Eq. (1.2) corresponds to the T-matrix renormalization of the interaction [81, 82].

interactions. In the specific case of a 2D Bose gas, this entails the absence of Bose-Einstein condensation for positive temperatures $T > 0$.[3] Indeed, the phase fluctuations of the field $\hat{\psi}$ destroy long-range order [47], so that the two-point correlation function $G_1(\boldsymbol{r}) \equiv \langle \hat{\psi}^\dagger(0)\hat{\psi}(\boldsymbol{r})\rangle$ always vanishes in the limit $r \to \infty$. However, the repulsive interactions tend to freeze the density fluctuations of the gas. Hence, a state of "quasi long-range order" can arise at very low temperatures, referred to as *quasi-condensation* [49], for which G_1 decays algebraically [65]

$$G_1(\boldsymbol{r}) \sim \left(\frac{\lambda}{|\boldsymbol{r}|}\right)^{\frac{1}{\rho_0\lambda^2}}, \tag{1.3}$$

with $\lambda = \sqrt{2\pi/(mT)}$ the thermal de Broglie wavelength. Quasi-condensed Bose gases are in general also superfluids (see Sec. 1.1.4).

The equilibrium law (1.3) is only valid at sufficiently small temperatures. On the other hand, when the total energy of the system is large enough, the G_1 function decays exponentially:

$$G_1(\boldsymbol{r}) \sim \exp(-|\boldsymbol{r}|/\mathcal{L}). \tag{1.4}$$

The two regimes characterized by Eqs. (1.3) and (1.4) are separated by a topological phase transition, known as the Berezinskii-Kosterlitz-Thouless (BKT) transition [66, 67, 85]. In the "normal" phase, where Eq. (1.4) applies, the phase coherence of the gas is destroyed by the proliferation of topological excitations (isolated vortices). We will not deal with the normal phase in this thesis nor the approach to the BKT transition. Instead, we will focus on the low temperature limit where quantum degeneracy is reached, i.e., $\rho_0\lambda^2 \gg 1$.

1.1.2 Hydrodynamic Hamiltonian

In dimension three, the properties of low-lying excitations can be understood from Bogoliubov theory [65, 86], which consists in expanding the field operator $\hat{\psi}$ around the condensate wave function $\Psi_c = \sqrt{\rho_c}e^{i\theta_c}$ as $\hat{\psi}(\boldsymbol{r}) = \Psi_c + \delta\hat{\psi}(\boldsymbol{r})$, treating $\delta\hat{\psi}(\boldsymbol{r})$ as a small perturbation. However, for two-dimensional Bose gases at low temperatures, such an expansion is no longer adequate. Indeed, unlike the spatially homogeneous condensate phase θ_c, the phase of the field $\hat{\psi}$ is expected to display variations at the scale of the de Broglie wavelength λ [as indicated by Eq. (1.3)], consistently with the Mermin-Wagner-Hohenberg theorem.[4] Instead, collective excitations of the Bose gas are most conveniently described within a quantum *hydrodynamic* formalism, where the field operator is expressed in the density-phase representation [49, 65]

$$\hat{\psi}(\boldsymbol{r}) = e^{i\hat{\theta}(\boldsymbol{r})}\sqrt{\hat{\rho}(\boldsymbol{r})}, \tag{1.5}$$

[3] Notable exceptions, distinct from the physical system described here, include finite-size systems and trapped configurations, for which condensation can occur [65]. It is also allowed at zero temperature [47, 78].

[4] From a perturbation theory point of view, the use of the "Cartesian" coordinates of the microscopic Hamiltonian (1.1) leads to the infrared divergence of the longitudinal propagator [87].

with the commutation rule $[\hat{\rho}(\boldsymbol{r}), \hat{\theta}(\boldsymbol{r}')] = i\delta(\boldsymbol{r}-\boldsymbol{r}')$. In a 2D Bose gas, density fluctuations and phase gradients are expected to be small [47–49] (see below Sec. 1.1.3 for specific requirements). By writing $\hat{\rho}(\boldsymbol{r}) = \rho_0 + \delta\hat{\rho}(\boldsymbol{r})$, we can then expand the Hamiltonian (1.1) with respect to $\delta\hat{\rho}$ and $\nabla_{\boldsymbol{r}}\hat{\theta}$. This leads to [48, 88, 89]

$$\hat{H} = \int d\boldsymbol{r}\Big[\frac{\rho_0}{2m}(\nabla_{\boldsymbol{r}}\hat{\theta})^2 + \frac{g}{2}(\delta\hat{\rho})^2 + \frac{1}{8m\rho_0}(\nabla_{\boldsymbol{r}}\delta\hat{\rho})^2 + \frac{1}{2m}(\nabla_{\boldsymbol{r}}\hat{\theta})\delta\hat{\rho}(\nabla_{\boldsymbol{r}}\hat{\theta})\Big], \tag{1.6}$$

where we have redefined the energy scale $\hat{H} \to \hat{H} - g\rho_0/2$ and we have dropped a cubic term $\propto (\nabla_{\boldsymbol{r}}\delta\hat{\rho})^2\delta\hat{\rho}$, negligible at low energy [48, 88].

1.1.3 Conditions of validity

Much like microscopic fields $\hat{\psi}(\boldsymbol{r}), \hat{\psi}^\dagger(\boldsymbol{r})$, the density-phase operators of the hydrodynamic language are plagued by ultraviolet divergences [49]. In all rigor, it is not possible to find two operators $\hat{\rho}(\boldsymbol{r}), \hat{\theta}(\boldsymbol{r})$, defined on the whole two-dimensional position space, which simultaneously satisfy Eq. (1.5) and the commutation relation $[\hat{\rho}(\boldsymbol{r}), \hat{\theta}(\boldsymbol{r}')] = i\delta(\boldsymbol{r}-\boldsymbol{r}')$. Mora and Castin showed in Ref. [49] that it was possible to ignore this issue by discretizing space, provided the vacuum state of a $\boldsymbol{r}$-centered box can be neglected. Therefore, based on their findings, the continuous $\boldsymbol{r}$-space must be seen as a grid of characteristic scale ℓ, each unit cell containing a large number $\rho_0\ell^2 \gg 1$ of physical particles. The resulting coarse-grain average amounts to introducing an ultraviolet cutoff in momentum space at $q \sim 1/\ell$, which was already discussed by Popov [47, 48]. Strictly speaking, integro-differential operators in Eq. (1.6) should be replaced by their discrete counterpart, and the thermodynamic limit should be carefully taken at the end of the calculations. In practice, because the excitations we will typically consider have a phononic nature (cf. Chapter 3), a reasonable choice for the size of the hydrodynamic cell is $\ell \sim \xi$. The hydrodynamic treatment (1.5) can thus be considered valid as soon as $\rho_0\xi^2 \gg 1$ (dilute regime) and $\rho_0\lambda^2 \gg 1$ (degenerate regime) [49].

1.1.4 Bogoliubov transformation

Let us now introduce the Bogoliubov theory based on the hydrodynamic Hamiltonian (1.6). The latter is the sum of a quadratic part $\hat{H}_0$ and a cubic interaction term $\hat{H}_{\text{int}}$. The quadratic part is non-diagonal, but can be diagonalized by means of a Bogoliubov transformation [90]. To proceed, we first rewrite Eq. (1.6) in momentum space, introducing the Fourier variables

$$\hat{\theta}_{\boldsymbol{q}} \equiv \rho_0 \int d\boldsymbol{r} e^{-i\boldsymbol{q}\cdot\boldsymbol{r}}\hat{\theta}(\boldsymbol{r}), \quad \delta\hat{\rho}_{\boldsymbol{q}} \equiv \int d\boldsymbol{r} e^{-i\boldsymbol{q}\cdot\boldsymbol{r}}\hat{\rho}(\boldsymbol{r}). \tag{1.7}$$

Importantly, the above Fourier expansion of the phase $\hat{\theta}(\boldsymbol{r})$ neglects vortices [91]. Indeed, the speed of the fluid is proportional to $\nabla_{\boldsymbol{r}}\hat{\theta}_{\boldsymbol{q}} \propto \boldsymbol{q}\cdot\hat{\theta}_{\boldsymbol{q}}$, and hence excitations

orthogonal to $\boldsymbol{q}$ are not considered here, which is a fair approximation well below the BKT transition. The quadratic part of the Hamiltonian becomes

$$\hat{H}_0 = \int_{\boldsymbol{q}} \left[\frac{q^2}{2m} \hat{\theta}_{\boldsymbol{q}} \hat{\theta}_{-\boldsymbol{q}} + \left(\frac{g\rho_0}{2} + \frac{q^2}{8m} \right) \delta\hat{\rho}_{\boldsymbol{q}} \delta\hat{\rho}_{-\boldsymbol{q}} \right], \tag{1.8}$$

where we have introduced the short-hand notation $\int_{\boldsymbol{q}} \equiv \int d^2\boldsymbol{q}/[(2\pi)^2\rho_0]$. To diagonalize $\hat{H}_0$, we introduce new operators $\hat{a}_{\boldsymbol{q}}$ and $\hat{a}^\dagger_{\boldsymbol{q}}$, defined through the Bogoliubov transformation

$$\delta\hat{\rho}_{\boldsymbol{q}} = -\sqrt{\frac{E_{\boldsymbol{q}}}{\epsilon_{\boldsymbol{q}}}} (\hat{a}^\dagger_{\boldsymbol{q}} + \hat{a}_{-\boldsymbol{q}}), \tag{1.9}$$

$$\hat{\theta}_{\boldsymbol{q}} = \frac{i}{2} \sqrt{\frac{\epsilon_{\boldsymbol{q}}}{E_{\boldsymbol{q}}}} (\hat{a}^\dagger_{\boldsymbol{q}} - \hat{a}_{-\boldsymbol{q}}), \tag{1.10}$$

where $E_{\boldsymbol{q}} \equiv \boldsymbol{q}^2/(2m)$ and $\epsilon_{\boldsymbol{q}} \equiv \sqrt{E_{\boldsymbol{q}} \left(E_{\boldsymbol{q}} + 2g\rho_0 \right)}$ is the well-known Bogoliubov dispersion relation. Inserting this basis change into Eq. (1.8), we obtain

$$\hat{H}_0 = \int_{\boldsymbol{q}} \epsilon_{\boldsymbol{q}} \left(\hat{a}^\dagger_{\boldsymbol{q}} \hat{a}_{\boldsymbol{q}} + 1/2 \right), \tag{1.11}$$

which describes a gas of free quasiparticles with energy dispersion $\epsilon_{\boldsymbol{q}}$. At momenta $|\boldsymbol{q}| \ll 1/\xi$, the dispersion relation becomes phononic:

$$\epsilon_{\boldsymbol{q}} \simeq c|\boldsymbol{q}|, \tag{1.12}$$

where $c = \sqrt{g\rho_0/m}$ is the speed of sound. This implies, in particular, that according to Landau's criterion for superfluidity $\min_{\boldsymbol{q}} \epsilon_{\boldsymbol{q}}/|\boldsymbol{q}| > 0$ [65], the gas of bosons (1.1) is a superfluid. Unless stated otherwise, in the following we will mainly focus of the low-energy regime where Eq. (1.12) holds.

In the next chapter, we will see that in a nonequilibrium context, the description of thermalization in an isolated quantum gas requires to account for interactions between the quasiparticles. These interactions are encoded in the cubic term of the Hamiltonian (1.6). In terms of the Bogoliubov operators $\hat{a}_{\boldsymbol{q}}$ and $\hat{a}^\dagger_{\boldsymbol{q}}$, this term reads

$$\hat{H}_{\text{int}} = \int_{\boldsymbol{p},\boldsymbol{q}} \Lambda_{\boldsymbol{p},\boldsymbol{q}} \left(\hat{a}_{\boldsymbol{p}} \hat{a}_{\boldsymbol{q}} \hat{a}^\dagger_{\boldsymbol{p}+\boldsymbol{q}} + \text{h.c.} \right), \tag{1.13}$$

where, in the phononic regime $|\boldsymbol{q}| \ll 1/\xi$, the vertex function $\Lambda_{\boldsymbol{p},\boldsymbol{q}}$ is given by

$$\Lambda_{\boldsymbol{p},\boldsymbol{q}} \simeq \frac{3}{4m} \sqrt{\frac{g\rho_0}{2c}} \sqrt{|\boldsymbol{p}|\,|\boldsymbol{q}|\,|\boldsymbol{p}+\boldsymbol{q}|}. \tag{1.14}$$

The cubic interaction (1.13) describes a three-phonon scattering process with momentum conservation, which includes the well-known Landau and Beliaev processes [65, 88, 92–94]. Note that in two dimensions, such interaction process can also be

resonant, i.e., there exists a range of $\boldsymbol{p}, \boldsymbol{q}$-values satisfying $\epsilon_{\boldsymbol{p}} + \epsilon_{\boldsymbol{q}} = \epsilon_{\boldsymbol{p}+\boldsymbol{q}}$ *and* momentum conservation [95, 96]. As will be shown in Sec. 2.2.3, when the excitation spectrum is purely linear this property leads to a divergence of the self-energy, which makes this process the dominant one for the dynamics. For this reason, when writing Eq. (1.13) we have dropped interaction terms of the type $\hat{a}_{\boldsymbol{p}}\hat{a}_{\boldsymbol{q}}\hat{a}_{-\boldsymbol{p}-\boldsymbol{q}}$, which cannot be resonant and are therefore subdominant.

1.2 2D Bose gases out of equilibrium

In recent years, considerable efforts have been devoted to understanding the *out-of-equilibrium* dynamics of quantum gases. In practice, a possible protocol to initiate such time evolution consists in performing a "quantum quench" [97–105], i.e., starting from the system prepared in a thermal state, one abruptly changes a parameter of the Hamiltonian. If the quench is weak enough, the short-time dynamics can be understood from a *coherent* theory, where the Bogoliubov modes are assumed to be non-interacting and therefore evolve as $\hat{a}_{\boldsymbol{q},t} = \hat{a}_{\boldsymbol{q},0}e^{-i\epsilon_{\boldsymbol{q}}t}$. This description amounts to approximating the Hamiltonian (1.6) by its quadratic part $\hat{H}_0$. In general, however, at later times, the quasiparticles interactions, characterized by $\hat{H}_{\rm int}$, cannot be dismissed, prompting the need for more elaborate theoretical frameworks. To illustrate these concepts in two dimensions, in this section we choose to present three recent experiments of nonequilibrium physics with 2D Bose gases.

1.2.1 Structure factor oscillations in a 2D superfluid

In 2013, the authors of Ref. [44] cooled down cesium atoms to the degenerate regime to produce a uniform, weakly interacting, 2D Bose superfluid. By means of a Feshbach resonance [106], they engineered a quench of the interaction coupling constant g [cf. Fig. 1.1(a)], and measured the subsequent evolution of the time-dependent structure factor

$$S_{\boldsymbol{q},\tau} \equiv \langle \delta\hat{\rho}_{\boldsymbol{q},\tau}\delta\hat{\rho}_{-\boldsymbol{q},\tau}\rangle, \tag{1.15}$$

which is the Fourier transform of the spatial density-density correlator of the Bose gas.[5] It was observed that, at short times after the quench, the structure factor oscillates with a period proportional to $1/(2\epsilon_{\boldsymbol{q}})$, as illustrated in Fig. 1.1(c). This phenomenon was interpreted as an interference between (non-interacting) quasiparticles emitted at the quench, and correspondingly explained in terms of the Bogoliubov theory mentioned in the previous section. The corresponding temporal regime is dubbed *prethermal*, here in the sense that it precedes the full gas thermalization expected at long times. We will describe this problem more quantitatively in Sec. 1.3.2, as well as in the next chapter.

As a remark, such oscillations of $S_{q,\tau}$, here observed in the frame of a cold-atom experiment, turn out to be analogous to the famous Sakharov oscillations,

[5] We refer to Sec. 3.1.5 for additional details on $S_{\boldsymbol{q},\tau}$, such as its explicit expression (3.13).

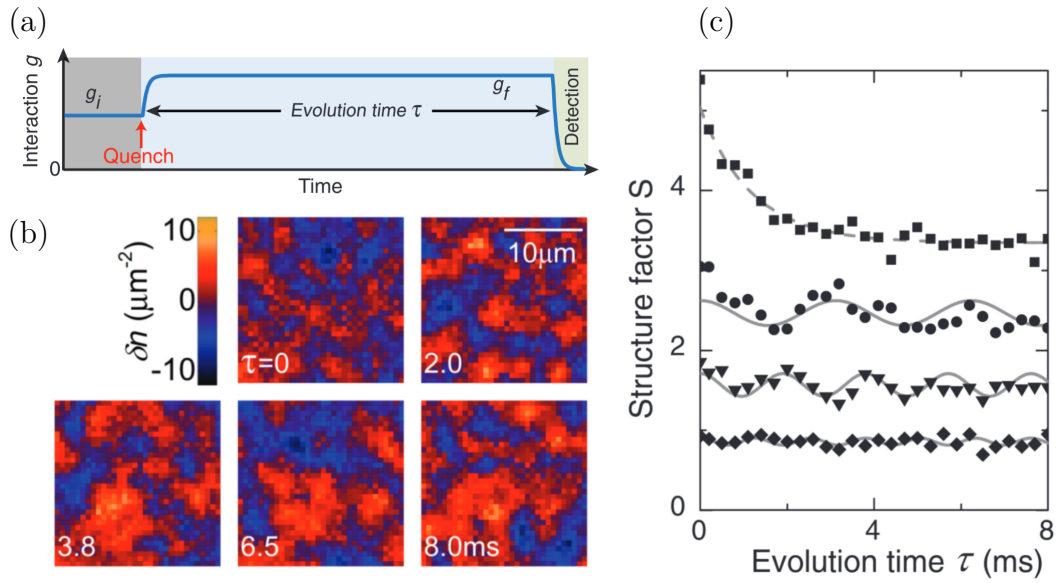

Figure 1.1: (a) Schematic quench protocol used in Ref. [44]. A 2D ultracold Bose gas is prepared in an equilibrium state with coupling constant g_i. The interaction strength is then abruptly switched on to a final value g_f, driving the system out of equilibrium. (b) The spatial density fluctuations $\delta n \equiv |\delta\hat{\rho}|$ are imaged *in situ* during the dynamics by an absorption technique described in Ref. [108]. (c) For a fixed momentum of the order $\sim 1/\xi$, the structure factor (1.15) exhibits temporal oscillations. The plain lines are numerically adjusted to extract the period of the oscillations.

a distinctive anisotropic pattern in the cosmic microwave background radiation, which originates from the interference between acoustic waves emitted in the early stages of the universe [107].

1.2.2 Interaction quench in a 2D fluid of light

The physics of 2D isolated Bose superfluids can also be addressed in optics using "quantum fluids of light" in "propagating geometries", see Fig. 1.2(a) for a sketch of the experimental setup. This type of experimental platform, which has gained popularity over the past decade [109], is based on the paraxial propagation of a laser of central wavelength $2\pi/k_0$ through a lossless, nonlinear material of refractive index n and Kerr susceptibility $\chi^{(3)}$. In practice, such systems are realized using photorefractive crystals [110, 111] or resonant hot atomic vapors [68, 112]. Indeed, in the paraxial approximation the evolution of the electric field envelope[6] ϕ of the

[6]The scalar electric field at time t in the space of coordinates $(\boldsymbol{r}, z) = (x, y, z)$ is given by $\mathcal{E}(\boldsymbol{r}, z, t) = \mathrm{Re}\left[\phi(\boldsymbol{r}, z, t)e^{ik_0 z - i\omega t}\right]$, where ω is the carrier frequency.

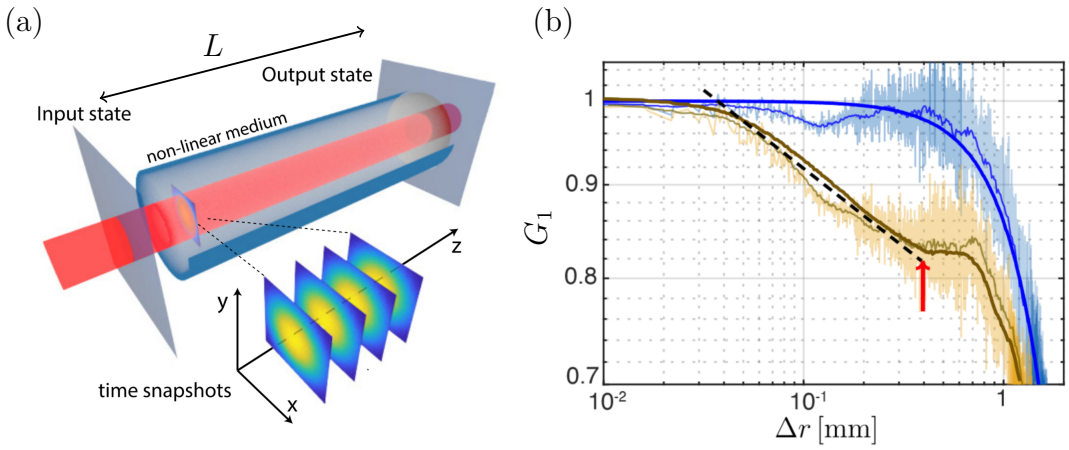

Figure 1.2: (a) Schematic representation of a fluid-of-light experiment in the propagating geometry, from Ref. [114]. L is the length of the cell along the z-axis and represents the effective time. (b) Plot of the measured first-order spatial correlation function $G_1(\Delta r)$ in a two-dimensional fluid of light, extracted from Ref. [68]. Thick colored curves correspond to experimental data at initial "time" $z = 0$ (blue, input state) and final "time" $z = L$ (brown, output state). Thin color curves and light colored data are raw experimental data, prior to various data processing stages. The red arrow indicates the "light cone" boundary $\Delta r = cL$, where c is the speed of sound of the collective excitations. The black dotted line highlights the algebraic decay of the G_1 function inside the light cone (cf. discussion of Sec. 1.3.3).

laser obeys a Gross-Pitaevskii-like equation [113]:

$$i\partial_z \phi = \left(-\frac{1}{2k_0} \Delta_{\boldsymbol{r}} - \frac{3k_0 \chi^{(3)}}{8n^2} |\phi|^2 \right) \phi, \tag{1.16}$$

where $\boldsymbol{r} \equiv (x, y)$ denotes the transverse vector and z refers to the longitudinal axis of the nonlinear medium represented in Fig. 1.2(a). By analogy with the mean-field description of the 2D Bose gas, the direction z plays here the role of time, $-3k_0\chi^{(3)}/(8n^2)$ is the effective coupling parameter g (which can be positive or negative), while the beam wave number k_0 serves as an analog of the particle's mass m. Therefore, the light beam entering the medium simulates an interaction quench of a Bose gas from $g = 0$ to $g > 0$.

In the recent experiment [68], which involved a hot rubidium vapor, the authors sent into the atomic cell a fluctuating beam (see Sec. 1.3.2 for details) and measured the resulting spatial correlation function $G_1(\Delta \boldsymbol{r}, z)$ at the exit of the atomic cell. They observed an algebraic decay within a light cone [cf. Fig. 1.2(b)], confirming a coherent theory previously developed in Ref. [113]. In the latter study, interactions between quasiparticles are neglected and the collective excitations of the system evolve harmonically, as in the Cheng Chin experiment. The dynamical behavior of

the G_1 function was thus also referred to as prethermalization. This terminology is even more transparent here, since the algebraic decay of Fig. 1.2(b) resembles the thermal law (1.3), albeit with a different exponent [113], cf. Sec. 1.3.2 below. In fact, in both experiments, the emergence of a prethermalization regime is, in turn, caused by the integrability of the underlying Bogoliubov Hamiltonian. Note that the experiment [68] also put forward the existence of a nonequilibrium transition from algebraic to exponential decay of the G_1 function, analogously to Bose gases at equilibrium. Such phenomenon was interpreted as a nonequilibrium precursor of the BKT transition, expected to emerge at long enough time.

1.2.3 Sound propagation in a rubidium billiard

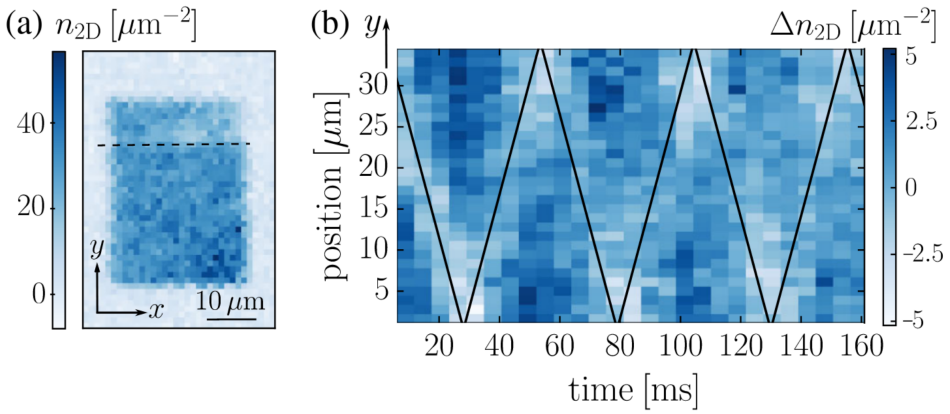

Figure 1.3: Experiment carried out in the "Rubidium group" at LKB (Collège de France), extracted from Ref. [69]. (a) The experiment consists in first preparing an inhomogeneous, boxed 2D superfluid with two flat components: the atomic density $n_{2D}(x, y)$ above the dashed black line is three times lower than the density in the rest of the box. (b) At initial time, external potentials are switched off and the density dip propagates in the box with a velocity v close to the speed of sound $c = \sqrt{gn_{2D}/m}$ given by Eq. (1.12). Here, the density dip is tracked by integrating over x and subtracting the mean average density; the corresponding triangular fit (black line) leads to $v \simeq 0.94c$ [69]. The temperature of the gas relative to the critical BKT temperature is $T/T_c \simeq 0.37$. For smaller temperatures, the ratio v/c approaches one [see Fig. 3(a) of Ref. [69]].

In 2018, another type of experiment on a nonequilibrium Bose gas was conducted in Jean Dalibard group at LKB [69] (see also [115]), where they confined a degenerate Bose gas of ^{87}Rb atoms in a quasi-two-dimensional box with open boundary conditions [116, 117]. While, in this setup, they were able to describe both sides of the BKT transition, their nonequilibrium experimental protocol also allowed to

explore the deep superfluid phase, where the temperature of the cloud is well below the critical BKT temperature T_c (temperatures as low as $T/T_c \simeq 0.2$ were reached).

More precisely, by means of a repulsive potential, they created a subregion of smaller density of particles [see Fig. 1.3(a)]. Once local equilibrium was established within each subregion, the quench experiment consisted in switching off the external potential. This allowed the system to relax into a state of uniform density, similarly to the phenomenon encountered in a Joule expansion. For very small temperatures, the density wave bounces several times off the walls, as demonstrated in Fig. 1.3 (b). The resulting time oscillations of the excited modes amplitude $A_q(t)$ in Fourier space (cf. [69] for proper definitions of these modes) can again be understood from the aforementioned coherent dynamics. Interestingly, at longer time scales it was also observed that the envelop of $A_q(t)/A_q(0)$ decays as $e^{-\Gamma_q t/2}$, where Γ_q was shown to be compatible with the 2D Landau damping rate first derived in Ref. [88]. This relaxation mechanism results from the interactions between quasiparticles, encoded in the Hamiltonian (1.13) and will be discussed at length in the next chapters.

1.3 Coherent dynamics

Under the dilute hypothesis $\rho_0\xi^2 \gg 1$, the Hamiltonian (1.6) can be approximated by its integrable part $\hat{H}_0$ and diagonalized following the steps of Sec. 1.1.4. The ensuing *coherent* dynamics is known exactly. In this section, we apply this method to explain qualitatively some of the above experimental observations, in particular the oscillations of the structure factor [Fig. 1.1(c)] and the behavior of the G_1 function [Fig. 1.2(b)].

1.3.1 Harmonic evolution

The Bogoliubov modes arising from the diagonalization of $\hat{H}_0$ evolve harmonically, i.e., as $\hat{a}_{\boldsymbol{q},t} = \hat{a}_{\boldsymbol{q},0}e^{-i\epsilon_{\boldsymbol{q}}t}$. This evolution defines a coherent time scale $\tau_g \sim 1/\epsilon_q$. In other words, interactions between quasiparticles are neglected, although the quartic term $\hat{\psi}^\dagger\hat{\psi}^\dagger\hat{\psi}\hat{\psi}$ describing interactions between *physical* particles is contained in $\hat{H}_0$. At the core of the latter Hamiltonian's integrability is the conservation of the quasiparticle occupation numbers $n_{\boldsymbol{q}}(t) = \langle\hat{a}^\dagger_{\boldsymbol{q},t}\hat{a}_{\boldsymbol{q},t}\rangle$, which are fixed by their initial values $n_{\boldsymbol{q}}(t=0) \equiv n^0_{\boldsymbol{q}}$. On the other hand, the expectation value of the destruction of a pair of quasiparticles typically oscillates in time as:

$$\langle\hat{a}_{\boldsymbol{q},t}\hat{a}_{-\boldsymbol{q},t}\rangle = \langle\hat{a}_{\boldsymbol{q},0}\hat{a}_{-\boldsymbol{q},0}\rangle e^{-2i\epsilon_{\boldsymbol{q}}t} \neq 0. \tag{1.17}$$

This is due to the creation of pairs of quasiparticles after the quench, cf. Ref. [118] for an experimental characterization. A specific example of quench protocol will be given in Sec. 3.1.1 of Chapter 3, as well as explicit expressions for, e.g., $n^0_{\boldsymbol{q}}$. The oscillating exponential in Eq. (1.17) is the signature of interferences between the counterpropagating quasiparticles. As will be demonstrated explicitly in Chapter 3,

the above quadratic expectation values $\langle \hat{a}^\dagger_{\boldsymbol{q},t}\hat{a}_{\boldsymbol{q},t}\rangle$ and $\langle \hat{a}_{\boldsymbol{q},t}\hat{a}_{-\boldsymbol{q},t}\rangle$ are the building blocks of the structure factor measured in the Cheng Chin experiment [44]. Therefore, the oscillations presented in Fig. 1.1(c) directly emerge from Eq. (1.17). At short enough times, the harmonic behavior of the density dip in Jean Dalibard experiment has the same physical origin, despite the initial inhomogeneity of the gas.

1.3.2 Prethermalization

A similar Bogoliubov approach was carried out by the authors of Ref. [113] to compute the G_1 function measured in the aforementioned fluid-of-light experiment (Sec. 1.2.2), with the slight difference that, in this optical context, the dynamics is purely classical [i.e., governed by the nonlinear wave equation (1.16)]. This requires to adapt a little the formalism of Sec. 1.1.4 in the form of a classical-statistical field theory. The precise connection between quantum classical field theories will be addressed in Sec. 2.3.3; nevertheless, at this stage let us briefly mention how to adapt the preceding arguments to fluids of light. In the optical experiment, the quantum fields $\hat{\psi}, \hat{\psi}^\dagger$ are replaced by their (commuting) classical counterparts ϕ, ϕ^*. In this framework, the initial state designed in [68, 113] was the sum of a uniform background and small spatial fluctuations modeled by a speckle field

$$\phi(\boldsymbol{r}, t=0) \propto \sqrt{\rho_0} + \epsilon\phi_\sigma(\boldsymbol{r}), \tag{1.18}$$

up to a normalization constant. Here, $\epsilon \ll 1$ is the amplitude of the speckle field $\phi_\sigma(\boldsymbol{r})$. The latter is a complex random variable with Gaussian correlations on the scale $\sigma \gg \xi$ [113]. The quantum expectation value $\langle \cdots \rangle$ is here replaced by an ensemble average over the random speckle field.

It was shown in Ref. [68, 113] that, after a few tens of the coherent time scale[7] τ_g, the G_1 function displays an algebraic decay for distances smaller than $|\Delta\boldsymbol{r}| = 2ct$ [Fig. 1.2(b)]. Within the light cone, the prediction of Bogoliubov theory is

$$G_1(\sigma \ll |\Delta\boldsymbol{r}| < 2ct, t/\tau_g \gg 1) \simeq \rho_0 e^{\psi(1/2)\alpha/2} \left(\frac{4\sigma}{|\Delta\boldsymbol{r}|}\right)^\alpha, \tag{1.19}$$

where $\psi(1/2)$ is the digamma function evaluated in $1/2$ and

$$\alpha = \epsilon^2\sigma^2/2\xi^2 \tag{1.20}$$

is the power-law exponent. Interestingly, the law (1.19) takes the thermal form (1.3), which also displays an algebraic decay in $|\Delta\boldsymbol{r}|$, but with the exponent $1/(\rho_0\lambda^2) \sim mT/\rho_0$. Here, α depends on the initial conditions through ϵ and σ, which is reminiscent of the underlying Hamiltonian's integrability. Nevertheless, α is distinct

[7] From the estimate in Sec. 1.3.1, i.e., $\tau_g \sim 1/\epsilon_{\boldsymbol{q}}$, one obtains that $\tau_g \sim 1/(g\rho_0)$ by using that $\epsilon_{\boldsymbol{q}} = c|\boldsymbol{q}|$ and that the typical momentum is $|\boldsymbol{q}| \sim 1/\xi$.

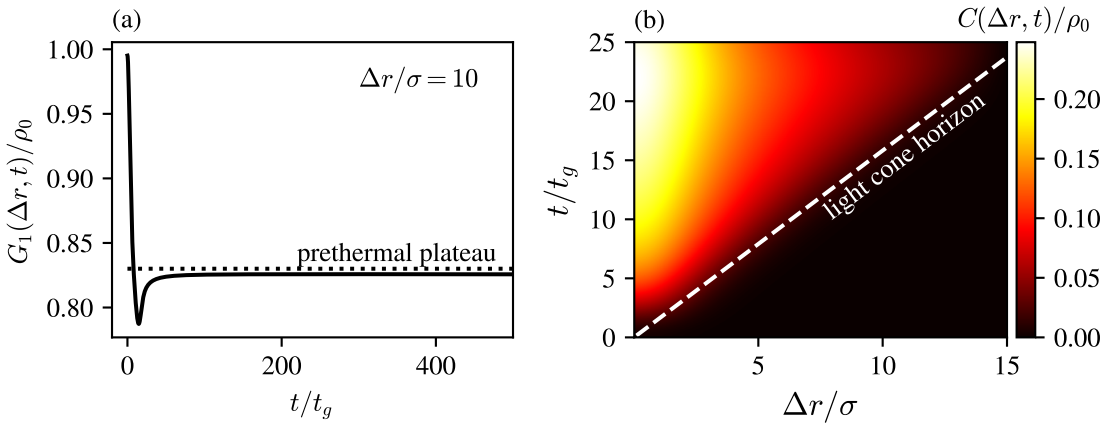

Figure 1.4: (a) Dynamical evolution of the two-point spatial correlation function G_1 for a *fixed* distance $\Delta r/\sigma = 10$, with $|\Delta \boldsymbol{r}| \equiv \Delta r$. The solid curve is the theoretical result given by Bogoliubov approach [cf. Eq. (2) of Ref. [113]]. In units of the rescaled time, G_1 exhibits a fast relaxation towards a "prethermal plateau", in the sense that it approaches the asymptotic value given by Eq. (1.19) (dotted line). The discrepancy between the dotted and solid curves vanishes when $\Delta r/\sigma$ increases. (b) Spreading of correlations, illustrated by the spacetime diagram of the connected correlator (1.21). Information propagates at the speed of sound c, along the light cone boundary given by $t = \Delta r/(2c)$(dashed line). Outside of the light cone (bottom right corner), the correlations are strongly suppressed, in agreement with Lieb-Robinson bounds [120, 121]. In both subplots, the initial state is characterized by $\epsilon = 0.07$ and $\xi/\sigma = 0.158$.

from the thermal exponent given by Eq. (1.3) [68], indicating that the optical field within the light cone is not described by a Gibbs ensemble. For all these reasons, the fast equilibration process towards the above algebraic decay has been termed *prethermalization* [33, 34, 119], i.e., it corresponds to the equilibration process of a *local* observable taking place long before the true thermalization, when interactions between quasiparticles can still be neglected. The local observable in question is here given by the G_1 function for a fixed spacing $|\Delta \boldsymbol{r}|$. As shown in Fig. 1.4(a), it rapidly reaches a long-lasting (prethermal) plateau, whose value is inferred from the conserved quantities of the integrable part of the Hamiltonian, i.e., the occupation numbers in the Bogoliubov basis.

1.3.3 Spreading of correlations

For larger distances $|\Delta \boldsymbol{r}| > 2ct$, the two-point correlation function $G_1(\Delta \boldsymbol{r}, t) = \langle \phi^*(0,t)\phi(\boldsymbol{r},t)\rangle$ becomes independent of the spatial variable, as counterpropagating quasiparticles separated by a distance $|\Delta \boldsymbol{r}|$ cannot travel faster than the speed of sound c. By analogy with relativistic quantum theory, where information propagation is bounded by the speed of light, the spreading of correlations is more clearly

represented in a spacetime diagram. For a better visualization of the "light cone" (sound cone), we introduce the connected correlator

$$C(\Delta\boldsymbol{r},t) = \langle\phi^*(0,t)\phi(\boldsymbol{r},t)\rangle - \langle\phi^*(0,t)\rangle\langle\phi(0,t)\rangle, \tag{1.21}$$

which can be equivalently rewritten as $C(\Delta\boldsymbol{r},t) = g_1(\Delta\boldsymbol{r},t) - g_1(\Delta\boldsymbol{r}\to\infty,t)$. This correlation function is represented in Fig. 1.4(b), obtained by solving the Bogoliubov theory starting from the initial state (1.18) (see [113] for details). The connected correlator C reveals a significant suppression of the correlations in the exterior of the light cone, compatible with the long-known findings of Lieb and Robinson [120, 121].

1.4 Thermalization

In the sound-wave experiment discussed in Sec. 1.2.3, we mentioned that a phenomenon of damping was observed in the quasiparticle modes at long times. This damping originates from collisions between quasiparticles, described by the Hamiltonian (1.13) and is, theorefore, beyond the scope of the Bogoliubov theory. In this final section, we provide elementary considerations about the theoretical description of these collisions, and the associated phenomenon of thermalization.

1.4.1 Quantum Boltzmann equation

The process of thermalization that establishes after the regime of coherent dynamics is in general driven by interactions between quasiparticles [due to the term (1.13) of the Hamiltonian], which makes the occupation number $n_{\boldsymbol{q}}$ evolve as a function of time. Here, we quickly explain how to study the relaxation rate $\partial_\tau n_{\boldsymbol{q}}$ under this mechanism, which for weak interactions can be achieved in the simplest way by using the Fermi's golden rule, as done, for example, in Refs [93, 94]. A possible decay process that can deplete $n_{\boldsymbol{q}}$ is the absorption by a $\boldsymbol{q}$-labeled phonon of another excitation of momentum $\boldsymbol{p}$ to create a third quasiparticle of momentum $\boldsymbol{p}+\boldsymbol{q}$. This mechanism is known as Landau damping. In Fock space, the matrix elements of the creation and annihilation operators are $\langle n_{\boldsymbol{q}}-1|\hat{a}_{\boldsymbol{q}}|n_{\boldsymbol{q}}\rangle = \langle n_{\boldsymbol{q}}|\hat{a}^\dagger_{\boldsymbol{q}}|n_{\boldsymbol{q}}-1\rangle = \sqrt{n_{\boldsymbol{q}}}$, so that the expectation value of the described scattering process is

$$|\langle n_{\boldsymbol{q}}-1, n_{\boldsymbol{p}}-1, n_{\boldsymbol{p}+\boldsymbol{q}}+1|\hat{a}_{\boldsymbol{q}}\hat{a}_{\boldsymbol{p}}\hat{a}^\dagger_{\boldsymbol{p}+\boldsymbol{q}}|n_{\boldsymbol{q}}, n_{\boldsymbol{p}}, n_{\boldsymbol{p}+\boldsymbol{q}}\rangle|^2 = n_{\boldsymbol{q}}n_{\boldsymbol{p}}(n_{\boldsymbol{p}+\boldsymbol{q}}+1). \tag{1.22}$$

Here, the $+1$ factor corresponds to spontaneous emission, while the cubic term refers to stimulated emission. Alternatively, the state of occupation number $n_{\boldsymbol{q}}$ can *gain* quasiparticles from the hermitian conjugated process $\hat{a}_{\boldsymbol{p}+\boldsymbol{q}}\hat{a}^\dagger_{\boldsymbol{p}}\hat{a}^\dagger_{\boldsymbol{q}}$, with squared matrix elements $n_{\boldsymbol{p}+\boldsymbol{q}}(n_{\boldsymbol{p}}+1)(n_{\boldsymbol{q}}+1)$. Therefore, the total decay rate given by Fermi's golden rule follows a *detailed balance* principle, where all processes scattered

into the state $\boldsymbol{q}$ are counted with a positive sign, while processes scattered out are subtracted:

$$\partial_\tau n_{\boldsymbol{q}} \sim \int_{\boldsymbol{p}} \Lambda^2_{\boldsymbol{p},\boldsymbol{q}}\, \delta(\epsilon_{\boldsymbol{p}} + \epsilon_{\boldsymbol{q}} - \epsilon_{\boldsymbol{q}+\boldsymbol{p}}) \Big[n_{\boldsymbol{p}+\boldsymbol{q}}(n_{\boldsymbol{p}}+1)(n_{\boldsymbol{q}}+1) - n_{\boldsymbol{q}} n_{\boldsymbol{p}} (n_{\boldsymbol{p}+\boldsymbol{q}}+1) \Big]. \quad (1.23)$$

In this formula, the Dirac δ imposes the conservation of energy. Furthermore, it can be readily verified that the Bose equilibrium distribution $n^{\rm th}_{\boldsymbol{q}} = (e^{\epsilon_{\boldsymbol{q}}/T} - 1)^{-1}$ cancels out the right hand side of Eq. (1.23): this equation thus describes a process of thermalization. The aim of the next chapter is precisely to give a more systematic derivation of such *kinetic equation*, so that we will refrain here from delving into a deeper analysis. However, let us provide a glimpse of what awaits us in Sec (2.3.2). Upon injecting $n_{\boldsymbol{q},\tau} = n^{\rm th}_{\boldsymbol{q}} + \delta n_{\boldsymbol{q},\tau}$ and linearizing around $\delta n_{\boldsymbol{q},\tau}$, we find an *exponential* relaxation towards equilibrium [cf. Eq. (2.77)]. The corresponding inverse relaxation time, known as Landau damping rate, was first obtained in two dimensions in Ref. [88]. This relaxation mechanism is precisely responsible for the damping of the density oscillations observed in the experiment [69] and discussed in Sec. 1.2.3.

Note that, at zero temperature, Landau damping becomes negligible, leading to the emergence of an alternative relaxation mechanism. This mechanism involves the disintegration of a phonon $\epsilon_{\boldsymbol{q}}$ into two smaller quasiparticles, and is referred to as Beliaev damping [65]. This process will be also discussed in the next chapter.

The arguments developed above give a simple physical interpretation of the dynamics of the occupation number $n_{\boldsymbol{q}}$. The latter evolves in time similarly to the one-particle distribution function of a classical gas governed by the Boltzmann equation [122]. More precisely, it is controlled by a collision integral (1.23) that enforces the detailed balance between scattering processes allowed by the conservation of energy. However, if the principle of detailed balance is *a priori* well suited to describe the dynamics of distribution functions, it is not clear how it can be generalized to observables such as, e.g., $\langle \hat{a}_{\boldsymbol{q},t} \hat{a}_{-\boldsymbol{q},t} \rangle$.

1.4.2 Equation-of-motion theory

EOM theory covers a variety of techniques that apply to *any* observable [77, 123, 124]. The starting point of these approaches is the Heisenberg equation of motion

$$i d_t \hat{O} = [\hat{O}, \hat{H}]. \quad (1.24)$$

In general, the commutator in the right-hand side gives rise to operators that are distinct from $\hat{O}$. Thus, additional equations of motion must be derived to solve Eq. (1.24), leading to an infinite hierarchy of coupled equations, equivalent to the full many-body problem. In the Schrödinger picture, a closely related system of differential equations is known as the Bogoliubov–Born–Green–Kirkwood–Yvon (BBGKY) hierarchy [77] that tackles the dynamics of reduced density matrices.

In principle, EOM theory can be employed in any basis, e.g., for microscopic variables $\hat{O} \equiv \hat{\psi}^\dagger, \hat{\psi}$, hydrodynamic ones $\hat{O} \equiv \hat{\rho}, \hat{\theta}$, etc. However, this approach is most effective when implemented in a basis where the Hamiltonian is approximately diagonal [125, 126] (assuming that such a basis exists). In the case of the 2D Bose gas (1.1), the quasiparticles language (1.9) provides such weakly interacting framework. In this basis, observables like the number operators $n_{\boldsymbol{q}}$ are slowly varying compared to the coherent time scale $\sim 1/\epsilon_{\boldsymbol{q}}$, a property known as the *separation of time scales*.

The full hierarchy resulting from Eq. (1.24), however, is plagued by the exponential complexity of the many-body problem. To obtain a closed differential system that is numerically tractable, it is necessary to truncate the EOM hierarchy at a given order. The first option is to neglect all terms of degree higher than a certain rank (the so-called "hard cutoff" [127]). Such approximations are expected to provide good results for short times in the limit of low energies. However, they typically lead to divergences at late times. The second type of truncation schemes consists in using an educated Ansatz on the expectation value of high-order operator. For instance, in some cases, Wick's theorem can be applied, so that expectations values of quartic operators are broken into a product of quadratic ones, etc; the added difficulty is that the differential system then becomes nonlinear. Importantly, such "factorized cutoff" allows to derive analytically Boltzmann-like equations such as Eq. (1.23) [41, 128]. To achieve this, in addition to using the proper hierarchy truncation, one must also average out fluctuations of the expectations values on small time scales [41], which amounts, again, to assuming a separation of time scales between microscopic scattering processes and macroscopic relaxation phenomena.

Conclusion

In this chapter, we have introduced 2D uniform Bose gases with weak contact interactions. After quickly reviewing their equilibrium properties, we have discussed several recent quench experiments. In these setups, the physics could be mostly explained in terms of independent quasiparticles (Bogoliubov theory), corresponding to a coherent dynamics. In Sec. 1.4, we then discussed two techniques allowing to go beyond the Bogoliubov approach by including quasiparticle interactions. These methods lead to "kinetic equations", i.e., integro-differential coupled equations that resemble the classical Boltzmann equation. The first of these methods is based on detailed balance arguments combined with the Fermi golden rule. The other one, EOM theory, allows to microscopically derive the kinetic equation (1.23) by relying on a separation of time scales between coherent phenomena (described by free quasiparticles), and macroscopic processes like thermalization. However, EOM theory, even when brought into a Boltzmann form, suffers from several limitations. A first obstacle is that calculations quickly become difficult to follow, as there is no diagrammatic representation. Second, the separation of time scales is not imple-

mented in a transparent way, in the sense that it is stated as an Ansatz, instead of emerging as the first order of a controlled expansion. Finally, it is inherently perturbative and cannot be extended beyond the weakly interacting (near integrable) regime. In the next chapter, we will introduce the Keldysh formalism to overcome these issues, while gaining other benefits in the process: clear connection between quantum and classical-statistical field theories, possible extension to non-Gaussian initial state, and others.

Chapter 2

Keldysh approach to two-dimensional Bose superfluids

In this chapter, we introduce the Keldysh approach to nonequilibrium quantum systems, and use it to derive quantum kinetic equations describing two-dimensional, dilute Bose superfluids. To explain the purpose of the Keldysh technique, we first outline the limitations of Feynman path integrals, which are typically restricted to the evolution of *pure* states in time, or to the computation of expectations values of *mixed* states *at equilibrium*. The Feynman path integral is unable to combine the above aspects simultaneously, i.e., it cannot describe the nonequilibrium dynamics of a mixed state. This gap is filled by the Keldysh formalism, at the price of a doubling of degrees of freedom. After these preliminary discussions, we construct the nonequilibrium Keldysh action within the hydrodynamic formalism for 2D superfluids. We then introduce the corresponding perturbation theory, and exploit it to derive quantum kinetic equations for the phonon distribution of the superfluid. The resolution of these equations for a specific quench protocol is postponed to the next chapter. In the whole chapter, we set $\hbar = 1$.

2.1 Keldysh technique in a nutshell

2.1.1 Feynman path integral

Evolution of pure states Suppose we want to compute the dynamical evolution of a pure state $|\psi_0\rangle$. In other words, we search for the solution of the Schrödinger equation $i\partial_t|\psi\rangle = \hat{h}|\psi\rangle$, with $|\psi(t=0)\rangle = |\psi_0\rangle$. As an example, $\hat{h}$ can here be the Hamiltonian of a single particle in a two-dimensional potential $\hat{v}$. The kinetic part $\hat{k} = \hat{\boldsymbol{p}}^2/2m$ is diagonal in momentum space, while $\hat{v}$ is more conveniently expressed in position space as $\langle \boldsymbol{r}'|\hat{v}|\boldsymbol{r}\rangle = v(\boldsymbol{r})\delta(\boldsymbol{r}-\boldsymbol{r}')$. Clearly, $\hat{k}$ and $\hat{v}$ do not commute. Formally, one can integrate the Schrödinger equation as $|\psi(t)\rangle = \hat{\mathcal{U}}_{t,0}|\psi_0\rangle$, where $\hat{\mathcal{U}}_{t,0} = e^{-i\hat{h}t}$ is the *forward* evolution operator, i.e., it represents the unitary dynamics

from the initial time to t.

At this stage, one could introduce the basis of energy eigenstates to express the dynamics of ψ in terms of the spectral decomposition of $\hat{h}$. Instead of this Hamiltonian approach, however, it is instructive to aim at a Lagrangian formulation of the dynamics, as introduced by Feynman [129]. The idea is to use Trotter's formula to split $\hat{\mathcal{U}}_{t,0}$ into a time-ordered product of n evolution operators:

$$\hat{\mathcal{U}}_{t,0} = \prod_{l=1}^{n} \hat{\mathcal{U}}_{lt/n,(l-1)t/n}. \tag{2.1}$$

The computation of the matrix elements of $\hat{\mathcal{U}}$ in, e.g., position space, is then facilitated by the insertion of $n-1$ resolutions of unity such as $\hat{1} = \int d\boldsymbol{r}|\boldsymbol{r}\rangle\langle\boldsymbol{r}|$. Indeed, in the position basis $e^{-i\hat{v}t/n}$ is diagonal and can thus be expressed explicitly. Similarly, $n-1$ resolutions of unity in momentum basis allow to simplify terms like $e^{-i\hat{k}t/n}$. Taking the limit $n \to \infty$, the matrix elements of $\hat{\mathcal{U}}$ can then be represented as the path integral [130]

$$\langle \boldsymbol{r}''|\hat{\mathcal{U}}_{t,0}|\boldsymbol{r}'\rangle = \int_{\boldsymbol{r}(0)=\boldsymbol{r}'}^{\boldsymbol{r}(t)=\boldsymbol{r}''} [d\boldsymbol{r}(u)] \exp[iS(\boldsymbol{r})], \tag{2.2}$$

where S is the *classical* action, $S(\boldsymbol{r}) = \int_0^t du\, [m(\partial_u \boldsymbol{r})^2/2 - v(\boldsymbol{r})]$. Eq. (2.2) establishes a spectacular relation between the operatorial formalism, whose dynamics is characterized by $\hat{\mathcal{U}}_{t,0}$, and a "classical" average over all possible trajectories $\boldsymbol{r}(u)$, where $0 \leq u \leq t$ and the boundary conditions are fixed by the vectors $\boldsymbol{r}', \boldsymbol{r}''$. These paths, weighted by e^{iS}, appear in the measure of the integral (2.2) as

$$\int [d\boldsymbol{r}(u)] \equiv \lim_{n\to\infty} \left(\frac{mn}{2\pi i t}\right)^n \int \prod_{l=1}^{n-1} d\boldsymbol{r}_l, \tag{2.3}$$

where $\boldsymbol{r}_l \equiv \boldsymbol{r}(lt/n)$. Finally, the solution of the problem is

$$|\psi(t)\rangle = \int d\boldsymbol{r}'\, d\boldsymbol{r}''\, \langle \boldsymbol{r}''|\hat{\mathcal{U}}_{t,0}|\boldsymbol{r}'\rangle \psi_0(\boldsymbol{r}')|\boldsymbol{r}''\rangle, \tag{2.4}$$

where $\psi_0(\boldsymbol{r}') = \langle \boldsymbol{r}'|\psi_0\rangle$ is the initial wave function of the particle in position representation.

Equilibrium mixed states Assume we are now interested in the quantum average $\langle\hat{\mathcal{O}}\rangle = \mathrm{Tr}(\hat{\rho}\hat{\mathcal{O}})$ of the canonical equilibrium density matrix $\hat{\rho} = e^{-\beta\hat{h}}/\mathrm{Tr}(e^{-\beta\hat{h}})$, where $\hat{h}$ is the Hamiltonian introduced in the previous paragraph, and β is the inverse temperature. The trace implies a summation over all possible states. For instance, in the position representation:

$$\langle\hat{\mathcal{O}}\rangle = Z^{-1} \int d\boldsymbol{r} \langle \boldsymbol{r}|e^{-\beta\hat{h}}\hat{\mathcal{O}}|\boldsymbol{r}\rangle. \tag{2.5}$$

The denominator of this expression is the partition function of the system in thermal equilibrium: $Z = \int d\boldsymbol{r} \langle \boldsymbol{r}|e^{-\beta\hat{h}}|\boldsymbol{r}\rangle$. Provided that the transformation $t \to -i\beta$ is performed, Z is formally equivalent to the sum over all states of the diagonal amplitude $\langle \boldsymbol{r}|e^{-i\hat{h}t}|\boldsymbol{r}\rangle$ computed in Eq. (2.2). As for the numerator of Eq. (2.5), it can be brought into a field integral representation following the same method, with the only difference that the matrix elements of $\hat{\mathcal{O}}$ in position basis must be computed explicitly. Therefore, the rotation to imaginary times establishes a direct connection between Feynman path integrals and quantum expectation values at thermal equilibrium. It is, indeed, the starting point of the Matsubara formalism [90, 131].

To summarize the main insights of this section, the Feynman path integral allows to propagate pure states in time, as Eq. (2.2) demonstrates. It also opens up a way to compute equilibrium quantum averages like (2.5).

2.1.2 Closed time contour

We would like now to investigate the case of genuinely out-of-equilibrium quantum evolutions where the initial density matrix $\hat{\rho}_0$ can be a *mixed* state. Such a dynamics is governed by the von Neumann equation $i\partial_t\hat{\rho} = [\hat{H}, \hat{\rho}]$, where for $\hat{H}$ we now take the microscopic Hamiltonian (1.1) that describes a gas of two-dimensional bosons with contact interactions. Formal integration yields $\hat{\rho}(t) = \hat{\mathcal{U}}_{t,0}\hat{\rho}_0\hat{\mathcal{U}}_{0,t}$, so that the quantum expectation value of an operator $\hat{\mathcal{O}}$ can be written as

$$\langle\hat{\mathcal{O}}\rangle(t) = \mathrm{Tr}(\hat{\mathcal{U}}_{0,t}\hat{\mathcal{O}}\hat{\mathcal{U}}_{t,0}\hat{\rho}_0)/\mathrm{Tr}(\hat{\rho}_0), \tag{2.6}$$

implying that both the forward *and* backward evolution operators are involved [compare, e.g., with Eq. (2.5)]. Pictorially, this expectation value is described by the closed, real time contour C:

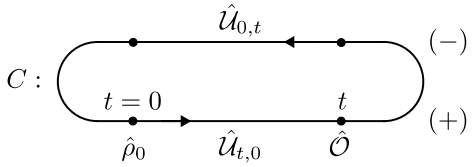

This representation is slightly inconvenient, because the contour depends on the time t at which the observable is measured. However, it is easy to obtain a time-independent contour, by introducing the identity $\hat{\mathcal{U}}_{t,+\infty}\hat{\mathcal{U}}_{+\infty,t} = \hat{1}$ at time t between the two branches, i.e., by formally extending the contour to infinite times. The equivalent contour

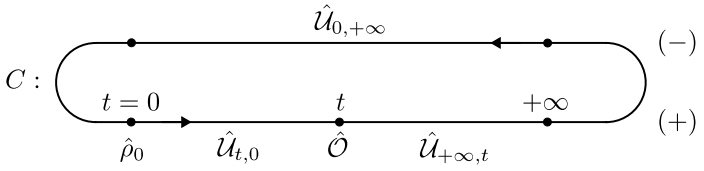

is composed of two branches: The forward (+) branch, related to forward time evolution, extends from the initial time, where the density matrix $\hat{\rho}_0$ is known, to a distant future, and the backward (−) branch, related to backward time evolution, expressed by $\hat{\mathcal{U}}_{0,+\infty}$. At time $t = 0$, the two branches are glued together by the trace operation. Furthermore, the contour is *oriented* (the direction is given by the arrows on C). It means that, for instance, times on the (−) part of C are considered to occur *after* times on the forward branch. Formally, we will resort to the time-ordering operator $\mathbf{T}$ to sort time-dependent operators along this contour.

Finally, let us mention that, in this thesis, we restrict our attention to uncorrelated initial states, i.e. initial density matrices $\hat{\rho}_0$ that admit a Wick decomposition [132]. Extension of the theory to non-Gaussian initial density matrices implies inclusion of additional vertices in the classical action, as explained in, e.g., Ref. [133]. However, it should be noted that, even for a Gaussian initial state $\hat{\rho}_0$, non-Gaussian high-order correlations will in general build up for $t > 0$ [134]. In the following framework these generic correlations will be properly accounted for, i.e., $\hat{\rho}(t > 0)$ will not approximated by a Gaussian density matrix.

2.1.3 Coherent state representation

A remarkable feature of the Feynman path integral is that it allows to express quantum mechanical averages (expectation values of operators in a given Hilbert space) in terms of functional integrals over classical fields. This point of view is conceptually appealing, because it bridges the gap between quantum and classical physics.

The Keldysh field theory is based on the partition function

$$Z = \mathrm{Tr}\left(\hat{\mathcal{U}}_C \hat{\rho}_0\right) / \mathrm{Tr}\left(\hat{\rho}_0\right), \tag{2.7}$$

where the evolution operator $\hat{\mathcal{U}}_C = \mathbf{T}\exp[-i\int_C dt\, \hat{H}(t)]$ is defined along the closed time contour C. By construction, $\hat{\mathcal{U}}_C = \hat{1}$ and therefore $Z = 1$, so that at first sight it may seem strange to construct a path integral on this quantity. However, as we will see, such a partition function does contain non-trivial information on the dynamics of quadratic correlators. More generic observables can be obtained by means of generating functionals [131, 135], which have a strong structural analogy with the partition function, although we will not need this formalism in this thesis.

Feynman's approach suggests to first discretize the Keldysh double contour C in a finite number of time steps, using Trotter's formula. Then, the trick is to introduce, along C, as many resolutions of unity as needed, in the relevant eigenstate basis of the quantum operators. For the simple single particle Hamiltonian discussed in Sec. (2.1.1), these operators were $\hat{\boldsymbol{r}}, \hat{\boldsymbol{p}}$ and thus the position and momentum eigenstates were employed. However, the Hamiltonian (1.1) is expressed in terms of the second-quantized operator fields $\hat{\psi}, \hat{\psi}^\dagger$, whose eigenstates are the coherent states ϕ, defined as $\hat{\psi}|\phi\rangle = \phi|\phi\rangle$. Eq. (2.7) may then be written as a path integral

in coherent-state representation [135]:

$$Z = \int [D\phi]\,[D\phi^*]\,e^{iS[\phi,\phi^*]}, \tag{2.8}$$

with

$$S\,[\phi,\phi^*] = \int d\boldsymbol{r} \int_C dt\,\phi^*(i\partial_t + \frac{1}{2m}\Delta_{\boldsymbol{r}})\phi - \frac{g}{2}\int d\boldsymbol{r}\int_C dt\,|\phi|^4 \tag{2.9}$$

the *classical* action along the Keldysh contour C, obtained from $\hat{H}$, the *quantum* microscopic Hamiltonian (1.1). In Eq. (2.8), ϕ and ϕ^* are treated as independent variables; an alternative choice would be $\mathrm{Re}\phi$, $\mathrm{Im}\phi$. The measure itself $[D\phi]\,[D\phi^*]$ is a generalization of Eq. (2.3) for coherent states on the closed time contour. Finally, notice that restoring $\hbar$ in the notations leads to $Z = \int [D\phi]\,[D\phi^*]\,e^{iS[\phi,\phi^*]/\hbar}$. In the semiclassical limit $\hbar \to 0$, the partition function is thus dominated by the paths that verify $\delta S/\delta\phi^* = 0$. These paths minimizing the action are the solution of the well-known Gross-Pitaevskii equation [65, 130].

2.1.4 Hydrodynamic formulation

As mentioned in Sec. 1.1.3, density-phase variables in the operator representation are ill-defined. The path integral formulation of the interacting Hamiltonian (1.1) is subject to the same issue. However, Popov justified the use of a hydrodynamic formalism starting from the microscopic (Cartesian) Hamiltonian [47, 48]. His conclusion is equivalent to the result of Ref. [49]: The hydrodynamic variables emerge from coarse-grained averaging over small spatial scales. In the following, we ignore this problem and write the classical field ϕ in the polar basis as

$$\phi(\boldsymbol{r}) = \sqrt{\rho(\boldsymbol{r})}e^{i\theta(\boldsymbol{r})}. \tag{2.10}$$

Following the steps of Sec. 1.1.2, we now expand the action (2.9) in powers of the density fluctuations $\delta\rho$ and of the phase gradient $\nabla_{\boldsymbol{r}}\theta$. The Bogoliubov transformation

$$\theta(\boldsymbol{r}) \equiv \int \frac{i d\boldsymbol{q}}{2(2\pi)^2\rho_0}\sqrt{\frac{\epsilon_{\boldsymbol{q}}}{E_{\boldsymbol{q}}}}\,e^{i\boldsymbol{q}\cdot\boldsymbol{r}}(a^*_{\boldsymbol{q}} - a_{-\boldsymbol{q}}), \tag{2.11}$$

$$\delta\rho(\boldsymbol{r}) \equiv -\int \frac{d\boldsymbol{q}}{(2\pi)^2}\sqrt{\frac{E_{\boldsymbol{q}}}{\epsilon_{\boldsymbol{q}}}}\,e^{i\boldsymbol{q}\cdot\boldsymbol{r}}(a^*_{\boldsymbol{q}} + a_{-\boldsymbol{q}}), \tag{2.12}$$

then leads to the hydrodynamic action

$$\begin{aligned} &S[a,a^*] = S_0 + S_{\mathrm{int}} = \\ &\int_{\boldsymbol{q},C} a^*_{\boldsymbol{q},t}(i\partial_t - \epsilon_{\boldsymbol{q}})a_{\boldsymbol{q},t} + \int_{\boldsymbol{p},\boldsymbol{q},C}\Lambda_{\boldsymbol{p},\boldsymbol{q}}\left(a_{\boldsymbol{p},t}a_{\boldsymbol{q},t}a^*_{\boldsymbol{p}+\boldsymbol{q},t} + \text{c.c.}\right), \end{aligned} \tag{2.13}$$

where the vertex function $\Lambda_{\boldsymbol{p},\boldsymbol{q}}$ is given by Eq. (1.14). The first term in this equation describes a gas of free quasiparticles, while the second term accounts for the interactions between them at leading order.

Finally, let us point out that the choice of basis has some important technical consequences. Indeed, this choice conditions the number and types of diagrams to be obtained within perturbation theory (see Sec. 2.2.3 below), making more difficult the comparisons with other possible approaches. As an example, some authors [88] chose to follow Popov [47, 48] by working directly with the density-phase variables. Others [136, 137] integrated out one the two fields $\theta, \delta\rho$ and proceeded with a simpler effective action depending only either on the phase or the density fluctuations. The action (2.13) represents yet another strategy, whose interest is to exploit the perturbative expansion of the action in the quasiparticles basis. Of course, the physical quantities themselves, such as the damping rates close to equilibrium (cf. Sec. 2.3.2), are the same regardless of the basis choice.

2.1.5 Keldysh rotation

The time integrals over the forward and backward contours C_+ and C_- in Eq. (2.13) are conveniently reduced to a single integral over $t > 0$ by introducing two sets of fields a_+, a_+^* and a_-, a_-, which are the restrictions of a, a^* to the $(\pm)$ branches of C. One can then rewrite the partition function as

$$Z = \int D[a_+, a_+^*, a_-, a_-^*] e^{iS_>[a_+,a_+^*]-iS_>[a_-,a_-^*]}. \tag{2.14}$$

The notation $S_> = \int_{t>0} \cdots$ emphasizes that the temporal integration of the action is now done for $t > 0$, instead of $S = \int_{t\in C} \cdots$ in Eq. (2.13). The minus sign in the exponential comes from the reverse direction of time on the backward branch, which reverses the bounds of the time integral. In the following, the slight abuse of notation $S_> \equiv S$ is implied.

As illustrated by Eq. (2.14), the closed contour leads to a doubling of the degrees of freedom. However, this representation of Z is still not completely satisfying, partly because it contains a redundancy, which we will not address in this work (see, e.g., Refs. [90, 135]). To overcome this problem, it is customary to introduce the "classical" and "quantum" field variables $\alpha = (a_+ + a_-)/\sqrt{2}$ and $\tilde{\alpha} = (a_+ - a_-)/\sqrt{2}$. A rationale for this semantic choice will be given in Sec. 2.3.3. Under this transformation, the quadratic action becomes

$$S_0 = \int_{\boldsymbol{q},t>0} \begin{pmatrix} \alpha_{\boldsymbol{q},t}^* & \tilde{\alpha}_{\boldsymbol{q},t}^* \end{pmatrix} [\mathbf{G}^0]^{-1}_{\boldsymbol{q},t,t} \begin{pmatrix} \alpha_{\boldsymbol{q},t} \\ \tilde{\alpha}_{\boldsymbol{q},t} \end{pmatrix} \tag{2.15}$$

where

$$[\mathbf{G}^0]^{-1}_{\boldsymbol{q},t,t} = \begin{pmatrix} 0 & i\partial_t - \epsilon_{\boldsymbol{q}} - i0^+ \\ i\partial_t - \epsilon_{\boldsymbol{q}} + i0^+ & 2i0^+(2n_{\boldsymbol{q},0}+1) \end{pmatrix}, \tag{2.16}$$

while the interaction part is expressed as

$$S_{\text{int}} = \frac{1}{\sqrt{2}} \int_{\boldsymbol{p},\boldsymbol{q},t>0} \Lambda_{\boldsymbol{p},\boldsymbol{q}} (2\alpha^*_{\boldsymbol{p}+\boldsymbol{q},t}\tilde{\alpha}_{\boldsymbol{p},t}\alpha_{\boldsymbol{q},t} + \tilde{\alpha}^*_{\boldsymbol{p}+\boldsymbol{q},t}\alpha_{\boldsymbol{p},t}\alpha_{\boldsymbol{q},t} + \tilde{\alpha}^*_{\boldsymbol{p}+\boldsymbol{q},t}\tilde{\alpha}_{\boldsymbol{p},t}\tilde{\alpha}_{\boldsymbol{q},t} + \text{c.c.}). \tag{2.17}$$

The Keldysh actions (2.15) and (2.17) constitute the starting point of the nonequilibrium perturbation theory that is presented in Sec. 2.2.

2.1.6 From operators to fields

In this work, we consider a 2D Bose gas initially described by an equilibrium density matrix $\hat{\rho}_0$, and we wish to examine its subsequent dynamics following, e.g., a quantum quench performed at $t = 0$. Specifically, we are interested in the time evolution of the phonon normal and anomalous momentum distributions, defined as

$$n_{\boldsymbol{q},t} \equiv \langle \hat{a}^\dagger_{\boldsymbol{q},t} \hat{a}_{\boldsymbol{q},t} \rangle \tag{2.18}$$
$$m_{\boldsymbol{q},t} \equiv |\langle \hat{a}_{\boldsymbol{q},t} \hat{a}_{-\boldsymbol{q},t} \rangle|, \tag{2.19}$$

where the quantum-mechanical averages are performed over the initial density matrix: $\langle \ldots \rangle = \mathrm{Tr}(\hat{\rho}_0 \ldots)/\mathrm{Tr}(\hat{\rho}_0)$.

On the other hand, with the nonequilibrium action (2.15, 2.17), we have developed a functional integral formalism where the quantum operators are expressed in the $\alpha, \tilde{\alpha}$ representation (or in the a, a^* representation before the Keldysh rotation). Because of the non-commutativity of the quantum operators $\hat{a}, \hat{a}^\dagger$ on the closed contour, however, the connection between quadratic correlators in the two formalisms is a non-trivial question. As an example, the expectation values $\langle \hat{a}_{t_1} \hat{a}^\dagger_{t_2} \rangle$ and $\langle \hat{a}^\dagger_{t_2} \hat{a}_{t_1} \rangle$ are in general different, whereas, in the coherent-state representation, the corresponding fields a_{t_1} and $a^*_{t_2}$ always commute. To avoid ambiguities, it is customary to use the time-ordering operator $\mathbf{T}$ on the Keldysh contour. In practice, $\mathbf{T}\hat{A}_t \hat{B}_{t'} = \hat{A}_t \hat{B}_{t'}$ if $t \geq t'$ and $\mathbf{T}\hat{A}_t \hat{B}_{t'} = \hat{B}_{t'} \hat{A}_t$ otherwise. For convenience, we also define the inverse time-ordering operator $\tilde{\mathbf{T}}$ that performs the opposite operation, which is useful on the backward branch. Note that this problem already arises in the usual Feynman path integral, where ordering prescriptions are common [130].

Normal correlators Let us first deal with correlators involving a single complex conjugation, such as $\langle \alpha \alpha^* \rangle$. To connect with correlators of quantum operators, it is necessary to first go back to the forward a^+ and backward a^- fields:

$$\begin{aligned} \langle \alpha_{\boldsymbol{q},t} \alpha^*_{\boldsymbol{q},t'} \rangle &= \frac{1}{2} \langle (a^+_{\boldsymbol{q},t} + a^-_{\boldsymbol{q},t})(a^{+\,*}_{\boldsymbol{q},t'} + a^{-\,*}_{\boldsymbol{q},t'}) \rangle \\ &= \frac{1}{2} \langle a^+_{\boldsymbol{q},t} a^{+\,*}_{\boldsymbol{q},t'} + a^+_{\boldsymbol{q},t} a^{-\,*}_{\boldsymbol{q},t'} + a^-_{\boldsymbol{q},t} a^{+\,*}_{\boldsymbol{q},t'} + a^-_{\boldsymbol{q},t} a^{-\,*}_{\boldsymbol{q},t'} \rangle. \end{aligned} \tag{2.20}$$

In the right hand side of Eq. (2.20), the fields $a^\pm, a^{\pm\,*}$ are classical quantities that always commute with each other. However, it is not the case for quantum operators. Therefore, it is required to explicitly indicate the time ordering, as imposed by the direction of the Keldysh contour. After close inspection, one finds the following identification [135, 138]

$$\langle \alpha_{\boldsymbol{q},t} \alpha^*_{\boldsymbol{q},t'} \rangle = \frac{1}{2} \langle \mathbf{T} \hat{a}_{\boldsymbol{q},t} \hat{a}^\dagger_{\boldsymbol{q},t'} + \{ \hat{a}_{\boldsymbol{q},t}, \hat{a}^\dagger_{\boldsymbol{q},t'} \} + \tilde{\mathbf{T}} \hat{a}_{\boldsymbol{q},t} \hat{a}^\dagger_{\boldsymbol{q},t'} \rangle, \tag{2.21}$$

Clearly, here, no matter how t and t' compare, the correlator has the following form:

$$\langle \alpha_{\boldsymbol{q},t} \alpha^*_{\boldsymbol{q},t'} \rangle = \langle \{ \hat{a}_{\boldsymbol{q},t}, \hat{a}^\dagger_{\boldsymbol{q},t'} \} \rangle. \tag{2.22}$$

In particular, this yields $\langle \alpha_{\boldsymbol{q},t} \alpha^*_{\boldsymbol{q},t} \rangle = 2\langle \hat{a}^\dagger_{\boldsymbol{q},t} \hat{a}_{\boldsymbol{q},t} \rangle + 1$, which will be used extensively in Sec. 2.2.

Similarly, for the quantum-classical normal correlator, we have

$$\langle \alpha_{\boldsymbol{q},t} \tilde{\alpha}^*_{\boldsymbol{q},t'} \rangle = \frac{1}{2} \langle (a^+_{\boldsymbol{q},t} + a^-_{\boldsymbol{q},t})(a^{+*}_{\boldsymbol{q},t'} - a^{-*}_{\boldsymbol{q},t'}) \rangle \tag{2.23}$$

$$= \frac{1}{2} \langle a^+_{\boldsymbol{q},t} a^{+*}_{\boldsymbol{q},t'} - a^+_{\boldsymbol{q},t} a^{-*}_{\boldsymbol{q},t'} + a^-_{\boldsymbol{q},t} a^{+*}_{\boldsymbol{q},t'} - a^-_{\boldsymbol{q},t} a^{-*}_{\boldsymbol{q},t'} \rangle. \tag{2.24}$$

$$= \frac{1}{2} \langle \mathbf{T} \hat{a}_{\boldsymbol{q},t} \hat{a}^\dagger_{\boldsymbol{q},t'} + [\hat{a}_{\boldsymbol{q},t}, \hat{a}^\dagger_{\boldsymbol{q},t'}] - \tilde{\mathbf{T}} \hat{a}_{\boldsymbol{q},t} \hat{a}^\dagger_{\boldsymbol{q},t'} \rangle. \tag{2.25}$$

Hence,

$$\langle \alpha_{\boldsymbol{q},t} \tilde{\alpha}^*_{\boldsymbol{q},t'} \rangle = \Theta(t - t') \langle [\hat{a}_{\boldsymbol{q},t}, \hat{a}^\dagger_{\boldsymbol{q},t'}] \rangle. \tag{2.26}$$

Anomalous correlators Let us now quickly mention how the previous results (2.22, 2.26) generalize to the case of "anomalous" correlation functions such as $\langle \alpha\alpha \rangle$. The same reasoning leads to

$$\langle \alpha_{q,t} \alpha_{-q,t'} \rangle = \langle \{ \hat{a}_{q,t}, \hat{a}_{-q,t'} \} \rangle, \tag{2.27}$$

and

$$\langle \alpha_{q,t} \tilde{\alpha}_{-q,t'} \rangle = 0. \tag{2.28}$$

2.2 Pertubation theory

When the interaction term (1.13) in the Hamiltonian is neglected, the Heisenberg equation of motion following from Eq. (1.11) leads to a purely harmonic evolution of the Bogoliubov operators, $\hat{a}_{\boldsymbol{q},t} = \hat{a}_{\boldsymbol{q},0} e^{-i\epsilon_{\boldsymbol{q}} t}$, so that

$$n_{\boldsymbol{q},t} = n_{\boldsymbol{q},0}, \quad m_{\boldsymbol{q},t} = m_{\boldsymbol{q},0}. \tag{2.29}$$

The normal and anomalous phonon momentum distributions thus remain stuck to their initial value, as already mentioned in the previous chapter (Sec. 1.3.1). We now wish to describe the time dependence of $n_{\boldsymbol{q},t}$ and $m_{\boldsymbol{q},t}$ pertained to the cubic interaction (1.13), using the Keldysh formalism introduced above.

2.2.1 Quantum kinetic equation

To construct the perturbation theory, we introduce three fundamental correlators, the retarded G^R, advanced G^A, and Keldysh G^K Green's functions:

$$G^R_{\boldsymbol{q},t,t'} \equiv -i\Theta(t - t') \langle [\hat{a}_{\boldsymbol{q},t}, \hat{a}^\dagger_{\boldsymbol{q},t'}] \rangle = -i \langle \alpha_{\boldsymbol{q},t} \tilde{\alpha}^*_{\boldsymbol{q},t'} \rangle, \tag{2.30}$$

$$G^A_{\boldsymbol{q},t,t'} \equiv i\Theta(t' - t) \langle [\hat{a}_{\boldsymbol{q},t}, \hat{a}^\dagger_{\boldsymbol{q},t'}] \rangle = -i \langle \tilde{\alpha}_{\boldsymbol{q},t} \alpha^*_{\boldsymbol{q},t'} \rangle, \tag{2.31}$$

$$G^K_{\boldsymbol{q},t,t'} \equiv -i \langle \{ \hat{a}_{\boldsymbol{q},t}, \hat{a}^\dagger_{\boldsymbol{q},t'} \} \rangle = -i \langle \alpha_{\boldsymbol{q},t} \alpha^*_{\boldsymbol{q},t'} \rangle. \tag{2.32}$$

While G^R and G^A correspond to response functions to an external excitation, the Keldysh Green's function contains information on the system's correlations. In particular, it gives access to the quasiparticle momentum distribution via the relation

$$iG^K_{\boldsymbol{q},t,t} = 2n_{\boldsymbol{q},t} + 1, \tag{2.33}$$

deduced from Eq. (2.18). The description of the anomalous distribution $m_{\boldsymbol{q},t}$ requires to introduce a corresponding anomalous Keldysh Green's function and is postponed to Sec. 2.2.4 for clarity.

In the absence of phonon interactions, the Green's functions reduce to their bare values $G^{0,R}, G^{0,A}, G^{0,K}$ and follow from Gaussian integrations on the quadratic action (2.15). This allows us to identify the elements of the matrix kernel (2.16) as:

$$[\mathbf{G}^0]^{-1} = \begin{pmatrix} 0 & [G^{0,A}]^{-1} \\ [G^{0,R}]^{-1} & -[G^{0,R}]^{-1} \circ G^{0,K} \circ [G^{0,A}]^{-1} \end{pmatrix} \tag{2.34}$$

and, correspondingly,

$$\mathbf{G}^0 = \begin{pmatrix} G^{0,K} & G^{0,R} \\ G^{0,A} & 0 \end{pmatrix}. \tag{2.35}$$

In Eq. (2.34), the symbol $\circ$ denotes a convolution in the time coordinates. In momentum-time representation, the bare retarded, advanced and Keldysh Green's functions take the explicit expressions

$$G^{0,R}_{\boldsymbol{q},t,t'} = -i\Theta(t-t')e^{-i\epsilon_{\boldsymbol{q}}(t-t')}, \tag{2.36}$$
$$G^{0,A}_{\boldsymbol{q},t,t'} = i\Theta(t'-t)e^{-i\epsilon_{\boldsymbol{q}}(t-t')}, \tag{2.37}$$
$$G^{0,K}_{\boldsymbol{q},t,t'} = -i(2n_{\boldsymbol{q},0}+1)e^{-i\epsilon_{\boldsymbol{q}}(t-t')}. \tag{2.38}$$

In the presence of phonon interactions, one rewrites the dressed Green function in the form

$$[\mathbf{G}]^{-1}_{\boldsymbol{q},t,t'} = \begin{pmatrix} 0 & [G^{0,A}]^{-1} - \Sigma^A \\ [G^{0,R}]^{-1} - \Sigma^R & -\Sigma^K \end{pmatrix}_{\boldsymbol{q},t,t'}. \tag{2.39}$$

This structure generalizes Eq. (2.34) by including finite self-energies $\Sigma^{R,A,K}$ that encapsulate the effect of interactions. The self-energies can be computed from perturbation theory with the action (2.17), a task that will be undertaken in the next section. Comparing Eq. (2.39) with the definition of $\mathbf{G}$, of the same triangular form as (2.35), we infer the following Dyson equations :

$$[G^R]^{-1} = [G^{0,R}]^{-1} - \Sigma^R \tag{2.40}$$
$$[G^A]^{-1} = [G^{0,A}]^{-1} - \Sigma^A \tag{2.41}$$
$$G^K = G^R \circ \Sigma^K \circ G^A. \tag{2.42}$$

Within this formalism, the computation of response and correlation functions thus essentially amounts to evaluating the self-energies $\Sigma^{R,A,K}$ at a certain level of approximation.

While retarded and advanced Green's functions verify $(G^R)^\dagger = G^A$ and $(G^A)^\dagger = G^R$, the Keldysh Green's function is anti-hermitian, $(G^K)^\dagger = -G^K$ (with the hermitian conjugate obtained by taking the complex conjugate and reversing time indices). This allows us to parametrize G^K as

$$G^K = G^R \circ F - F \circ G^A, \tag{2.43}$$

where the hermitian distribution function F will be related to the phonon momentum distribution below. Combining Eqs. (2.42) and (2.43), we infer:

$$\Sigma^K = F \circ [G^A]^{-1} - [G^R]^{-1} \circ F, \tag{2.44}$$

which, by virtue of the Dyson equations (2.40) and (2.41), becomes

$$F \circ \left[G^{0,A}\right]^{-1} - \left[G^{0,R}\right]^{-1} \circ F = \Sigma^K - \left(\Sigma^R \circ F - F \circ \Sigma^A\right).$$

Direct evaluation of the left-hand side leads to the following quantum kinetic equation for the distribution function in real-time representation:

$$i(\partial_t + \partial_{t'}) F_{\boldsymbol{q},t,t'} = -\Sigma^K_{\boldsymbol{q},t,t'} + \left(\Sigma^R \circ F - F \circ \Sigma^A\right)_{\boldsymbol{q},t,t'}. \tag{2.45}$$

An evaluation of this evolution equation requires the knowledge of the Keldysh and retarded self-energies, which will be both computed in Sec. 2.2.3. Before that, we introduce an important assumption that will bring about a first simplification of Eq. (2.45).

2.2.2 Separation of time scales and on-shell approximation

Two-time nonequilibrium functions such as $F_{\boldsymbol{q},t,t'}$ are most conveniently expressed using the Wigner coordinates $\tau \equiv (t+t')/2$ and $\Delta t \equiv t - t'$. The Wigner transform of a given two-time function $X_{t,t'}$ is defined as $X_{\omega,\tau} = \int d\Delta t\, e^{i\Delta t \omega} X_{\tau+\Delta t/2, \tau-\Delta t/2}$. In the present context, the central time τ is associated with the slow relaxation of the phonons, while the time difference Δt is related to their fast, coherent dynamics [139], cf. Appendix A for additional details.

In the presence of interactions, Bogoliubov quasiparticles acquire a finite lifetime $\tau_{\boldsymbol{q}} \sim -1/\mathrm{Im}\Sigma^R_{\boldsymbol{q}}$. As long as interactions are weak, this lifetime is typically very long compared to the coherent time scale $1/\epsilon_{\boldsymbol{q}}$:

$$\tau_{\boldsymbol{q}} \sim -1/\mathrm{Im}\Sigma^R_{\boldsymbol{q}} \gg 1/\epsilon_{\boldsymbol{q}}. \tag{2.46}$$

This condition, which we will verify *a posteriori* below, also implies that quasiparticles remain well defined during of the out-of-equilibrium evolution. In the limit

(2.46), it can be shown that the Wigner transform of a time convolution reduces [at leading order in $1/(\epsilon_{\boldsymbol{q}}\tau_{\boldsymbol{q}}) \ll 1$] to the product of Wigner transforms: see Appendix A and Ref. [135] for more details. The Wigner transform of Eq. (2.45) thus simplifies to

$$i\partial_\tau F_{\boldsymbol{q},\omega,\tau} \simeq -\Sigma^K_{\boldsymbol{q},\omega,\tau} + 2iF_{\boldsymbol{q},\omega,\tau}\mathrm{Im}(\Sigma^R_{\boldsymbol{q},\omega,\tau}). \tag{2.47}$$

Within the separation of time scales (2.46), application of the Wigner transform to Eq. (2.43) also yields:

$$iG^K_{\boldsymbol{q},\omega,\tau} \simeq F_{\boldsymbol{q},\tau,\omega}A_{\boldsymbol{q},\omega,\tau}, \tag{2.48}$$

where

$$A_{\boldsymbol{q},\omega,\tau} \equiv -2\,\mathrm{Im}(G^R_{\boldsymbol{q},\omega,\tau}) = \frac{-2\,\mathrm{Im}(\Sigma^R_{\boldsymbol{q},\omega,\tau})}{|\omega - \epsilon_{\boldsymbol{q}} - \Sigma^R_{\boldsymbol{q},\omega,\tau}|^2}. \tag{2.49}$$

$A_{\boldsymbol{q},\tau,\omega}$ is called the spectral function. It gives the probability density that a quasiparticle with energy ω has the dispersion $\epsilon_{\boldsymbol{q}}$ at a time τ after the start of the dynamics. Under the condition (2.46) of well defined quasiparticles, the spectral function is strongly peaked around $\omega = \epsilon_{\boldsymbol{q}}$ [with $A_{\boldsymbol{q},\tau,\omega} \to 2\pi\delta(\omega - \epsilon_{\boldsymbol{q}})$ in the non-interacting limit]. Integrating Eq. (2.48) over ω then leads to

$$\int \frac{d\omega}{2\pi} iG^K_{\boldsymbol{q},\omega,\tau} \simeq F_{\boldsymbol{q},\epsilon_{\boldsymbol{q}},\tau} = 2n_{\boldsymbol{q},\tau} + 1, \tag{2.50}$$

where we have used Eq. (2.33) in the last equality. This relation shows that as long as the separation of time scales (2.46) holds, the phonon momentum distribution coincides with the distribution function $F_{\boldsymbol{q},\omega,\tau}$ evaluated at $\omega = \epsilon_{\boldsymbol{q}}$, a property known as the on-shell approximation. To evaluate $n_{\boldsymbol{q},\tau}$, it is thus sufficient to solve the on-shell version of the kinetic equation (2.45). This is achieved by multiplying the latter by the spectral function and integrating over ω, similarly to Eq. (2.50). The kinetic equation simplifies to:

$$\partial_\tau F_{\boldsymbol{q},\tau} \simeq i\Sigma^K_{\boldsymbol{q},\tau} + 2F_{\boldsymbol{q},\tau}\mathrm{Im}(\Sigma^R_{\boldsymbol{q},\tau}), \tag{2.51}$$

where we have introduced the simpler notations $F_{\boldsymbol{q},\tau} \equiv F_{\boldsymbol{q},\epsilon_{\boldsymbol{q}},\tau}$ and $\Sigma_{\boldsymbol{q},\tau} \equiv \Sigma_{\boldsymbol{q},\epsilon_{\boldsymbol{q}},\tau}$. Together with Eq. (2.50), Eq. (2.51) constitutes a quantum kinetic equation for the momentum distribution of the interacting phonons, which can be directly solved once an approximation for the self-energies is provided.

2.2.3 One-loop approximation

We now evaluate the retarded and Keldysh self-energies $\Sigma^R_{\boldsymbol{q},\tau}$ and $\Sigma^K_{\boldsymbol{q},\tau}$ for a 2D, weakly interacting Bose gas using perturbation theory. In practice, this is achieved by comparing Dyson equations with the path integral expressions of the corresponding dressed correlators.

Retarded sector On the one hand, Dyson equation (2.40) *defines* the retarded self-energy as

$$G^R_{\boldsymbol{q},t,t'} = G^{0,R}_{\boldsymbol{q},t,t'} + \int dt_1 dt_2 G^{0,R}_{\boldsymbol{q},t,t_1} \Sigma^R_{\boldsymbol{q},t_1,t_2} G^{0,R}_{\boldsymbol{q},t_2,t'} + \cdots , \tag{2.52}$$

where $G^{0,R}_{\boldsymbol{q},t,t_1}$ and $G^{0,R}_{\boldsymbol{q},t_2,t'}$ are the "legs" of $\Sigma^R_{\boldsymbol{q},t_1,t_2}$. On the other hand, the dressed retarded Green's function is expressed as the functional integral

$$G^R_{\boldsymbol{q},t,t'} = -i\langle \alpha_{\boldsymbol{q},t} \tilde{\alpha}^*_{\boldsymbol{q},t'} \rangle = -i \int \mathcal{D}[\alpha,\tilde{\alpha}] \alpha_{\boldsymbol{q},t} \tilde{\alpha}^*_{\boldsymbol{q},t'} e^{i(S_0+S_{\rm int})}. \tag{2.53}$$

For a dilute Bose gas, $e^{iS_{\rm int}}$ can be expanded at first order in the interaction parameter $g\rho_0$ (one-loop approximation, or Born approximation):

$$G^R_{\boldsymbol{q},t,t'} \simeq -i \int \mathcal{D}[\alpha,\tilde{\alpha}] \alpha_{\boldsymbol{q},t} \tilde{\alpha}^*_{\boldsymbol{q},t'} e^{iS_0} (1 - S^2_{\rm int}/2!). \tag{2.54}$$

In Eq. (2.54), the zeroth-order term in $S_{\rm int}$ is exactly $G^{0,R}_{\boldsymbol{q},t,t'}$. There is no linear term in $S_{\rm int}$, because the Gaussian average of a product of five fields vanish, according to Wick's theorem. As for the term proportional to $\int \mathcal{D}[\alpha,\tilde{\alpha}] \alpha\tilde{\alpha} S^2_{\rm int} e^{iS_0}$, it is a non-zero Gaussian integral that can be computed by means of Wick's theorem. The corresponding Wick contractions include products of four free Green functions ($\alpha\tilde{\alpha} S^2_{\rm int}$ contains eight fields). They are more easily enumerated through a diagrammatic representation based on the pictorial convention

$iG^{0,R} = \langle \alpha \tilde{\alpha}^* \rangle$ $\quad$ $iG^{0,A} = \langle \tilde{\alpha} \alpha^* \rangle$ $\quad$ $iG^{0,K} = \langle \alpha \alpha^* \rangle$

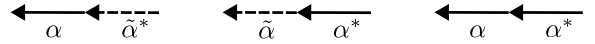

where dashed (solid) lines refer to a quantum $\tilde{\alpha}$ (classical α) field variable. Arrows are directed from a conjugated field variable to a non-conjugated one. The "allowed" Wick contractions must verify the following rules:

- The selected diagrams should be connected (in "one piece") and one-particle irreducible (i.e., they cannot be split into two parts by "cutting" a single line),
- Momentum conservation should be enforced in all Wick pairings,
- The "legs" of the diagrams should be those indicated in Eq. (2.52), represented as

$iG^{0,R}_{\boldsymbol{q},t,t_1} = \langle \alpha_{\boldsymbol{q},t} \tilde{\alpha}^*_{\boldsymbol{q},t_1} \rangle$ $\quad$ $iG^{0,R}_{\boldsymbol{q},t_2,t'} = \langle \alpha_{\boldsymbol{q},t_2} \tilde{\alpha}^*_{\boldsymbol{q},t'} \rangle$

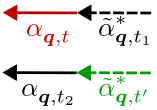

  where colored arrows identify fields that do not originate from $S^2_{\rm int}$,

– No diagrams should involve quantum-quantum field correlators; indeed, $\langle\tilde{\alpha}\tilde{\alpha}^*\rangle_0$ vanishes due to the triangular structure of the matrix Green function [135],

– Diagrams involving anomalous correlators are neglected ("linear-resonance approximation"). This requirement is not obvious, since anomalous correlators are in general nonzero in a nonequilibrium problem. For instance, the average of a quartic term $\alpha_1\alpha_2\alpha_3^*\alpha_4^*$ weighted by a free (Gaussian) factor e^{iS_0} is, without any particular constraints, given by

$$\langle\alpha_1\alpha_2\alpha_3^*\alpha_4^*\rangle_0 = \langle\alpha_1\alpha_2\rangle_0\langle\alpha_3^*\alpha_4^*\rangle_0 + \langle\alpha_1\alpha_3^*\rangle_0\langle\alpha_2\alpha_4^*\rangle_0 + \langle\alpha_1\alpha_4^*\rangle_0\langle\alpha_2\alpha_3^*\rangle_0, \quad (2.55)$$

which does contain anomalous correlators [first term in Eq. (2.55)]. However, in the context of nonequilibrium, 1D interacting Luttinger liquids, it was shown that these anomalous contractions could still be excluded from the diagrammatic expansion of Σ^R [96]. To show this, the authors of Ref. [96] exploited both the *resonance* condition (i.e., the simultaneous conservation of energy and momentum [140]) as well as the *linearity* of the dispersion relation (i.e., the purely phononic nature of the excitations). The same arguments also apply in two dimensions, resulting in the same diagrammatic restriction. Note that, for a 2D Bose gas, $\epsilon_{\boldsymbol{p}}$ has a small cubic correction, but at low energy we expect the corresponding diagrammatic corrections to be small. From now on, we will thus neglect anomalous correlators in the expansion of the normal self-energy, and proceed as if the scattering events were purely linear-resonant.

Lastly, it is worth noting that in dimension three, the Popov approximation [135], an alternative theoretical framework, completely neglects anomalous correlators. In fact, the *normal* self-energy in Popov approximation is identical to the one obtained in this section (except for dimensional specificities). However, within our approach a nonzero *anomalous* self-energy also exists (see Sec. 2.2.4), and thus goes beyond the more drastic Popov approximation.

The Gaussian integral $\int\mathcal{D}[\alpha,\tilde{\alpha}]\alpha\tilde{\alpha}S_{\text{int}}^2e^{iS_0}$ includes three contributions that meet these criteria, each appearing with multiplicity 8, represented by the one-loop diagrams in Fig. 2.1. The comparison with Eq. (2.40) thus results in:

$$\Sigma^R_{\boldsymbol{q},t_1,t_2} = 8\times\frac{i}{2!}\times\frac{1}{2}\int_{\boldsymbol{p}}\Big[\Lambda^2_{\boldsymbol{p},\boldsymbol{q}}G^K_{\boldsymbol{p}+\boldsymbol{q},t_1,t_2}G^{0,A}_{\boldsymbol{p},t_2,t_1} + \Lambda^2_{\boldsymbol{p},\boldsymbol{q}-\boldsymbol{p}}G^K_{\boldsymbol{q}-\boldsymbol{p},t_1,t_2}G^{0,R}_{\boldsymbol{p},t_1,t_2} + \Lambda^2_{\boldsymbol{p},\boldsymbol{q}}G^K_{\boldsymbol{p},t_2,t_1}G^{0,R}_{\boldsymbol{p}+\boldsymbol{q},t_1,t_2}\Big]. \quad (2.56)$$

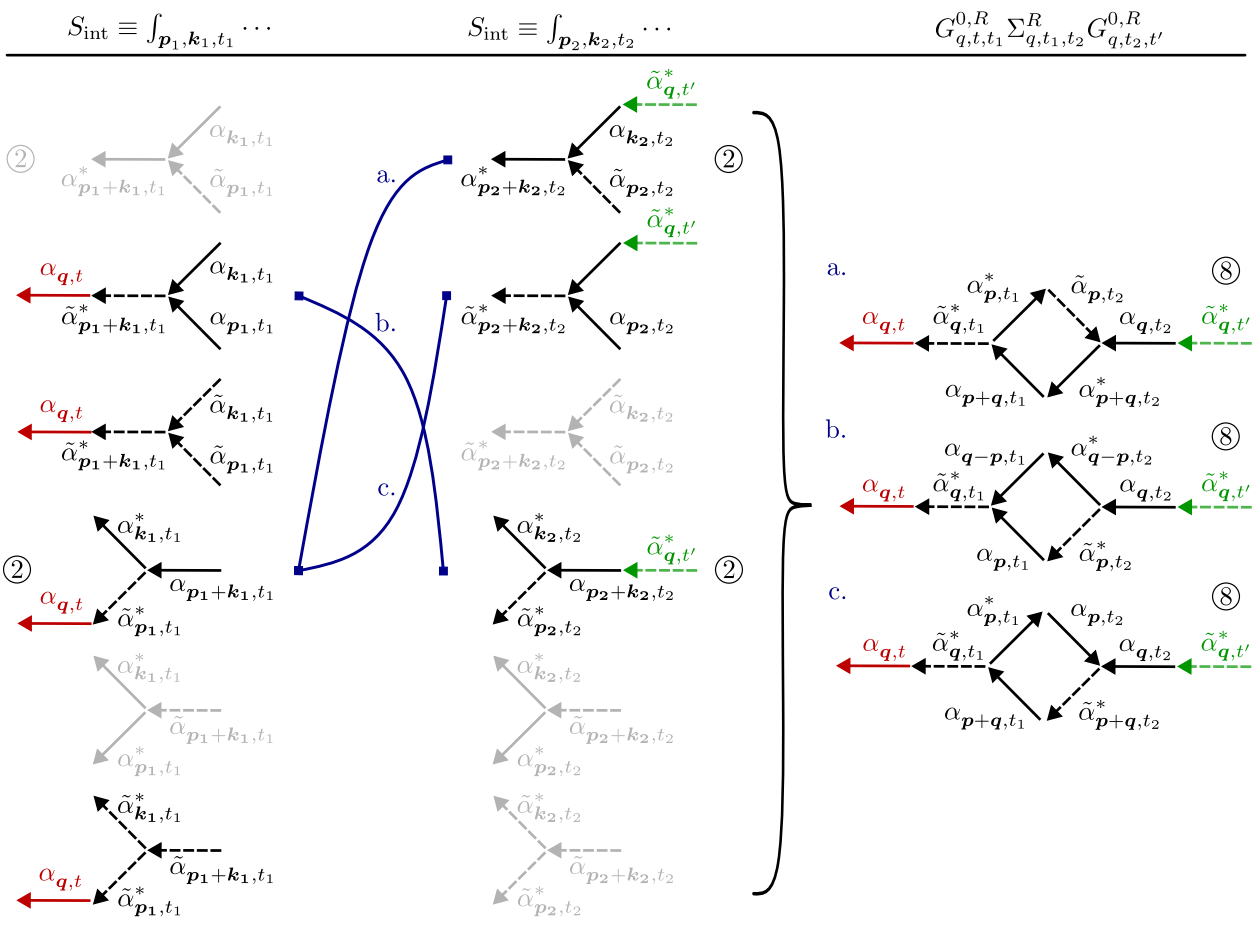

Figure 2.1: Wick-pairing procedure used to obtain the leading-order (one-loop) diagrams for the retarded self-energy Σ^R [Eq. (2.56)]. The left and central columns represent all the vertices of $S_{\rm int}$ at momenta $\boldsymbol{p}_1, \boldsymbol{k}_1$ and $\boldsymbol{p}_2, \boldsymbol{k}_2$ respectively. Calculation of Σ^R involves the Wick pairing of the two columns, with intermediate momenta $\boldsymbol{p}_i, \boldsymbol{k}_i$ to be integrated over. Shaded vertices cannot fulfill the condition on the self-energy "legs" (green and red arrows), required by Eq. (2.52), and must be discarded. The blue lines indicate the permitted diagram associations. The resulting three possible diagrams are shown in the rightmost column; energy conservation reduces integration variables as $\int_{\boldsymbol{p}_1,\boldsymbol{k}_1,\boldsymbol{p}_2,\boldsymbol{k}_2} \equiv \int_{\boldsymbol{p}}$. Multiplicities (circled numbers) arise from both coefficients in the action and other combinatorics factors, including the global exchange of variables $1 \leftrightarrow 2$. As an example, the multiplicity of the diagram labeled b can be analyzed as follows: a factor of 2 comes from the coefficient of $\tilde{\alpha}^*_{\boldsymbol{p}_2,t_2} \alpha^*_{\boldsymbol{k}_2,t_2} \alpha_{\boldsymbol{p}_2+\boldsymbol{k}_2,t_2}$ in the interacting action (to which corresponds a circled multiplicity in the middle column), another factor of 2 comes from the equivalent possibility of contracting $\alpha^*_{\boldsymbol{k}_2,t_2}$ with either $\alpha_{\boldsymbol{k}_1,t_1}$ or $\alpha_{\boldsymbol{p}_1,t_1}$, and the last factor of 2 comes from the global permutation of indices 1 and 2.

In Eq. (2.56), we have made the substitution $G^{0,K} \to G^K$, which amounts to a self-consistent approximation on the Keldysh Green function. Furthermore, one can check that $\Sigma^R_{\boldsymbol{q},t_1,t_2} \propto \theta(t_1 - t_2)$, which expresses causality. In the Wigner representation, this reads:

$$\Sigma^R_{\boldsymbol{q},\omega,\tau} = 2i \int_{\boldsymbol{p},\nu} \Big\{ \Lambda^2_{\boldsymbol{p},\boldsymbol{q}-\boldsymbol{p}} G^K_{\boldsymbol{p},\nu,\tau} G^{0,R}_{\boldsymbol{q}-\boldsymbol{p},\omega-\nu} + \Lambda^2_{\boldsymbol{p},\boldsymbol{q}} \left[G^K_{\boldsymbol{p},\nu} G^{0,R}_{\boldsymbol{p}+\boldsymbol{q},\omega+\nu} + G^K_{\boldsymbol{p}+\boldsymbol{q},\nu+\omega,\tau} G^{0,A}_{\boldsymbol{p},\nu} \right] \Big\}. \tag{2.57}$$

Next, we use that $G^{0,R}_{\boldsymbol{p},\nu} = -i\pi\delta(\nu - \epsilon_{\boldsymbol{p}})$, $G^{0,A}_{\boldsymbol{p},\nu} = i\pi\delta(\nu - \epsilon_{\boldsymbol{p}})$ and that similarly $G^K_{\boldsymbol{p},\tau,\nu} \simeq -2i\pi F_{\boldsymbol{p},\nu,\tau}\delta(\nu - \epsilon_{\boldsymbol{p}})$ [cf Eqs. (2.36, 2.37, 2.38)]; we multiply Eq. (2.57) by the spectral function $A_{\boldsymbol{q},\omega,\tau}$ and integrate over ω and ν using that the latter is peaked around $\omega \simeq \epsilon_{\boldsymbol{q}}$. This yields the on-shell self-energy

$$\Sigma^R_{\boldsymbol{q},\tau} \simeq -2i\pi \int_{\boldsymbol{p}} \Big[\Lambda^2_{\boldsymbol{p},\boldsymbol{q}} \left(F_{\boldsymbol{p},\tau} - F_{\boldsymbol{p}+\boldsymbol{q},\tau}\right) \delta(\epsilon_{\boldsymbol{q}} + \epsilon_{\boldsymbol{p}} - \epsilon_{\boldsymbol{p}+\boldsymbol{q}}) + \Lambda^2_{\boldsymbol{p},\boldsymbol{q}-\boldsymbol{p}} F_{\boldsymbol{p},\tau}\, \delta(\epsilon_{\boldsymbol{q}} - \epsilon_{\boldsymbol{p}} - \epsilon_{\boldsymbol{q}-\boldsymbol{p}}) \Big]. \tag{2.58}$$

For a purely phononic dispersion (1.12), the angular integration in Eq. (2.58) is divergent, cf. Appendix B for details. In two and three dimensions, this divergence is customarily regularized by taking into account the first nonlinear correction to the Bogoliubov dispersion: $\epsilon_{\boldsymbol{q}} \simeq c|\boldsymbol{q}| + (c\xi^2/2)|\boldsymbol{q}|^3$ [88, 93]. This is also the approach we adopt here. Note, however, that in strongly interacting one-dimensional gases, it has been proposed that the divergence should be instead resolved via a self-consistent Born approximation [95, 96]. This alternative regularization will be investigated in Sec. 3.2 of the next chapter.

Including the leading-order corrections to the linear dispersion and performing the angular integrations in Eq. (2.58) as detailed in Appendix B, we finally obtain

$$\Sigma^R_{\boldsymbol{q},\tau} = -\frac{i}{2} \int_0^\infty dp\, \mathcal{K}^L_{\boldsymbol{p},\boldsymbol{q}} (F_{\boldsymbol{p},\tau} - F_{\boldsymbol{p}+\boldsymbol{q},\tau}) - i \int_0^q dp\, \mathcal{K}^B_{\boldsymbol{p},\boldsymbol{q}} F_{\boldsymbol{q},\tau} \tag{2.59}$$

where

$$\mathcal{K}^L_{\boldsymbol{p},\boldsymbol{q}} = \frac{3\sqrt{3}c}{8\pi\rho_0} p(p+q), \quad \mathcal{K}^B_{\boldsymbol{p},\boldsymbol{q}} = \frac{3\sqrt{3}c}{16\pi\rho_0} p(q-p). \tag{2.60}$$

Keldysh sector We now come to the Keldysh self-energy Σ^K, which is calculated perturbatively from the Dyson equation (2.42). At the one-loop (Born) approximation, this is achieved by approximating the left-hand side by

$$G^K_{\boldsymbol{q},t,t'} \simeq -i \int \mathcal{D}[\alpha]\, \alpha_{\boldsymbol{q},t} \alpha^*_{\boldsymbol{q},t'} e^{iS_0} (1 - S^2_{\rm int}/2). \tag{2.61}$$

Evaluation of the Gaussian integral involves the six one-loop diagrams represented in Fig. 2.2:

$$\Sigma^K_{\boldsymbol{q},t_1,t_2} = i\int_{\boldsymbol{p}} \Big[2\Lambda^2_{\boldsymbol{p},\boldsymbol{q}} \Big(G^K_{\boldsymbol{p}+\boldsymbol{q},t_1,t_2} G^K_{\boldsymbol{p},t_2,t_1} + G^{0,A}_{\boldsymbol{p},t_2,t_1} G^{0,R}_{\boldsymbol{p}+\boldsymbol{q},t_1,t_2} + G^{0,R}_{\boldsymbol{p},t_2,t_1} G^{0,A}_{\boldsymbol{p}+\boldsymbol{q},t_1,t_2} \Big) + \Lambda^2_{\boldsymbol{p},\boldsymbol{q}-\boldsymbol{p}} \Big(G^K_{\boldsymbol{q}-\boldsymbol{p},t_1,t_2} G^K_{\boldsymbol{p},t_1,t_2} + G^{0,A}_{\boldsymbol{q}-\boldsymbol{p},t_1,t_2} G^{0,A}_{\boldsymbol{p},t_1,t_2} + G^{0,R}_{\boldsymbol{q}-\boldsymbol{p},t_1,t_2} G^{0,R}_{\boldsymbol{p},t_1,t_2} \Big) \Big]. \tag{2.62}$$

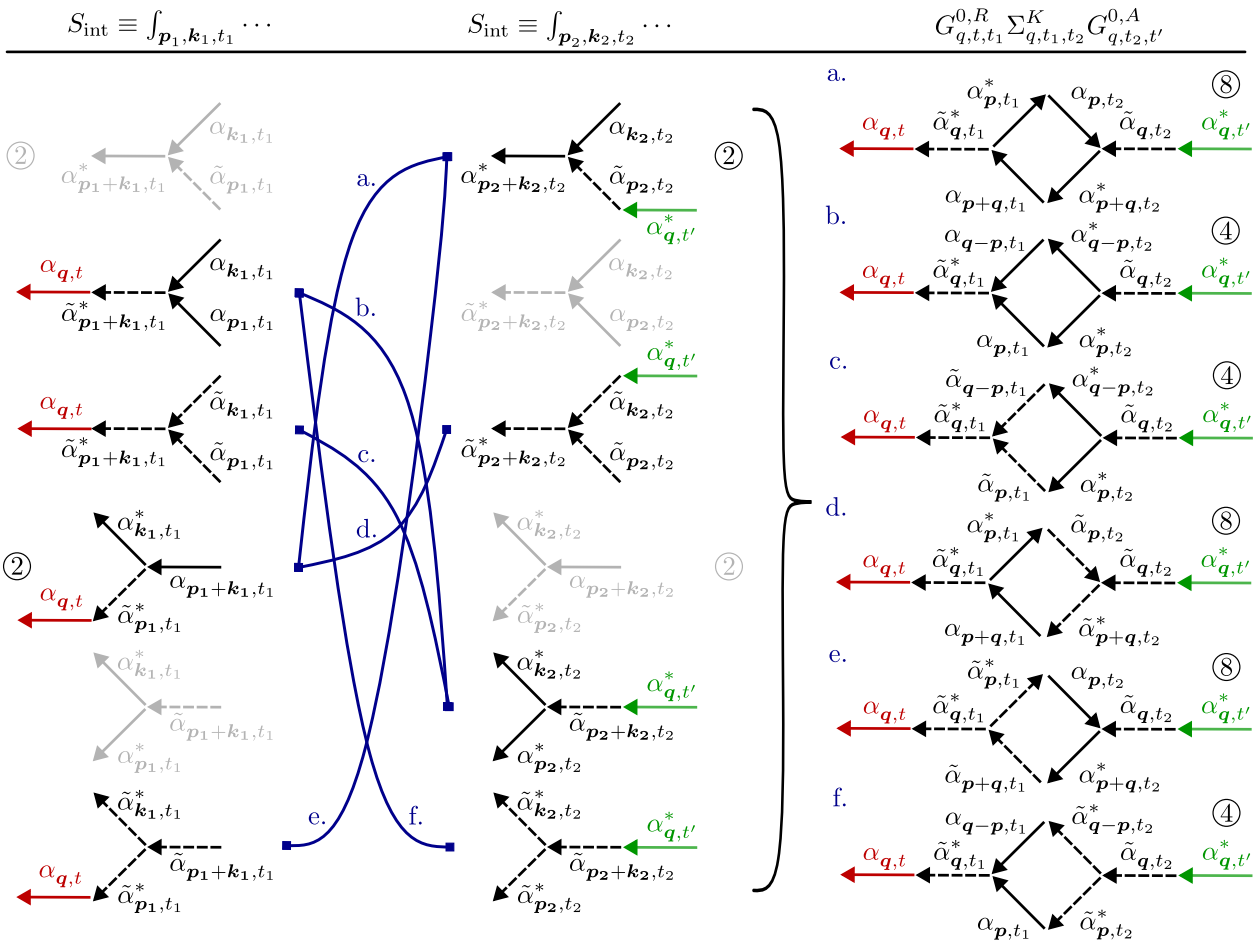

Figure 2.2: Diagrams contributing to the Keldysh self-energy Σ^K [Eq. (2.62)]. The six possible associations are represented in the rightmost column, following the same rules used in Fig. 2.1.

To evaluate this expression, we proceed as for Σ^R, namely, we move to Wigner representation, multiply Eq. (2.62) by the spectral function and integrate over

Wigner frequencies. This leads to the on-shell value

$$\Sigma^K_{\boldsymbol{q},\tau} = -2i\pi \int_{\boldsymbol{p}} \Big[2\Lambda^2_{\boldsymbol{p},\boldsymbol{q}} \, (F_{\boldsymbol{p}+\boldsymbol{q}} F_{\boldsymbol{p}} - 1) \, \delta(\epsilon_{\boldsymbol{q}} + \epsilon_{\boldsymbol{p}} - \epsilon_{\boldsymbol{p}+\boldsymbol{q}}) + \Lambda^2_{\boldsymbol{p},\boldsymbol{q}-\boldsymbol{p}} \, (F_{\boldsymbol{q}-\boldsymbol{p}} F_{\boldsymbol{p}} + 1) \, \delta(\epsilon_{\boldsymbol{q}} - \epsilon_{\boldsymbol{p}} - \epsilon_{\boldsymbol{q}-\boldsymbol{p}}) \Big]. \tag{2.63}$$

By finally computing the angular integration using the regularization procedure explained in Appendix B, we find:

$$\Sigma^K_{\boldsymbol{q},\tau} = -i \int_0^\infty dp \, \mathcal{K}^L_{\boldsymbol{p},\boldsymbol{q}} \, (F_{\boldsymbol{p}+\boldsymbol{q},\tau} F_{\boldsymbol{p},\tau} - 1) - i \int_0^q dp \, \mathcal{K}^B_{\boldsymbol{p},\boldsymbol{q}} \, (F_{\boldsymbol{q}-\boldsymbol{p},\tau} F_{\boldsymbol{p},\tau} + 1) \, . \tag{2.64}$$

Eqs. (2.59) and (2.64) constitute the final expressions for the normal self-energies, which once inserted in Eq. (2.51) provide a kinetic equation for the momentum distribution $n_{\boldsymbol{q},\tau}$. Before coming to that point, however, we now discuss the perturbation theory for the anomalous distribution.

2.2.4 Anomalous momentum distribution

In order to derive a quantum kinetic equation for the anomalous phonon distribution $m_{\boldsymbol{q},\tau}$, one is naturally led to define a Keldysh Green's function from the anomalous anti-commutator $\langle\{\hat{a}_{\boldsymbol{q},t}, \hat{a}_{-\boldsymbol{q},t'}\}\rangle$, in analogy with Eq. (2.32). Such a definition, however, gives rise to fast temporal oscillations at the scale of $1/\epsilon_{\boldsymbol{q}}$, which are incompatible with the requirement of time scales separation discussed in Sec. 2.2.2. This can already be seen at the level of the free-field theory, which yields $\langle\{\hat{a}_{\boldsymbol{q},t}, \hat{a}_{-\boldsymbol{q},t'}\}\rangle = 2\langle \hat{a}_{\boldsymbol{q},0}\hat{a}_{-\boldsymbol{q},0}\rangle \exp(-2i\epsilon_{\boldsymbol{q}}\tau)$, where $\tau = (t+t')/2$. To get rid of these fast variations, we move to the rotating time frame by employing the transformation $\alpha_{\boldsymbol{q},t} \to \alpha_{\boldsymbol{q},t} \exp(i\epsilon_{\boldsymbol{q}} t)$, following [96, 141]. In this rotating frame, we can now safely define the anomalous Keldysh Green's function as

$$i\mathscr{G}^K_{\boldsymbol{q},t,t'} = \langle\{\hat{a}_{\boldsymbol{q},t}, \hat{a}_{-\boldsymbol{q},t'}\}\rangle = \langle \alpha_{\boldsymbol{q},t}\alpha_{-\boldsymbol{q},t'}\rangle. \tag{2.65}$$

From its definition (2.19), the anomalous momentum distribution follows from $2m_{\boldsymbol{q},t} = i\mathscr{G}^K_{\boldsymbol{q},t,t}$. It should be noted that the quantity $\langle\{\hat{a}_{\boldsymbol{q},t}, \hat{a}_{-\boldsymbol{q},t'}\}\rangle$ is *a priori* a complex number, even after moving to the rotating time frame. However, in the present work we always consider initial states such that $i\mathscr{G}^K_{\boldsymbol{q},t,t}$ is real, cf., e.g., Eq. (3.3). In the general case, one should define the anomalous Keldysh Green function as a matrix in Nambu space to ensure the anti-hermiticity of $\mathscr{G}^K$, as presented in Ref. [96]. Here, we have chosen to keep the theory as simple as possible, working with scalars rather than matrices, and using calligraphic letters to refer to anomalous Green's functions.

In the presence of phonon interactions, $\mathscr{G}^K$ acquires a finite (anomalous) self-energy $\mathscr{S}^K$, defined through a Dyson equation similar to Eq. (2.42):

$$\mathcal{G}^K = G^R \circ \mathscr{S}^K \circ G^A. \tag{2.66}$$

In the rotating frame, $\mathscr{G}^K$ is also anti-hermitian, and can therefore be parameterized in a similar manner as G^K [see Eq. (2.43)]:

$$\mathscr{G}^K = G^R \circ \mathscr{F} - \mathscr{F} \circ G^A. \tag{2.67}$$

Combining the four relations (2.40), (2.41), (2.66) and (2.67) and making use of the condition of time scales separation, as explained in Sec. 2.2.2, we infer the anomalous version of the on-shell kinetic equation (2.51):

$$\partial_\tau \mathscr{F}_{\boldsymbol{q},\tau} \simeq i\mathscr{S}^K_{\boldsymbol{q},\tau} + 2\mathscr{F}_{\boldsymbol{q},\tau}\mathrm{Im}(\Sigma^R_{\boldsymbol{q},\tau}). \tag{2.68}$$

As compared to Eq. (2.51), the difference lies in the anomalous Keldysh self-energy $\mathscr{S}^K_{\boldsymbol{q},\tau}$, which can be computed by perturbation theory from Eq. (2.66). Similarly to the normal correlator, this is done by approximating the left-hand side of Eq. (2.66) by

$$\mathcal{G}^K_{\boldsymbol{q},t,t'} \simeq -i \int \mathcal{D}[\alpha]\, \alpha_{\boldsymbol{q},t}\alpha_{-\boldsymbol{q},t'} e^{iS_0}(1 - S^2_{\mathrm{int}}/2). \tag{2.69}$$

It should be noted that, unlike the calculation of Σ^K, here the Wick decomposition resulting from the Gaussian integral (2.53) takes into account only pairings of anomalous correlators, which is a consequence of the linear-resonant character of the interaction, see [96] for details. This leads to the two self-energy diagrams displayed in Fig. 2.3, which explicitly read:

$$\mathscr{S}^K_{\boldsymbol{q},t,t'} = i\int_{\boldsymbol{p}} [2\Lambda^2_{\boldsymbol{p},\boldsymbol{q}}\, \mathscr{G}^K_{\boldsymbol{p}+\boldsymbol{q},t,t'}\mathscr{G}^K_{\boldsymbol{p},t',t} + \Lambda^2_{\boldsymbol{p},\boldsymbol{q}-\boldsymbol{p}}\, \mathscr{G}^K_{\boldsymbol{p},t,t'}\mathscr{G}^K_{\boldsymbol{q}-\boldsymbol{p},t,t'}]. \tag{2.70}$$

We then proceed as in Sec. 2.2.3, i.e., we compute the Wigner transform of $\mathscr{S}^K_{\boldsymbol{q},t,t'}$, multiply by the spectral function and integrate over Wigner frequencies. This eventually yields

$$\mathscr{S}^K_{\boldsymbol{q},\tau} = -i\int_0^\infty dp \mathcal{K}^L_{\boldsymbol{p},\boldsymbol{q}} \mathscr{F}_{\boldsymbol{p}+\boldsymbol{q},\tau}\mathscr{F}_{\boldsymbol{p},\tau} - i\int_0^q dp\, \mathcal{K}^B_{\boldsymbol{p},\boldsymbol{q}} \mathscr{F}_{\boldsymbol{q}-\boldsymbol{p},\tau}\mathscr{F}_{\boldsymbol{p},\tau}. \tag{2.71}$$

Once inserted in (2.68), this provides an explicit expression for the kinetic equation for $m_{\boldsymbol{q},\tau}$.

2.3 Phonon quantum kinetics

2.3.1 Kinetic equations

Inserting the expressions (2.59) and (2.64) of the normal self-energies into Eq. (2.51) and using Eq. (2.50), we obtain the final form of the kinetic equation for the phonon momentum distribution $n_{\boldsymbol{q},\tau}$ at the one-loop approximation:

$$\begin{aligned}\partial_\tau n_{\boldsymbol{q},\tau} = {} & 2\int_0^\infty dp\, \mathcal{K}^L_{\boldsymbol{p},\boldsymbol{q}} \left[n_{\boldsymbol{p}+\boldsymbol{q}}\,(n_{\boldsymbol{p}}+n_{\boldsymbol{q}}+1) - n_{\boldsymbol{p}}n_{\boldsymbol{q}}\right] + \\ & 2\int_0^q dp\, \mathcal{K}^B_{\boldsymbol{p},\boldsymbol{q}} \left[n_{\boldsymbol{p}}n_{\boldsymbol{q}-\boldsymbol{p}} - n_{\boldsymbol{q}}\,(n_{\boldsymbol{p}}+n_{\boldsymbol{q}-\boldsymbol{p}}+1)\right],\end{aligned} \tag{2.72}$$

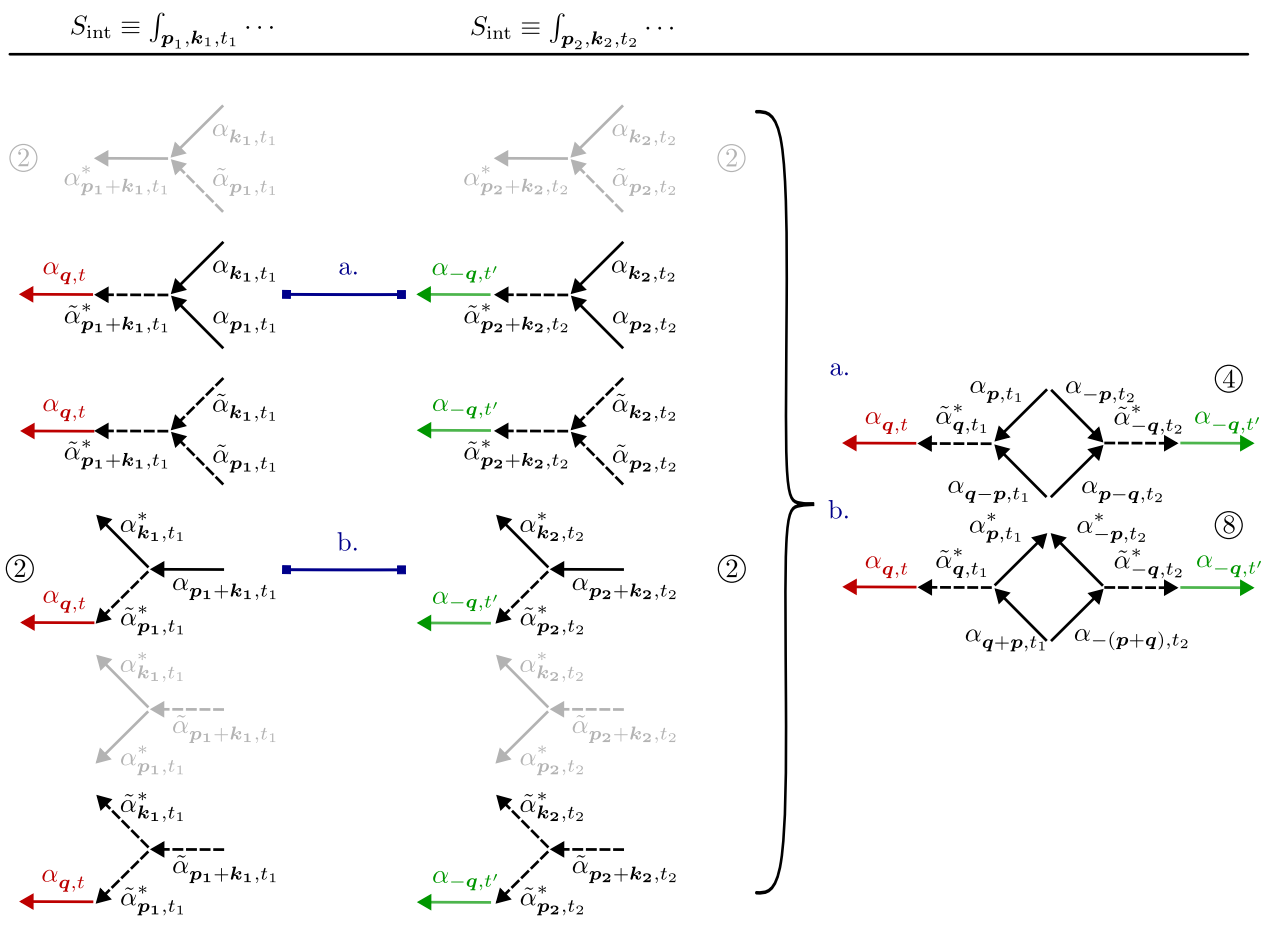

Figure 2.3: Diagrams contributing to the anomalous Keldysh self-energy $\mathscr{S}^K$ [Eq. (2.70)]. The two possible associations are represented in the rightmost column, following the same rules used in Fig. 2.1.

where for notation simplicity we have dropped the τ indices in the collision integrals, and we recall that the kernels $\mathcal{K}^L_{\boldsymbol{p},\boldsymbol{q}}$ and $\mathcal{K}^B_{\boldsymbol{p},\boldsymbol{q}}$ are given by Eq. (2.60). The only quantity conserved during the time evolution pertained to Eq. (2.72) is the (phononic) energy: $\partial_\tau \int_{\boldsymbol{q}} c|\boldsymbol{q}| n_{\boldsymbol{q},\tau} = 0$ for all τ. The kinetic equation includes two collision integrals, which correspond to the well-known Beliaev (B) and Landau (L) three-particle scattering processes. The Beliaev process describes the splitting $q \to (p, q-p)$ of the probe phonon of momentum q into two phonons of momenta p and $q-p$, while the Landau process describes the recombination $(q,p) \to p+q$ of the probe phonon with another one, each process coming together with its reversed version. Both Landau and Beliaev processes yield a relaxation of the momentum distribution toward a thermal equilibrium at long time:

$$n_{\boldsymbol{q},\tau\to\infty} \equiv n^{\text{th}}_{\boldsymbol{q}} = \frac{1}{\exp(\epsilon_{\boldsymbol{q}}/T) - 1}, \tag{2.73}$$

a solution which cancels both collision integrals in Eq. (2.72). In the present nonequilibrium scenario, the temperature T characterizes the effective thermal equilibrium reached by the phonon gas at late times. In practice, this temperature is determined from the law of energy conservation mentioned above. A concrete example of this will be given in Sec. 3.1. Finally, note that Eq. (2.72) is equivalent to the Fermi Golden Rule combined with the detailed balance principle, cf. Eq. (1.23).

The kinetic equation for the anomalous phonon distribution is similarly derived, by inserting Eq. (2.59) and (2.71) into Eq. (2.68):

$$\begin{aligned}\partial_\tau m_{\boldsymbol{q},\tau} = 2\int_0^\infty dp\, \mathcal{K}^L_{\boldsymbol{p},\boldsymbol{q}} \left(n_{\boldsymbol{p}+\boldsymbol{q}} m_{\boldsymbol{q}} + m_{\boldsymbol{p}} m_{\boldsymbol{p}+\boldsymbol{q}} - n_{\boldsymbol{p}} m_{\boldsymbol{q}}\right) + \\ 2\int_0^q dp\, \mathcal{K}^B_{\boldsymbol{p},\boldsymbol{q}} \left[m_{\boldsymbol{p}} m_{\boldsymbol{q}-\boldsymbol{p}} - m_{\boldsymbol{q}} \left(n_{\boldsymbol{p}} + n_{\boldsymbol{q}-\boldsymbol{p}} + 1\right)\right].\end{aligned} \tag{2.74}$$

Notice that the dynamics of the anomalous distribution is coupled to the evolution of $n_{\boldsymbol{q}}$. Furthermore, unlike $n_{\boldsymbol{q}}$ the anomalous distribution vanishes at long time:

$$m_{\boldsymbol{q},\tau\to\infty} = 0, \tag{2.75}$$

a result expected for a quantum gas at thermal equilibrium. At any finite time, however, $m_{\boldsymbol{q}}$ is in general nonzero and may significantly impact the intermediate-time dynamics of physical observables.

2.3.2 Near-equilibrium solutions

Before examining the consequences of the phonon relaxation on a concrete scenario, it is useful to discuss the near-equilibrium case, which typically corresponds to the long-time regime where the distributions $m_{\boldsymbol{q},\tau}$ and $n_{\boldsymbol{q},\tau}$ become close to their equilibrium values (2.73) and (2.75). To this aim, we substitute $n_{\boldsymbol{q},\tau} = n^{\text{th}}_{\boldsymbol{q}} + \delta n_{\boldsymbol{q},\tau}$

with $\delta n_{\boldsymbol{q},\tau} \ll n^{\rm th}_{\boldsymbol{q}}$ in the kinetic equation (2.72) and linearize. If only the Beliaev collision integral is kept, this leads to

$$\partial_\tau \delta n_{\boldsymbol{q},\tau} \simeq -2\gamma^B_{\boldsymbol{q}} \delta n_{\boldsymbol{q},\tau}, \quad \gamma^B_{\boldsymbol{q}} = \frac{\sqrt{3}c}{32\pi\rho_0} q^3. \tag{2.76}$$

This describes an exponential relaxation governed by the Beliaev damping rate $\gamma^B_{\boldsymbol{q}}$. Note that, alternatively, the latter could have been directly derived from the self-energy (2.59) evaluated at equilibrium: $\gamma^B_{\boldsymbol{q}} = -{\rm Im}\Sigma^R_{\boldsymbol{q}}(n^{\rm th}_{\boldsymbol{q}})$. In two dimensions, the Beliaev damping rate (2.76) has been previously derived in [88, 142] using Matsubara formalism.

If, on the other hand, only the Landau collision integral in Eq. (2.72) is considered, the linearization procedure provides

$$\partial_\tau \delta n_{\boldsymbol{q},\tau} \simeq -2\gamma^L_{\boldsymbol{q}} \delta n_{\boldsymbol{q},\tau}, \quad \gamma^L_{\boldsymbol{q}} = \frac{\sqrt{3}\pi}{8\rho_0 c} q T^2, \tag{2.77}$$

which now involves the Landau damping rate $\gamma^L_{\boldsymbol{q}}$ [88]. Comparison of Eqs. (2.76) and (2.77) shows that Beliaev processes are mostly effective when the long-time equilibrium temperature vanishes. Landau processes, on the contrary, typically dominate at finite temperature. In the relaxation following a quantum quench (see next chapter), this is the most common situation since a brutal quench at $t = 0$ naturally injects a certain amount of energy into the system, eventually leading to a finite-temperature state at long time.

A near-equilibrium expansion, finally, can also be used for the anomalous momentum distribution, using that $m_{\boldsymbol{q}} \ll 1$ at long time. Expanding Eq. (2.74) for small $\delta n_{\boldsymbol{q}}$ and small $m_{\boldsymbol{q}}$ then yields

$$\partial_\tau m_{\boldsymbol{q},\tau} \simeq -2\gamma^{L,B}_{\boldsymbol{q}} m_{\boldsymbol{q},\tau}, \tag{2.78}$$

depending on which of the Beliaev or Landau processes dominates.

2.3.3 Classical-statistical limit

In the context of optics, a number of experiments involving "fluids of light" [109, 143] have emerged in recent years, in particular in cavityless, nonlinear materials where the propagation of a laser mimics the out-of-equilibrium dynamics of 2D dilute ultracold Bose gases [68, 144–147]. At leading order, these experiments are well-described by classical-statistical field theory, where quantum fluctuations are negligible but the initial state is defined statistically (see Sec. 1.3.2). It is therefore interesting to ask how to adapt the results of Sec. 2.3.1 to this setting. Another motivation for studying the classical limit is that it can be readily checked numerically, since in that limit the field theory becomes equivalent to the Gross-Pitaevskii equation with a random initial state.

The appropriate framework to construct a path integral formulation of the nonequilibrium dynamics of classical systems with stochastic initial states can be found in, e.g., Refs. [134, 148–150]. It is a particular case of the Martin–Siggia–Rose path integral approach of stochastic differential equations [90, 151, 152], and is very similar to the theory presented in Sec. 2.1, although it does not use a mixed state or a closed contour, which are specific features of quantum systems. Instead, one should construct a field theory from the classical evolution in phase space. This leads to a nonequilibrium action $S_{\rm cl}$ analogous to the Keldysh actions (2.15) and (2.17). In detail, $S_{\rm cl}$ can be written as $S_{\rm cl}[\alpha,\tilde{\alpha}] = S_0 + S_{\rm int}^{\rm cl}$, where S_0 is still given by Eq. (2.15), but the interaction part of the action reads

$$S_{\rm int}^{\rm cl} = \int_{\boldsymbol{p},\boldsymbol{q},t} \Lambda_{\boldsymbol{p},\boldsymbol{q}} (2\alpha^*_{\boldsymbol{p}+\boldsymbol{q},t}\tilde{\alpha}_{\boldsymbol{p},t}\alpha_{\boldsymbol{q},t} + \tilde{\alpha}^*_{\boldsymbol{p}+\boldsymbol{q},t}\alpha_{\boldsymbol{p},t}\alpha_{\boldsymbol{q},t} + \text{c.c.}). \tag{2.79}$$

Therefore, the main difference between the quantum and classical field theories is the presence of vertices of order $\tilde{\alpha}^3$ in the quantum case [cf. Eq. (2.17)]. In fact, this close connection also constitutes another motivation for performing the Keldysh rotation, since the latter brings the quantum field theory in a form that can be compared with the classical-statistical theory. It also justifies the terminology of "classical" and "quantum" fields respectively used for α and $\tilde{\alpha}$.

The perturbation theory presented in Sec. (2.2) is essentially unchanged in the classical-statistical case. The retarded self-energy Σ^R remains the same because the diagrams of Fig. 2.1 do not involve the triple quantum field vertices. However, Σ^K is modified: the diagrams c-d-e-f drawn in Fig. 2.2 are not involved in the classical field theory. These diagrams are responsible for the terms ± 1 in the kinetic equation (2.63). Furthermore, using that, classically, the on-shell distribution function is simply $F_{\boldsymbol{q}} \simeq n_q$, one eventually finds that the phonon momentum distribution evolves according to

$$\begin{aligned}\partial_\tau n_{\boldsymbol{q},\tau} = {} & 2\int_0^\infty dp\, \mathcal{K}^L_{\boldsymbol{p},\boldsymbol{q}} \left[n_{\boldsymbol{p}+\boldsymbol{q}}\,(n_{\boldsymbol{p}}+n_{\boldsymbol{q}}) - n_{\boldsymbol{p}} n_{\boldsymbol{q}}\right] + \\ & 2\int_0^q dp\, \mathcal{K}^B_{\boldsymbol{p},\boldsymbol{q}} \left[n_{\boldsymbol{p}} n_{\boldsymbol{q}-\boldsymbol{p}} - n_{\boldsymbol{q}}\,(n_{\boldsymbol{p}}+n_{\boldsymbol{q}-\boldsymbol{p}})\right].\end{aligned} \tag{2.80}$$

This could have been deduced directly with Eq. (2.72) by using that the large occupation case $n_{\boldsymbol{q}} \gg 1$ represents the classical limit of the quantum field theory. The momentum distribution that cancels the collision integral (2.80) is now the Rayleigh-Jeans distribution $n_{\boldsymbol{q}} = T/\epsilon_{\boldsymbol{q}}$. Note that this distribution suffers from the well-known ultraviolet catastrophe, namely it is neither normalizable nor admit a second moment [90]. In practice, the quantitative description of thermalization in classical-field systems thus requires the introduction of a ultraviolet cutoff. This cutoff is typically introduced in realistic physical scenarios, such as multimode optical fibers [153].

Finally, let us mention that, in the classical-statistical limit, the anomalous kinetic equation (2.74) is modified similarly to Eq. (2.80): the approximation $n_{\boldsymbol{p}}+$

$n_{\boldsymbol{q}-\boldsymbol{p}}+1 \simeq n_{\boldsymbol{p}}+n_{\boldsymbol{q}-\boldsymbol{p}}$ can be introduced, as well as an ultraviolet cutoff to regularize the integrals.

Conclusion

We have presented a general field-theoretical framework for studying the many-body nonequilibrium dynamics of 2D dilute Bose superfluids. The approach is based on a low-energy quantum hydrodynamic framework, and assumes that the time scales associated with the coherent dynamics of the Bogoliubov phonons and with their three-particle interaction processes are well separated. Under this condition, we were able to fully describe the time evolution of the phonon normal and anomalous momentum distributions, from the coherent regime to the final thermalization stage.

Chapter 3

Applications of the quantum kinetic theory: quench dynamics and self-consistent approach

In the previous chapter, we have derived quantum kinetic equations describing the nonequilibrium evolution of 2D uniform Bose superfluids starting from a Gaussian initial density matrix. Here, we apply this formalism to a concrete example, a quench of the interaction strength in a 2D superfluid, and analyze the subsequent time evolution of two observables, the structure factor and the spatial coherence function, recently measured in cold-atom [44] and optical-fluid [68, 147] experiments. Our approach, in particular, includes recent developments [154] allowing for a proper treatment of the finite quench duration, crucial to avoid unphysical divergences of the post-quench superfluid's energy. Eventually, it provides a consistent and unified theoretical description of the dynamics of 2D superfluids, from the short-time coherent regime to the long-time thermalization.

Next, in Sec. 3.2, we extend the perturbation theory presented in Chapter 2 to a self-consistent treatment, where the free propagators are replaced by their dressed counterparts. Focusing on the near-equilibrium case, we then explore the possibility of a regime where the perturbative approach may not be sufficient. In particular, our analysis reveals the existence of an "anomalous" Landau damping rate in the infrared region, where the quasiparticles exhibit significantly longer relaxation times than predicted by the perturbative calculation. Following an argument developed in Refs. [150, 155–158], we attribute this deviation to multiple scatterings caused by the high occupancy of the distribution function in the infrared limit $q \to 0$.

3.1 Nonequilibrium structure factor and coherence

3.1.1 Quench protocol

From now on, we consider a uniform two-dimensional Bose gas initially at equilibrium at temperature T_0 in a superfluid state with interaction strength g_0. The initial (pre-quench) quasiparticle distributions are thus given by

$$n^0_{\boldsymbol{q}} = \frac{1}{\exp(\epsilon^0_{\boldsymbol{q}}/T_0) - 1}, \quad m^0_{\boldsymbol{q}} = 0, \tag{3.1}$$

where $\epsilon^0_{\boldsymbol{q}} = \sqrt{E_{\boldsymbol{q}}(E_{\boldsymbol{q}} + 2g_0\rho_0)}$, with $E_{\boldsymbol{q}} = \boldsymbol{q}^2/2m$. As a quench protocol, we suppose that around the time $\tau = 0$ the interaction strength is changed from $g_0 > 0$ to another positive value $g \neq g_0$. The simplest description of this problem, studied, e.g., in [102, 154], consists in assuming that the interaction change occurs *instantaneously* at $\tau = 0$. In that case, applying the Bogoliubov transformation (1.9) at both $\tau = 0^-$ and $\tau = 0^+$ and using the continuity of the field operator (1.5), we obtain the following relation between the post-quench $(\hat{a}^{\rm ps}_{\boldsymbol{q}}, \hat{a}^{\rm ps\dagger}_{\boldsymbol{q}})$ and pre-quench $(\hat{a}^0_{\boldsymbol{q}}, \hat{a}^{0\dagger}_{\boldsymbol{q}})$ Bogoliubov operators:

$$\begin{pmatrix} \hat{a}^{\rm ps\dagger}_{\boldsymbol{q}} \\ \hat{a}^{\rm ps}_{-\boldsymbol{q}} \end{pmatrix} = \frac{1}{2\sqrt{\epsilon_{\boldsymbol{q}}\epsilon^0_{\boldsymbol{q}}}} \begin{pmatrix} \epsilon_{\boldsymbol{q}} + \epsilon^0_{\boldsymbol{q}} & \epsilon_{\boldsymbol{q}} - \epsilon^0_{\boldsymbol{q}} \\ \epsilon_{\boldsymbol{q}} - \epsilon^0_{\boldsymbol{q}} & \epsilon_{\boldsymbol{q}} + \epsilon^0_{\boldsymbol{q}} \end{pmatrix} \begin{pmatrix} \hat{a}^{0\dagger}_{\boldsymbol{q}} \\ \hat{a}^0_{-\boldsymbol{q}} \end{pmatrix}.$$

where $\epsilon_{\boldsymbol{q}} = \sqrt{E_{\boldsymbol{q}}(E_{\boldsymbol{q}} + 2g\rho_0)}$. The post-quench normal and anomalous momentum distributions then take the form

$$n^{\rm ps}_{\boldsymbol{q}} = n^0_{\boldsymbol{q}}\left(2d^2_{\boldsymbol{q}} + 1\right) + d^2_{\boldsymbol{q}}, \tag{3.2}$$

$$m^{\rm ps}_{\boldsymbol{q}} = \sqrt{d^2_{\boldsymbol{q}} + d^4_{\boldsymbol{q}}}\left(2n^0_{\boldsymbol{q}} + 1\right), \tag{3.3}$$

with $d_{\boldsymbol{q}} \equiv (\epsilon_{\boldsymbol{q}} - \epsilon^0_{\boldsymbol{q}})/(2\sqrt{\epsilon_{\boldsymbol{q}}\epsilon^0_{\boldsymbol{q}}})$. At this stage, it is instructive to examine the large-$|\boldsymbol{q}|$ asymptotics of this post-quench solution: for $q\xi \gg 1$, Eq. (3.2) leads to $n^{\rm ps}_{\boldsymbol{q}} \simeq [m\rho_0(g - g_0)]^2/q^4$. An instantaneous interaction quench thus turns the pre-quench exponential decay (3.1) into an algebraic one, provoking a logarithmic divergence of the total energy $\int_{\boldsymbol{q}} \epsilon_{\boldsymbol{q}} n^{\rm ps}_{\boldsymbol{q}}$ of the system after the quench. This underlines the somewhat pathological character of the instantaneous quench for a quantum gas, which needs to be regularized by including a finite switch-on time τ_s. Note that a similar divergence occurs in the problem of Tan's contact in Bose gases, originating from the zero-range character of the contact interaction [65, 159].

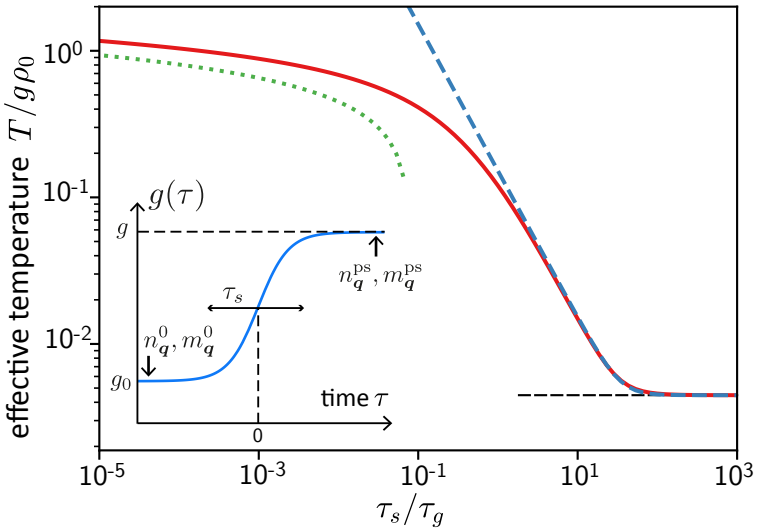

Figure 3.1: Inset: Sketch of the Wood-Saxon function modeling an interaction quench of finite duration, with the asymptotic limits $g(-\infty) = g_0$ and $g(\infty) = g$. Main panel: effective equilibrium temperature reached by the Bose gas a long time after the quench as a function of the quench duration τ_s [expressed in units of $\tau_g = 1/(g\rho_0)$]. The dotted and dashed curves show the asymptotic limits of the temperature for fast and slow quenches, Eqs. (3.11) and (3.12), respectively. Parameters are set to $g_0\rho_0 = 0.1$, $g\rho_0 = 0.5$, $T_0/g_0\rho_0 = 0.01$, $\rho_0\xi^2 \simeq 0.5$.

To overcome the ultraviolet divergence resulting from an instantaneous interaction quench, we rather consider the smooth Wood-Saxon quench $g(\tau) = g + (g_0 - g)/(1 + e^{\tau/\tau_s})$ [160], which was revisited recently in [154] and is sketched in the inset of Fig. 3.1. For this model, Eqs. (3.2) and (3.3) still hold but $n^0_{\boldsymbol{q}}$ ($m^0_{\boldsymbol{q}}$) and $n^{\rm ps}_{\boldsymbol{q}}$ ($m^{\rm ps}_{\boldsymbol{q}}$) should now be understood as the (anomalous) momentum distributions a long time $|\tau| \gg \tau_s$ before and after the interaction jump, respectively, and $d^2_{\boldsymbol{q}}$ is now given by [154]

$$d^2_{\boldsymbol{q}} = \frac{\sinh^2\left[\pi(\epsilon_{\boldsymbol{q}} - \epsilon^0_{\boldsymbol{q}})\tau_s\right]}{\sinh(2\pi\epsilon^0_{\boldsymbol{q}}\tau_s)\sinh(2\pi\epsilon_{\boldsymbol{q}}\tau_s)}. \tag{3.4}$$

At low momentum, the post-quench momentum distribution obeys the asymptotic law

$$n^{\rm ps}_{\boldsymbol{q}} \simeq \frac{T_0}{q}\frac{c^2 + c_0^2}{2cc_0^2}, \tag{3.5}$$

which involves the pre-quench $c_0 = \sqrt{g_0\rho_0/m}$ and post-quench $c = \sqrt{g\rho_0/m}$ speeds of sound. At large momentum, on the other hand, we have

$$n^{\rm ps}_{\boldsymbol{q}} \propto \exp(-2\pi\tau_s\boldsymbol{q}^2/m). \tag{3.6}$$

This asymptotic law is similar to that to the pre-quench thermal distribution, $n^0_{\boldsymbol{q}} \sim \exp[-\boldsymbol{q}^2/(2mT_0)]$, except that the inverse of the quench duration $1/\tau_s$ now takes the role of the pre-quench equilibrium temperature.

3.1.2 Momentum distributions and thermalization

Using the post-quench distributions (3.2) and (3.3) as initial conditions, we have performed numerical simulations of the kinetic equations (2.72) and (2.74). To do this, we used a logarithmically-scaled momentum axis with typically $N_p \sim 2^{11}$ points covering around ~ 10 orders of magnitude of $q\xi$. The time evolution was performed by a Runge-Kutta algorithm with time increment $\Delta t \sim 1/10$. We have verified that the energy is conserved during the evolution to an accuracy of at least $\sim 10^{-3}$, and we have adjusted the precise choice of N_p and h according to this requirement.

The resulting distributions $n_{\boldsymbol{q},\tau}$ and $m_{\boldsymbol{q},\tau}$ are shown in Fig. 3.2 for different times. As expected, we find that $n_{\boldsymbol{q},\tau}$ slowly evolves toward a thermal distribution of the form (2.73) at long time. Similarly, $m_{\boldsymbol{q},\tau}$ converges to zero, with the region where $m_{\boldsymbol{q},\tau}$ is nonzero shrinking to smaller and smaller $q-$values as time grows. For these simulations, we use as the unit time the Landau relaxation time (2.77) evaluated at the healing length $\xi = \sqrt{1/(4g\rho_0 m)}$:

$$\tau_\ell \equiv \frac{1}{2\gamma^L_{q=1/\xi}} = \frac{8}{\sqrt{3}\pi}\rho_0\xi^2\frac{g\rho_0}{T^2}, \tag{3.7}$$

where T is the final equilibration temperature. In order for the kinetic approach presented in Sec. 2.2 to be valid, the separation of time scale (2.46) should be verified, namely τ_ℓ should be large compared to the fast time scale $\tau_g \sim 1/(c|\boldsymbol{q}|)$ that governs the coherent dynamics of the Bogoliubov phonons. Evaluated at $q = 1/\xi$, the latter defines a "nonlinear time" that is sometimes used as a time scale in experiments [143]:

$$\tau_g \sim \frac{\xi}{c} \sim \frac{1}{g\rho_0} \ll \tau_\ell. \tag{3.8}$$

From the definition (3.7) of τ_ℓ, we find that, in practice, this inequality holds as long as the long-time equilibrium temperature is low enough, precisely when the product $(\rho_0\xi^2)(g\rho_0/T)^2 \gg 1$.

3.1.3 Dimensionless formulation

The definition of the time scale τ_ℓ opens up the opportunity to rescale the time variable of the kinetic equation (2.72) as $\tilde{t} \equiv t/\tau_\ell$. In addition, the momentum scale can be conveniently rendered dimensionless by means of the healing length: $\tilde{q} \equiv q\xi$.

In these units, the kinetic equation becomes

$$\frac{\partial n_{\tilde{q}}}{\partial \tilde{t}} = \frac{6}{\pi^2}\left(\frac{g\rho_0}{T}\right)^2 \left\{ \int_0^{+\infty} d\tilde{p}\, \tilde{p}(\tilde{p}+\tilde{q}) \left[n_{\tilde{p}+\tilde{q}} \left(n_{\tilde{p}} + n_{\tilde{q}} + 1 \right) - n_{\tilde{p}} n_{\tilde{q}} \right] + \frac{1}{2} \int_0^{\tilde{q}} d\tilde{p}\, \tilde{p}(\tilde{q}-\tilde{p}) \left[n_{\tilde{p}} n_{\tilde{q}-\tilde{p}} - n_{\tilde{q}} \left(n_{\tilde{p}} + n_{\tilde{q}-\tilde{p}} + 1 \right) \right] \right\}. \tag{3.9}$$

A similar rescaling can be performed for the anomalous kinetic equation (2.74). In the next section, we compute the equilibrium temperature and show that it is independent of the mass. Therefore, from the perspective of the resolution of the kinetic equations, the only parameter of Eq. (3.9) is $T/(g\rho_0) \ll 1$, which is independent from m. The quantity $\rho_0\xi^2 \sim 1/(mg)$ must large enough for the hydrodynamic theory to be valid, as stated in Sec. 1.1.3, but it does not appear in Eq. (3.9). We will use this property in numerical simulations to work with small $\rho_0\xi^2$, although, strictly speaking, the hydrodynamic treatment does not hold in this limit. This will enable us to plot the structure factor in Fig. 3.3 without having to cope with overly fast oscillations that would obscure the clarity of the plot.

3.1.4 Equilibrium temperature

The asymptotic thermal distribution (2.73) reached at long time $\tau \gg \tau_\ell$ is represented by the dashed curve in Fig. 3.2(a). The associated equilibrium temperature T is entirely determined from energy conservation during the whole time evolution:

$$\int_{\boldsymbol{q}} \frac{c|\boldsymbol{q}|}{\exp(c|\boldsymbol{q}|/T)-1} = \frac{\zeta(3)T^3}{\pi\rho_0 c^2} = \int_{\boldsymbol{q}} \epsilon_{\boldsymbol{q}} n^{\mathrm{ps}}_{\boldsymbol{q}}. \tag{3.10}$$

The temperature T, computed from this relation using Eqs. (3.2) and (3.4), is displayed in Fig. 3.1 as a function of the quench duration τ_s. As intuition suggests, T decreases when τ_s increases, i.e., as the quench is more and more adiabatic. The temperature admits a simple expression in the asymptotic regimes $\tau_s \gg \tau_g$ (slow quench) and $\tau_s \ll \tau_g$ (fast quench). For the fast quench we find

$$T \sim \sqrt{\frac{3(g-g_0)^2\rho_0^2}{\pi^2} \log\left[\sqrt{\frac{\tau_g}{4\pi\tau_s}}\right]}, \quad \tau_s/\tau_g \ll 1 \tag{3.11}$$

while

$$T \simeq \left[\left(\frac{cT_0}{c_0}\right)^3 + \frac{\pi(c-c_0)^2}{2^9\zeta(3)c_0 c\tau_s^3} \right]^{1/3}, \quad \tau_s/\tau_g \gg 1 \tag{3.12}$$

for the slow quench. Both Eqs. (3.11) and (3.12) are shown in Fig. 3.1, together with the exact result. The temperature is minimal for infinitely slow quenches $\tau_s/\tau_g \to \infty$, reaching $T \to (c/c_0)T_0$. As a remark, the curve in Fig. 3.1 also indicates that when τ_s is of the order of τ_g or larger, the equilibrium temperature is

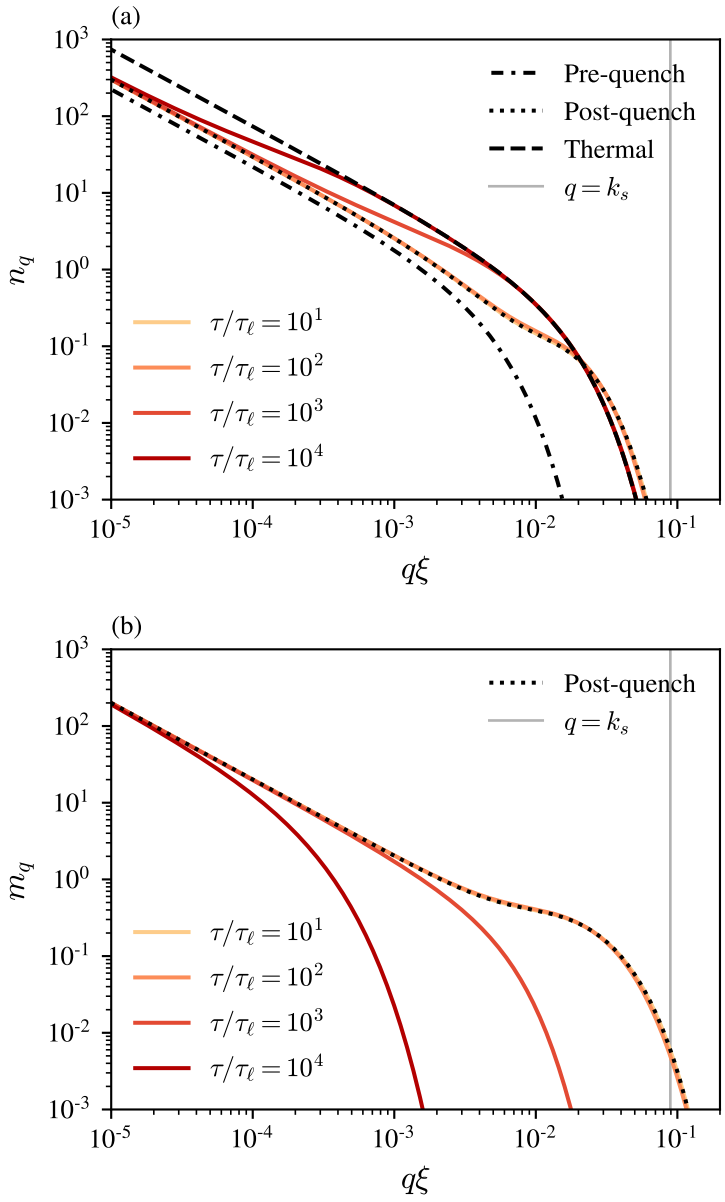

Figure 3.2: Time evolution of the phonon (a) momentum $n_{\boldsymbol{q},\tau}$ and (b) anomalous $m_{\boldsymbol{q},\tau}$ momentum distributions following an interaction quench $g_0 \to g$ near $\tau = 0$. Here we set $g_0\rho_0 = 0.1$, $g\rho_0 = 0.5$, $\rho_0\xi^2 = 0.5$, $\tau_s/\tau_g = 10$ and $T_0/g_0\rho_0 = 0.01$. The dashed-dotted curve shows the pre-quench thermal law (3.1), while dotted curves are the post-quench distributions computed from Eqs. (3.2) and (3.3), used as initial conditions for the kinetic equations. At long time, $n_{\boldsymbol{q},\tau}$ converges to the thermal distribution (2.73) (dashed curve), with an equilibrium temperature well approximated by Eq. (3.12).

such that $T \ll g\rho_0$. In this limit, the quasiparticles typically belong to the phononic branch of the dispersion and, at the same time, the condition of separation of time scales is satisfied. For this reason, in all subsequent numerical simulations we have chosen $\tau_s = 10\tau_g$.

3.1.5 Nonequilibrium structure factor

To illustrate the concrete impact of the phonon relaxation dynamics in a 2D quenched superfluid, we now study a specific observable, the nonequilibrium quantum structure factor $S_{\boldsymbol{q},\tau} \equiv \langle \delta\hat{\rho}_{\boldsymbol{q},\tau}\delta\hat{\rho}_{-\boldsymbol{q},\tau}\rangle$. The structure factor is the Fourier transform of the spatial density-density correlator of the superfluid. This quantity has been recently measured experimentally, in an ultra-cold Bose gas in two dimensions [44] and in a quantum fluid of light produced in a hot atomic vapor [147], both experiments involving a quench of the interaction strength. In practice, the nonequilibrium structure factor provides a simple observable to characterize the dynamical emergence of interference between quasiparticles emitted at the quench, which manifest themselves as oscillations of $S_{\boldsymbol{q},\tau}$ in space and time. Such oscillations, observed in laboratory superfluids, have also sparked interest because they are analogous to the famous Sakharov oscillations, a characteristic feature in the anisotropy of the cosmic microwave background radiation related to the emission of acoustic waves in the early universe [107]. Employing the Bogoliubov transformations (1.9) and (1.10), we can rewrite the structure factor as:

$$\begin{aligned} S_{\boldsymbol{q},\tau} &= \frac{E_{\boldsymbol{q}}}{\epsilon_{\boldsymbol{q}}}\left[2\langle \hat{a}^\dagger_{\boldsymbol{q},\tau}\hat{a}_{\boldsymbol{q},\tau}\rangle + 1 + 2\,\mathrm{Re}\,\langle \hat{a}_{\boldsymbol{q},\tau}\hat{a}_{-\boldsymbol{q},\tau}\rangle\right] \\ &= \frac{E_{\boldsymbol{q}}}{\epsilon_{\boldsymbol{q}}}\left[2n_{\boldsymbol{q},\tau} + 1 + 2\cos\left(2\epsilon_{\boldsymbol{q}}\tau\right) m_{\boldsymbol{q},\tau}\right], \end{aligned} \tag{3.13}$$

where in the second equality we have introduced the normal and anomalous phonon distributions. The structure factor primarily exhibits a fast, coherent dynamics described by the term $\propto \cos\left(2\epsilon_{\boldsymbol{q}}\tau\right)$. These oscillations stem from the interference between Bogoliubov quasiparticles with momenta $\boldsymbol{q}$ and $-\boldsymbol{q}$ emitted at the quench. On top these oscillations, $S_{\boldsymbol{q},\tau}$ is characterized by a slow relaxation dynamics due to the quasiparticle interactions that make $n_{\boldsymbol{q},\tau}$ and $m_{\boldsymbol{q},\tau}$ slowly vary in time.

The structure factor is shown in Fig. 3.3(a) for increasing times, from its post-quench to its long-time (thermal) value. Shortly after the quench, $S_{\boldsymbol{q},\tau}$ exhibits sizeable oscillations of period $\pi/(c\tau)$ in momentum space. In this regime [up to $\sim 10^2\tau_\ell$ in Fig. 3.3(a)], the dynamics is almost purely coherent, $m_{\boldsymbol{q},\tau}$ and $n_{\boldsymbol{q},\tau}$ remaining close to their initial, post-quench value. Within this short-time window, which was the main focus of previous experiments [44, 147], we can therefore approximate $m_{\boldsymbol{q},\tau} \simeq m^{\mathrm{ps}}_{\boldsymbol{q}}$ and $n_{\boldsymbol{q},\tau} \simeq n^{\mathrm{ps}}_{\boldsymbol{q}}$ in Eq. (3.13), so that:

$$S_{\boldsymbol{q},\tau} \simeq \frac{E_{\boldsymbol{q}}}{\epsilon_{\boldsymbol{q}}}\coth\left(\frac{\epsilon^0_{\boldsymbol{q}}}{2T_0}\right)\left[2d^2_{\boldsymbol{q}} + 1 + 2\sqrt{d^2_{\boldsymbol{q}} + d^4_{\boldsymbol{q}}}\cos(2\epsilon_{\boldsymbol{q}}\tau)\right], \tag{3.14}$$

which is nothing but the prediction of Bogoliubov perturbation theory.

The approximation (3.14) is shown in Fig. 3.3(a) at both times $\tau = 10^2\tau_\ell$ and $10^3\tau_\ell$. While in the former case it well captures the dynamics, in the latter case it is clearly inaccurate. Indeed, at long times quasiparticle interactions become prominent and lead to a damping of the coherent oscillations. The latter eventually completely disappear when the system has thermalized, with $S_{\boldsymbol{q},\infty} \simeq (E_{\boldsymbol{q}}/\epsilon_{\boldsymbol{q}})\coth(\epsilon_{\boldsymbol{q}}/2T)$. While a quantitative description of $S_{\boldsymbol{q},\tau}$ at an arbitrary time requires a numerical resolution of the kinetic equations, at long time the phonon distributions can be approximated by their near-equilibrium expressions, obtained from Eqs. (2.77) and (2.78). Inserting these solutions into Eq. (3.14), we find

$$\begin{aligned} S_{\boldsymbol{q},\tau} \simeq{}& \frac{E_{\boldsymbol{q}}}{\epsilon_{\boldsymbol{q}}}\coth\left(\frac{\epsilon_{\boldsymbol{q}}}{2T}\right)\left(1-e^{-\gamma_{\boldsymbol{q}}\tau}\right) \\ &+\frac{E_{\boldsymbol{q}}}{\epsilon_{\boldsymbol{q}}}\coth\left(\frac{\epsilon^0_{\boldsymbol{q}}}{2T_0}\right)\left[2d^2_{\boldsymbol{q}}+1+2\sqrt{d^2_{\boldsymbol{q}}+d^4_{\boldsymbol{q}}}\cos(2\epsilon_{\boldsymbol{q}}\tau)\right]e^{-\gamma_{\boldsymbol{q}}\tau} \end{aligned} \tag{3.15}$$

where $\gamma_{\boldsymbol{q}}$ coincides with either the Beliaev (2.76) or Landau (2.77) scattering rates depending on the range of momenta probed. In Fig. 3.3(a), Eq. (3.15) is superimposed onto the exact result for $\tau = 10^4\tau_\ell$, using $\gamma_{\boldsymbol{q}} = \gamma^L_{\boldsymbol{q}}$ (dashed black curve). The agreement is very good in the whole range of q (for the chosen parameters, we have typically $cq \ll T$, such that $\gamma^L_{\boldsymbol{q}}$ is always much larger than $\gamma^B_{\boldsymbol{q}}$). The impact of the relaxation dynamics of the phonons is seen even more dramatically in Fig. 3.3(b), which shows the structure factor at fixed momentum as a function of time. In the absence of phonon interactions (Bogoliubov approximation), $S_{\boldsymbol{q},\tau}$ oscillates harmonically. Comparing with the exact behavior for $q\xi = 10^{-3.5}$ shows how poor the Bogoliubov approximation becomes as time grows.

3.1.6 Nonequilibrium coherence function

As a second illustration, we study the time evolution of the coherence function of the Bose gas following the interaction quench:

$$G_1(r,\tau) \equiv \langle\hat\psi^\dagger(0,\tau)\hat\psi(\boldsymbol{r},\tau)\rangle. \tag{3.16}$$

In the density-phase representation (1.5), the coherence function can be expressed in terms of the variance of phase and density fluctuations [49]:

$$\begin{aligned} G_1(r,\tau) =\rho_0 \exp\Big\{ &-\frac{1}{2}\langle{:}\,[\hat\theta(0,\tau)-\hat\theta(\boldsymbol{r},\tau)]^2\,{:}\rangle \\ &-\frac{1}{8\rho_0}\langle{:}\,[\delta\hat\rho(0,\tau)-\delta\hat\rho(\boldsymbol{r},\tau)]^2\,{:}\rangle\Big\}, \end{aligned} \tag{3.17}$$

where the : symbol refers to normal ordering of operators in position representation. Notice that G_1 only depends $r = |\boldsymbol{r}|$ due to rotation invariance. In 2D Bose gases, the spatial dependence of this function is typically dominated by the spatial growth

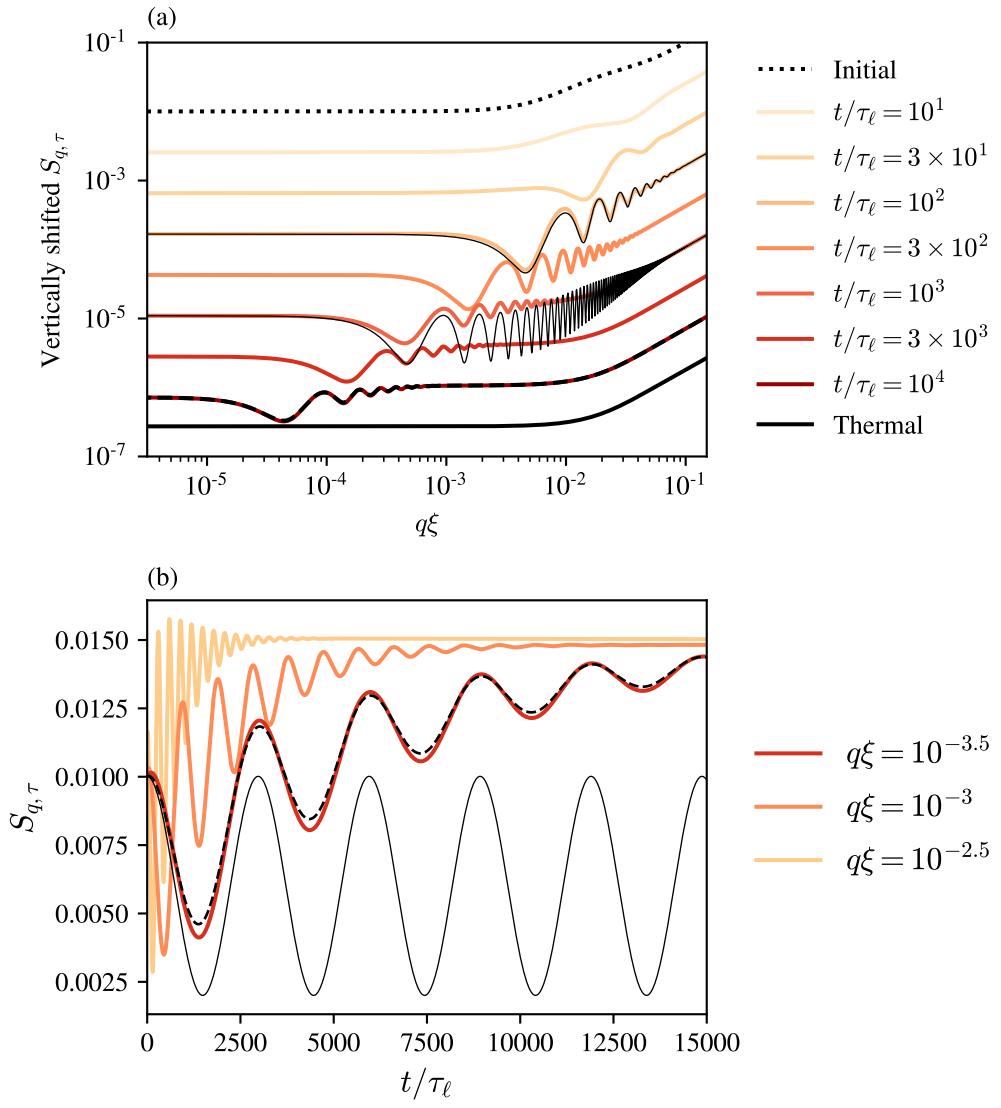

Figure 3.3: Nonequilibrium structure factor $S_{\boldsymbol{q},\tau}$, Eq. (3.13), versus (a) momentum at different times and (b) time at different momenta. For a better readability, in panel (a) the curves are shifted downward as time increases (except $S_{\boldsymbol{q},\tau=0}$, black dotted curve). In both panels, the thin black curves are the Bogoliubov prediction (3.14), while the dashed curves are the long-time approximation (3.15). Observe that the Bogoliubov result becomes clearly inaccurate as time increases. Parameters have the same values as in Fig. 3.2: $g_0\rho_0 = 0.1$, $g\rho_0 = 0.5$, $\rho_0\xi^2 = 5 \times 10^{-4}$, $\tau_s/\tau_g = 10$ and $T_0/g_0\rho_0 = 0.01$.

of phase fluctuations, eventually leading to an algebraic decay of G_1. This behavior is noticeably different from the one of 3D Bose gases, whose phase fluctuations are very small at low temperature. Using the Bogoliubov transformations (1.9-1.10) and definitions (2.18-2.19), we find that Eq. (3.17) can be rewritten as

$$G_1(r,\tau)/\rho_0 = \mathcal{G}_1(r) g_1(r,\tau). \tag{3.18}$$

Here

$$g_1(r,\tau) = \exp\Big\{-\int_{\boldsymbol{q}} \frac{1}{2}\left[1-\cos(\boldsymbol{q}\cdot\Delta\boldsymbol{r})\right]\Big[\left(\frac{\epsilon_{\boldsymbol{q}}}{E_{\boldsymbol{q}}}+\frac{E_{\boldsymbol{q}}}{\epsilon_{\boldsymbol{q}}}\right) n_{\boldsymbol{q},\tau} + \left(\frac{E_{\boldsymbol{q}}}{\epsilon_{\boldsymbol{q}}}-\frac{\epsilon_{\boldsymbol{q}}}{E_{\boldsymbol{q}}}\right) m_{\boldsymbol{q},\tau}\cos(2\epsilon_{\boldsymbol{q}}\tau)\Big]\Big\} \tag{3.19}$$

encodes the time evolution of the Bose gas coherence following the quench. The function $\mathcal{G}(r)$ is, in contrast, independent of time. It satisfies $\mathcal{G}_1(0) = 1$ and quickly decays to $\mathcal{G}_1(r \gg \xi) \simeq 1 - 1/(16\pi\rho_0\xi^2)$ at distances larger than the healing length, a value that coincides with the quantum depletion of zero-temperature Bose gases in two dimensions [78, 80]. Note that $\mathcal{G}_1$ purely originates from the non-commutation of the Bogoliubov operators involved in Eq. (3.17) and, as such, would be absent within a classical-field description.

From now on we focus our attention on $g_1(r,\tau)$, which we have computed from Eq. (3.19), using the numerical solutions of the quantum kinetic equations (2.72) and (2.74) for $n_{\boldsymbol{q},\tau}$ and $m_{\boldsymbol{q},\tau}$. The full time evolution of this function is shown in Fig. 3.4, and reveals the successive emergence of three characteristic regimes of algebraic decay. At very short times, first, g_1 mainly exhibits the algebraic decay of the pre-quench equilibrium state:

$$g_1(r,\tau) \sim \left(\frac{\lambda_0}{r}\right)^{\frac{1}{\rho_0\lambda_0^2}}, \tag{3.20}$$

with $\lambda_0 = \sqrt{2\pi/(mT_0)}$ the thermal de Broglie wavelength at the (pre-quench) temperature T_0. Shortly after the quench, then, a second algebraic law emerges at intermediate scales, typically within a light cone of radius $r = 2c\tau$. This characteristic decay can be described at the level of the Bogoliubov approximation, namely by simply replacing $n_{\boldsymbol{q},\tau}$ and $m_{\boldsymbol{q},\tau}$ by their post-quench values in Eq. (3.19). This leads to the "pre-thermal" algebraic law

$$g_1(r,\tau) = \left(\frac{\lambda_0}{r}\right)^{\frac{1+g/g_0}{2\rho_0\lambda_0^2}}. \tag{3.21}$$

At long time, finally, a third thermal algebraic scaling arises from short scales, and eventually extends to all scales as the system fully thermalizes with $n_{\boldsymbol{q},\tau} \to [\exp(cq/T)-1]^{-1}$ and $m_{\boldsymbol{q},\tau} \to 0$:

$$g_1(r,\tau\to\infty) = \left(\frac{\lambda}{r}\right)^{\frac{1}{\rho_0\lambda^2}}, \tag{3.22}$$

with the algebraic exponent now controlled by the thermal wavelength $\lambda = \sqrt{2\pi/(mT)}$.

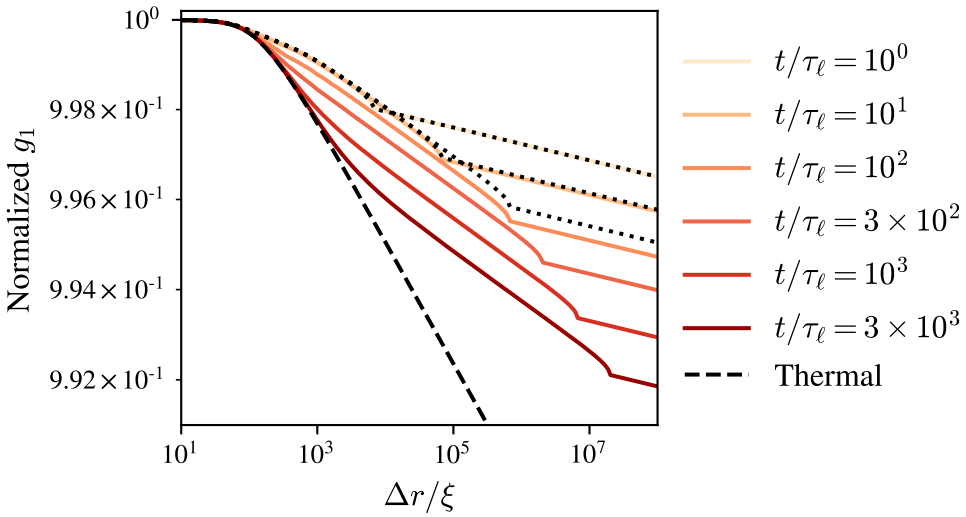

Figure 3.4: Nonequilibrium coherence function $g_1(r,\tau)$ versus position r at different times, computed from Eq. (3.19) together with the numerical solution of quantum kinetic equations for $n_{\boldsymbol{q},\tau}$ and $m_{\boldsymbol{q},\tau}$. The three black dotted curves are the Bogoliubov prediction at times $\tau = \tau_\ell, 10\tau_\ell$ and $100\tau_\ell$. Observe that at $\tau = 100\tau_\ell$ the Bogoliubov prediction becomes no longer accurate. The dashed curve shows the long-time, thermal asymptotic value. Parameters are set to $g_0\rho_0 = 0.1$, $g\rho_0 = 0.5$, $\rho_0\xi^2 = 0.5$, $\tau_s/\tau_g = 10$ and $T_0/g_0\rho_0 = 0.01$.

Note that in the case $g > g_0$ considered here, the three algebraic exponents satisfy the inequalities

$$\frac{1}{\rho_0\lambda_0^2} \leq \frac{1+g/g_0}{2\rho_0\lambda_0^2} \leq \frac{1}{\rho_0\lambda^2}, \tag{3.23}$$

with the two bounds being reversed in the case of a down-quench $g < g_0$. It is instructive, additionally, to compare the exact shape of the coherence function with its Bogoliubov approximation. The latter is shown in Fig. 3.4 for the three shortest times $\tau = \tau_\ell, 10\tau_\ell$ and $100\tau_\ell$. Again, while this approximation is acceptable at short time, it becomes clearly inaccurate starting from $\tau \sim 100\tau_\ell$. This shows that in 2D Bose gases, a description in terms of independent quasiparticles should be systematically questioned when dealing with nonequilibrium scenarios.

3.2 Nonperturbative corrections to the Landau relaxation rate

In the previous chapter, we have derived a quantum kinetic theory for a nonequilibrium gas of 2D bosons. An important object of our study was the self-energy Σ^R, whose imaginary part is related to the relaxation rates $\gamma^{L/B}$ of the quasiparticles. We have seen that for a purely linear dispersion $\epsilon_{\boldsymbol{q}} \simeq c|\boldsymbol{q}|$, the angular integration in Eq. (2.58) is divergent, leading to $\gamma^{L/B} \to \infty$. Following a common strategy in dimension $D > 1$ [88, 136, 137], we have cured this behavior by including the first nonlinear correction to the Bogoliubov dispersion, $\epsilon_{\boldsymbol{q}} \simeq c|\boldsymbol{q}| + (c\xi^2/2)|\boldsymbol{q}|^3$. The diagrams considered in this approach are the one-loop scattering terms depicted in Fig. 2.1. Our calculations thus constitute a perturbative expansion at leading order in the small parameter $1/(\rho_0\xi^2)$. It has led us to the perturbative Landau-Beliaev damping rates Eqs. (2.76) and (2.77), for which we recall the expressions:

$$\gamma^L_{\boldsymbol{q}} = \frac{\sqrt{3}\pi}{8\rho_0 c} q T^2, \quad \gamma^B_{\boldsymbol{q}} = \frac{\sqrt{3}c}{32\pi\rho_0} q^3. \tag{3.24}$$

However, we have mentioned that it is also possible to regularize the divergence of Σ^R in a completely different way, by means of a self-consistent extension of Eq. (2.58), which amounts to taking into account an infinite number of high-order scattering terms. Although this nonperturbative approach is strictly speaking uncontrolled (in the sense that infinitely many higher-order diagrams are neglected), it is nonetheless a standard scheme in dimension one, where the cubic regularization does not lead to any damping [136, 140], i.e., $\gamma^{B/L} = 0$. The idea of a self-consistent technique in one dimension dates back to the work of Andreev [95], and has also been used extensively in the context of non-quadratic Luttinger-liquid models (cf. [96, 141] and references therein).

In this section, we explore the possibility of combining the two approaches mentioned above, i.e., we keep *both* the cubic correction to the dispersion and the self-consistent scheme. We then derive the corresponding generalized Landau-Beliaev rates $\Gamma^{L/B}$. We find that, in most cases, the cubic regularization dominates the self-consistent one, validating the method used in Sec. 2.2. For instance, the Beliaev damping rate Eq. (2.76) is only slightly modified, i.e. $\Gamma^B_{\boldsymbol{q}} \sim q^3$, and the prefactor $\Gamma^B_{\boldsymbol{q}}/\gamma^B_{\boldsymbol{q}}$ remains close to one in the limit $\rho_0\xi^2 \gg 1$. However, we also show that, for any given microscopic parameters g, m, ρ_0, there exists an infrared range of momenta where the Landau damping rate is dominated by the self-consistent regularization. More precisely, for sufficiently small q, we find that $\Gamma^L_{\boldsymbol{q}} \sim q^{3/2}$.

3.2.1 Self-consistent Born approximation

The perturbative approach of Sec. 2.2 leads to the (on-shell) retarded self-energy (2.57). Alternatively, the self-consistent Born (one-loop) approximation (SCBA)

consists in substituting the free propagators $G^{0,R/A}$ in the integrand by their dressed counterparts $G^{R/A}$. By doing so, high-order interaction terms based on the one-loop diagrams of Fig. 2.1 are systematically resummed. In the self-consistent approach, the retarded self-energy is thus:

$$\Sigma^R_{\boldsymbol{q},\tau} = 2i \int_{\boldsymbol{p},\nu,\omega} A_{\boldsymbol{q},\omega,\tau} \left(\Lambda^2_{\boldsymbol{p},\boldsymbol{q}-\boldsymbol{p}} G^K_{\boldsymbol{p},\nu,\tau} G^R_{\boldsymbol{q}-\boldsymbol{p},\omega-\nu,\tau} + \Lambda^2_{\boldsymbol{p},\boldsymbol{q}} G^K_{\boldsymbol{p},\nu,\tau} G^R_{\boldsymbol{p}+\boldsymbol{q},\omega+\nu,\tau} + \Lambda^2_{\boldsymbol{p},\boldsymbol{q}} G^K_{\boldsymbol{p}+\boldsymbol{q},\nu+\omega,\tau} G^A_{\boldsymbol{p},\nu,\tau} \right). \tag{3.25}$$

In the following, we will focus on the equilibrium case for simplicity. Consequently, we will omit the τ index from the notations since the time dependence of self-energies and distributions functions is not relevant for our current purposes.

Let us first perform the integration over ω in Eq. (3.25), which amounts to a generalized on-shell approximation where the broadening of the spectral function is self-consistently taken into account. The spectral function is expressed as $A_{\boldsymbol{q},\omega} = i(G^R_{\boldsymbol{q},\omega} - G^A_{\boldsymbol{q},\omega})$, where the dressed components of $G^{R/A}$ are given by the Dyson equations (2.40) and (2.41), for which we recall the Wigner representation:

$$\begin{cases} G^R_{\boldsymbol{q},\omega} = \left(\omega - \omega^-_{\boldsymbol{q}}\right)^{-1}, & \omega^-_{\boldsymbol{q}} = \epsilon_{\boldsymbol{q}} + \Sigma^R_{\boldsymbol{q}}, \\ G^A_{\boldsymbol{q},\omega} = \left(\omega - \omega^+_{\boldsymbol{q}}\right)^{-1}, & \omega^+_{\boldsymbol{q}} = \epsilon_{\boldsymbol{q}} + \Sigma^{R*}_{\boldsymbol{q}}. \end{cases} \tag{3.26}$$

The poles $\omega^\pm_{\boldsymbol{q}}$ are distinguished according to the sign of their imaginary part. In Eq. (3.26), we have injected the ω-independent expression of the retarded self-energy [i.e., the left-hand side of Eq. (3.25)], in a self-consistent manner at the level of the on-shell approximation. The integration over ω is then achieved by means of the residue theorem:

$$\Sigma^R_{\boldsymbol{q}} = 2i \int_{\boldsymbol{p},\nu} \Lambda^2_{\boldsymbol{p},\boldsymbol{q}-\boldsymbol{p}} G^K_{\boldsymbol{p},\nu} G^R_{\boldsymbol{q}-\boldsymbol{p},\omega^+_{\boldsymbol{q}}-\nu} + \Lambda^2_{\boldsymbol{p},\boldsymbol{q}} G^K_{\boldsymbol{p},\nu} G^R_{\boldsymbol{p}+\boldsymbol{q},\omega^+_{\boldsymbol{q}}+\nu} + \Lambda^2_{\boldsymbol{p},\boldsymbol{q}} F_{\boldsymbol{p}+\boldsymbol{q},\nu+\epsilon_{\boldsymbol{q}}} \left(G^R_{\boldsymbol{p}+\boldsymbol{q},\omega^+_{\boldsymbol{q}}+\nu} - G^A_{\boldsymbol{p}+\boldsymbol{q},\omega^-_{\boldsymbol{q}}+\nu} \right) G^A_{\boldsymbol{p},\nu}, \tag{3.27}$$

where we employed the parametrization (2.43) to express the Keldysh Green function $G^K_{\boldsymbol{p}+\boldsymbol{q},\nu+\omega}$ in Eq. (3.25). By assuming the separation of time scales introduced in Sec. 2.2.2, the latter can be expressed as the product of the spectral function and the distribution function $G^K_{\boldsymbol{p}+\boldsymbol{q},\nu+\omega} = -iA_{\boldsymbol{p}+\boldsymbol{q},\nu+\omega} F_{\boldsymbol{p}+\boldsymbol{q},\nu+\omega}$, at leading order in the Wigner expansion.

A similar integration over ν leads to

$$\Sigma^R_{\boldsymbol{q}} = -2 \int_{\boldsymbol{p}} \left(\Lambda^2_{\boldsymbol{p},\boldsymbol{q}-\boldsymbol{p}} \frac{F_{\boldsymbol{p}}}{\epsilon_{\boldsymbol{p}} + \epsilon_{\boldsymbol{q}-\boldsymbol{p}} - \epsilon_{\boldsymbol{q}} + \Sigma^R_{\boldsymbol{p}} + \Sigma^R_{\boldsymbol{q}-\boldsymbol{p}} - \Sigma^{R*}_{\boldsymbol{q}}} + \Lambda^2_{\boldsymbol{p},\boldsymbol{q}} \frac{F_{\boldsymbol{p}} - F_{\boldsymbol{p}+\boldsymbol{q}}}{\epsilon_{\boldsymbol{p}+\boldsymbol{q}} - \epsilon_{\boldsymbol{p}} - \epsilon_{\boldsymbol{q}} + \Sigma^R_{\boldsymbol{p}+\boldsymbol{q}} - \Sigma^{R*}_{\boldsymbol{p}} - \Sigma^{R*}_{\boldsymbol{q}}} \right), \tag{3.28}$$

where we recall that $F_{\boldsymbol{p}} \equiv F_{\boldsymbol{p},\epsilon_{\boldsymbol{p}}}$. The first term in Eq. (3.28) describes a generalized Beliaev process, that is the disintegration of a phonon $\epsilon_{\boldsymbol{q}}$ into two smaller excitations

$\epsilon_{\boldsymbol{p}}, \epsilon_{\boldsymbol{q}-\boldsymbol{p}}$ with a self-consistent account of the relaxation rate itself. The second term corresponds to the Landau damping introduced in 2.3.2. Note that here $\Sigma^R_{\boldsymbol{q}}$ is typically a complex quantity with a non-vanishing real part, contrary to the previous perturbative analysis, where Σ^R was purely imaginary [cf. Eq. (2.59)]. It implies that within the self-consistent Born approximation, the energies $\epsilon_{\boldsymbol{p}}$ are rescaled by a shift of amplitude $\mathrm{Re}(\Sigma^R_{\boldsymbol{p}})$.

Before turning to the angular integration of Eq. (3.28), we mention two technical aspects that deserve a preliminary comment. The first point is the assumed existence and uniqueness of the solutions of the self-consistent equation (3.28). This assumption is supported by numerical simulations. One important consequence is the possibility to make progress in analytically solving Eq. (3.28) by making an educated guess about the unknown variable Σ^R. Specifically, if we propose an Ansatz for Σ^R that is self-consistent with the equation, then we can consider it to be correct, as there is only one solution. Secondly, we will heavily rely on the following complex analysis result:

$$\int_{-\pi}^{\pi} \frac{d\theta}{\theta^2+\Omega} \simeq \int_{\mathbb{R}} \frac{d\theta}{\theta^2+\Omega} = -\mathrm{sgn}\left(\mathrm{Im}\left[\Omega\right]\right) \frac{i\pi}{\sqrt{-\Omega}}. \tag{3.29}$$

The first approximation is correct provided $0 < |\Omega| \ll 1$, and the second equality requires $\mathrm{Im}\left[\Omega\right] \neq 0$.

3.2.2 Corrections to Beliaev damping

For convenience, we now treat separately the Landau and Beliaev contributions to the damping of quasiparticles characterized by Eq. (3.28). Let us first focus on the dominant contribution at zero temperature, i.e., the Beliaev damping mechanism:

$$\Sigma^R_{\boldsymbol{q}} \overset{T=0}{=} -2 \int_{\boldsymbol{p}} \Lambda^2_{\boldsymbol{p},\boldsymbol{q}-\boldsymbol{p}} \frac{F_{\boldsymbol{p}}}{\epsilon_{\boldsymbol{p}} + \epsilon_{\boldsymbol{q}-\boldsymbol{p}} - \epsilon_{\boldsymbol{q}} + \Sigma^R_{\boldsymbol{p}} + \Sigma^R_{\boldsymbol{q}-\boldsymbol{p}} - \Sigma^{R*}_{\boldsymbol{q}}}. \tag{3.30}$$

Similarly to what is done in Appendix B, we denote by θ the angle between $\boldsymbol{p}$ and $\boldsymbol{q}$. A Beliaev process involves a quasiparticle of energy $\epsilon_{\boldsymbol{q}}$ that disintegrates into two phonons of energies $\epsilon_{\boldsymbol{p}}$ and $\epsilon_{\boldsymbol{q}-\boldsymbol{p}}$, which implies that $|\boldsymbol{p}| < |\boldsymbol{q}|$. The boundaries of the integral are thus $\int_{\boldsymbol{p}} \equiv \int_0^q dp \int_{-\pi}^{\pi} d\theta/[\rho_0(2\pi)^2]$. Moreover, under the assumption of long-lived (well-defined) quasiparticles, i.e., $\mathrm{Im}(\Sigma^R_{\boldsymbol{p}}) \ll \epsilon_{\boldsymbol{p}}$, the main contribution of Eq. (3.30) comes from small angles θ, where the expansion

$$\epsilon_{\boldsymbol{p}} + \epsilon_{\boldsymbol{q}-\boldsymbol{p}} - \epsilon_{\boldsymbol{q}} \simeq \frac{cpq}{2(q-p)} \left(\theta^2 - \theta^2_{B,+}\right), \quad \theta_{B,+} = \frac{\sqrt{3}}{2mc}(q-p), \tag{3.31}$$

holds true at leading order in $|\theta| \ll 1$. $\theta_{B,+}$ is the angle at which the energy conservation is satisfied, when the dispersion relation is expanded at cubic order. Furthermore, the isotropy of space leads to $\Sigma_{\boldsymbol{q}} = \Sigma_q$ and $F_{\boldsymbol{q}} = F_q$. Following the insights of Appendix B, we also neglect the θ dependence of $\Lambda^2_{\boldsymbol{p},\boldsymbol{q}-\boldsymbol{p}}$, i.e., we use

Eq. (1.14) to obtain $\Lambda^2_{\boldsymbol{p},\boldsymbol{q}-\boldsymbol{p}} \simeq 9cpq(q-p)/(32m)$. At this stage, it is not obvious if one can neglect the θ dependence of $\Sigma^R_{\boldsymbol{q}-\boldsymbol{p}}$. To clarify this, let us take a leap forward, and look at the self-consistent solution Eq. (3.34) obtained below: it is of the form $\Sigma_{\boldsymbol{p}} \sim |\boldsymbol{p}|^3$. Now, the θ dependence of terms like $|\boldsymbol{q}-\boldsymbol{p}|^3$ has already been neglected in Eq. (3.31). The appropriate *self-consistent* treatment is therefore to rule out any angular dependence in the self-energy $\Sigma^R_{\boldsymbol{q}-\boldsymbol{p}}$ in Eq. (3.30).

We can now proceed to the angular integration, using Eq. (3.29) with

$$\Omega = -\theta^2_{B,+} + \frac{2(q-p)}{cpq}\left(\Sigma^R_p + \Sigma^R_{q-p} - \Sigma^{R*}_q\right), \tag{3.32}$$

under the assumption that $|\Omega| \ll 1$, which can be verified self-consistently using the final solution Eq. (3.34) (the underlying physical hypothesis is the separation of time scales). After performing the change of variable $u = p/q$, we find

$$\Sigma^R_q \overset{T=0}{=} -6i\gamma^B_q \int_0^1 \frac{du\, u(1-u)}{\sqrt{1 + \frac{8m^2c}{3q^3u(1-u)}\left(\Sigma^{R*}_q - \Sigma^R_{uq} - \Sigma^R_{q-uq}\right)}}, \tag{3.33}$$

where we have introduced the perturbative two-dimensional Beliaev damping rate γ^B_q, and we have used the on-shell value of the distribution function at zero temperature: $F_{uq} = 1$. From Eq. (3.33), one recovers the perturbative Born approximation $\Sigma^R_q \to -i\gamma^B_q$ by replacing the self-energies under the square root by $-i0^+$.

We now use the Ansatz $\Sigma^R_q = \gamma^B_q S$, where the dimensionless complex number $S \in \mathbb{C}$ does not depend on the momentum q. Importantly, the q^3 factor under the square root in Eq. (3.33) ensures the self-consistency of this Ansatz. After some algebra, the SCBA solution $\Gamma^B_q = -\mathrm{Im}\,(\Sigma^R_q)$ of the Beliaev damping can be written as

$$\Gamma^B_q \overset{T=0}{=} \gamma^B_q S, \quad S = 6\int_0^1 \frac{du\, u(1-u)}{\sqrt{1 + \frac{1}{\rho_0\xi^2}\frac{3u(1-u)S - 2i\,\mathrm{Im}(S)}{u(1-u)16\sqrt{3\pi}}}}, \tag{3.34}$$

where the value of S is easily calculated numerically.

As shown by Eq. (3.34), the nonperturbative correction is small as soon as $\rho_0\xi^2 \sim (mg)^{-1}$ is very large. As the latter condition is a prerequisite of the hydrodynamic approach (see Sec. 1.1.3 of Chapter 1), it can be inferred that the perturbative Born approximation of Sec. 2.2.3 is always valid for describing Beliaev damping. This conclusion is consistent with the findings of Kopietz *et al.* [161, 162], who applied the functional renormalization group (FRG) [163, 164] to the 2D interacting Bose gas at zero temperature (see also [87, 165]). The FRG is a functional theory (i.e., it uses a generalized path-integral representation of the many-body problem, similarly to what is done with the Keldysh approach of Sec. 2.1) that goes beyond perturbative treatments. It consists in systematically integrating out small scale degrees of freedom. More precisely, in the context of the FRG, a flow equation is derived for an effective action Γ_k that only includes fluctuations with momenta larger than k (cf. [164] and references therein). Although mostly limited

to equilibrium phenomena[1], the FRG can be taylored to compute nonperturbative corrections for the two-dimensional Bose gas. Specifically, it can address scenarios involving strong interactions or high occupancy of distribution functions, where multiple scatterings cannot be ignored [157, 158, 166].

3.2.3 Anomalous Landau damping

The second term in Eq. (3.28) corresponds to a generalized Landau relaxation, which is dominant at finite temperature for $q \ll T/c$ (otherwise, Beliaev damping gives the leading contribution, and the results of Sec. 3.2.2 are valid). Keeping the cubic correction in Bogoliubov dispersion relation, the energy conservation of these processes is written as

$$\epsilon_{\boldsymbol{p}+\boldsymbol{q}} - \epsilon_{\boldsymbol{p}} - \epsilon_{\boldsymbol{q}} = -\frac{cpq}{2(p+q)}\left(\theta^2 - \theta_{L,+}^2\right), \quad \theta_{L,+} = \frac{\sqrt{3}}{2mc}(p+q). \tag{3.35}$$

There are again two allowed scattering branches $\theta = \pm\theta_{L,+}$, which is an expected property of two dimensional systems [88]. However, unlike the case of Beliaev damping, here no particular restriction holds on the integration domain, i.e., $p \equiv |\boldsymbol{p}|$ can take all real positive values. By application of Eq. (3.29), the angular integration yields

$$\Sigma^R_{\boldsymbol{q}} \overset{q\ll T/c}{=} -i\frac{3\sqrt{3}c}{16\pi\rho_0}\int_0^\infty \frac{dp\, p(p+q)(F_p - F_{p+q})}{\sqrt{1 + \frac{8m^2c}{3pq(p+q)}\left(\Sigma^R_{p+q} - \Sigma^{R*}_p - \Sigma^{R*}_q\right)}}. \tag{3.36}$$

Eq. (3.36) represents the self-consistent expression of Landau damping. In the specific case of equilibrium, the on-shell distribution function reduces to $F_p = 2n_p + 1$, where n_p is the Bose-Einstein distribution.

The integral (3.36) is dominated by values of p such that $p \gg q$, where the following approximation holds true:

$$2p(p+q)\,(n_p - n_{p+q}) \simeq p^2\frac{e^{cq/T} - 1}{\cosh(cp/T) - 1}. \tag{3.37}$$

At the Born approximation, the square root in Eq (3.36) can be replaced by one. Employing $\int_0^\infty du\, u^2 e^u/(e^u-1)^2 = \pi^2/3$, this leads to the standard perturbative Landau damping rate (2.77).

At the self-consistent Born approximation, it turns out that in Eq. (3.36) one can replace $(\Sigma^R_{p+q} - \Sigma^{R*}_p - \Sigma^{R*}_q)/p(p+q)$ by $2i\,\mathrm{Im}(\Sigma^R_p)/p^2$ in excellent approximation. Therefore,

$$\Sigma^R_{\boldsymbol{q}} \overset{q\ll T/c}{\simeq} -i\frac{3\sqrt{3}c}{16\pi\rho_0}\frac{cq}{T}\int_0^\infty \frac{dp\, p^2}{\cosh(cp/T) - 1}\frac{1}{\sqrt{1 + \frac{8m^2c}{3p^2q}\left(2i\,\mathrm{Im}(\Sigma^R_p)\right)}}, \tag{3.38}$$

[1] We refer to [156] for a discussion on the out-of-equilibrium extension of the FRG.

where, under the square root, the two terms correspond to either the cubic regularization or the self-consistent one. Importantly, when q is sufficiently small, the self-consistent contribution dominates the square root expression for any given microscopic parameters (m, g, ρ_0). Therefore, in this infrared regime, a first reasonable approximation is to replace the sum in the square root with $16im^2c\,\mathrm{Im}(\Sigma_p^R)/(3p^2q)$. Consequently, the term $\sqrt{q}$ can be factored out of the integral over p, indicating that $\Sigma_{\boldsymbol{q}}^R \sim q^{3/2}$ at leading order. To make progress in evaluating the integral (3.38), we can then reintroduce the expected momentum dependence of the self-energy under the square root in a self-consistent manner. After some rearrangement, we find

$$\Sigma_q^R \overset{q\ll T/c}{\simeq} \frac{1-i}{2^5}\left(\frac{9\mathcal{I}}{2\pi\rho_0\xi^2}\right)^{2/3}\frac{T^3}{(g\rho_0)^2}\left(\frac{cq}{T}\right)^{3/2}, \tag{3.39}$$

where $\mathcal{I} = \int_0^\infty du\, u^{9/4}/[\cosh(u)-1]$. Strikingly, our results imply that $\Sigma_q^R \sim q^{3/2}$ for sufficiently small q, unlike the expected linear behavior of the perturbative rate (2.77). This suggests that the phononic relaxation time scales are underestimated by the perturbative approach. Note that, in Eq. (3.39), the requirements $\rho_0\xi^2 \gg 1$ (i.e., hydrodynamic regime) and $T \ll g\rho_0$ (i.e., phononic approximation) do not conflict with the assumption of small $|\Sigma^R|$ needed for the angle integration or the Landau regime condition $cq \ll T$.

In Fig. 3.5, we compare the full numerical solution of Eq. (3.28) with the deep infrared result (3.39), and the perturbative rates (2.76, 2.77). At large q, the SCBA calculation essentially coincides with the usual Landau and Beliaev scattering rates, which are separated by the momentum scale $q \sim T/c$. At low q, in contrast, the Landau rate is strongly impacted, in agreement with the above calculations. By equating Eq. (2.77) with Eq. (3.39), one can estimate the momentum at which the crossover between the self-consistent $q^{3/2}$ regime and perturbative Landau damping occurs:

$$q_* \sim \frac{T}{c}\left(\frac{\pi^5}{3^{5/2}\mathcal{I}^2\rho_0\xi^2}\right)^{2/3}. \tag{3.40}$$

In particular, in the limit of vanishing interaction strength $g \to 0$, we find $q_* \to 0$ so that the perturbative rate is recovered at all momentum scales. Finally, it is worth mentioning that in Fig. 3.5, the estimate (3.39) accurately captures the momentum scaling $\sim q^{3/2}$, but it falls short in determining the correct prefactor of $\Sigma_{\boldsymbol{q}}^R$. Furthermore, our numerical findings indicate that the error tends to be more pronounced as g decreases in value. In fact, the relative lack of success of Eqs. (3.39, 3.40) is due to the approximation $16m^2c\,\mathrm{Im}(\Sigma_p^R)/(3p^2q) \gg 1$, which is somewhat crude. To overcome this limitation, we present a refined self-consistent Ansatz in the next section.

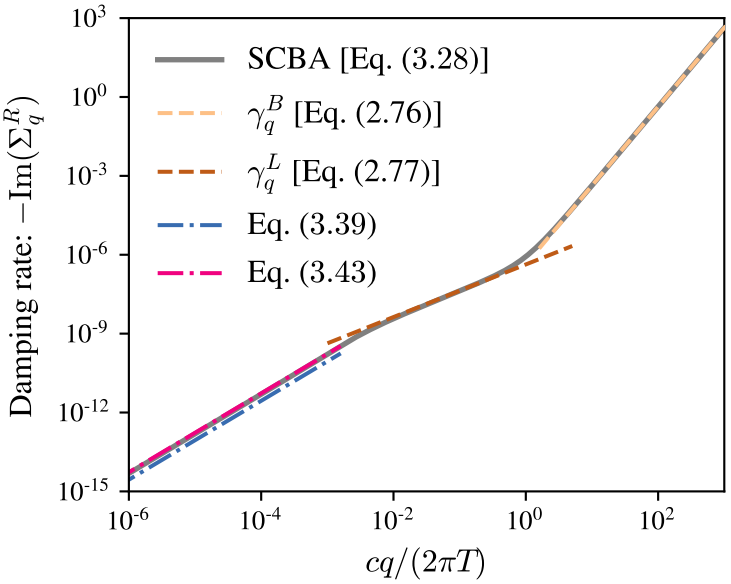

Figure 3.5: Landau damping rate as a function of q, computed by numerically solving Eq. (3.28) (plain grey line), and comparison with asymptotic approximations: The dashed curves correspond to the perturbative results given by Eqs. (2.76) and (2.77), while the dotted-dashed lines show the estimates provided by Eqs. (3.39) and (3.43). Parameters are set to $T/g\rho_0 = 0.1$, $\rho_0\xi^2 \simeq 25$.

3.2.4 Multiple-scattering interpretation

Although our self-consistent calculation, Eq. (3.39), suggests the existence of an anomalous Landau damping rate in the far infrared, the physical origin of this observation remains unclear. Here, we discuss an argument inspired of Refs. [150, 155, 156] that may corroborate our findings. The argument is that the many-body perturbation theory presented in Sec. 2.2.3 is inadequate in the strongly correlated regime where multiple scattering processes (i.e., terms of higher degree than the one-loop diagrams of Fig. 2.1) cannot be neglected. In practice, perturbation theory fails as soon as the occupation number n_q becomes large compared to the inverse of the small parameter of the Popov expansion (1.6). Within the hydrodynamic description of an interacting Bose gas in two dimensions, this small parameter is $1/(\rho_0\xi^2)$ [49]. The breaking of perturbation theory thus occurs when

$$n_q \geq \rho_0\xi^2, \tag{3.41}$$

which, in practice, is typically verified for strong interaction strengths, for which $\rho_0\xi^2$ is not large. Of course, this regime lies beyond the scope of the hydrodynamic theory. However, for a given small interaction strength g, the condition (3.41) is also satisfied for q-labelled states that are *largely occupied*. In momentum regimes where

Beliaev damping dominates, the occupation number is always very small. Indeed, n_q is exponentially damped at finite temperature for $q \gg T/c$, and it vanishes at $T = 0$. In contrast, for Landau damping, the momentum regime $q \ll T/c$ is such that the occupation number diverges, since $n_q \sim T/(cq)$. Eq. (3.41) thus leads to another estimate for the crossover between the perturbative and nonperturbative regimes of Landau damping:

$$\tilde{q}_* = \frac{T}{c} \frac{1}{\rho_0 \xi^2}, \tag{3.42}$$

which bears a strong resemblance to Eq. (3.40), albeit with a slightly different scaling of the interaction strength. Here, $\tilde{q}_* \propto g$, whereas we previously found $q_* \propto g^{2/3}$.

The exact numerical solution of Eq. (3.28) provides a way to decide which criterion works best, either Eq. (3.40) or Eq. (3.42). We find that the crossover momentum scales like g for small interaction strenghts, which validates Eq. (3.42). Combining the scaling $\Sigma^R_{\boldsymbol{q}} \sim q^{3/2}$ with Eq. (3.42) leads to the anomalous Landau damping rate

$$\Gamma^L_q \overset{q \ll T/c}{=} \frac{\sqrt{3}\pi}{2^5 \sqrt{\rho_0 \xi^2}} \frac{T^3}{(g\rho_0)^2} \left(\frac{cq}{T}\right)^{3/2}, \tag{3.43}$$

which provides an excellent approximation of the numerical solution of Eq. (3.28), for all values of g and T, as shown in Fig. 3.5.

In Sec. 3.2.2, we mentioned that the self-consistent corrections found for Beliaev damping align with findings from the functional renormalization group [161, 162]. To the best of our knowledge, however, there is currently no available FRG results on two-dimensional *Landau* damping. Consequently, it is not yet possible to establish with certainty whether the relaxation rate (3.43) is theoretically accurate or whether it can be measured experimentally. However, numerical simulations of the Gross-Pitaevskii equation with random initial conditions could potentially shed light on the self-consistent theory's predictions of anomalous Landau damping in the small q limit. Indeed, in this infrared regime, the classical-statistical field theory is expected to hold true, because the occupation number n_q is much greater than one (cf. Sec 2.3.3). Moreover, the Gross-Pitaevskii equation has been successfully used to verify the $\sim q^{3/2}$ damping rate that emerges from the SCBA theory in one dimension (see Ref. [140]). The fact that the exponent of the self-consistent damping rate does not depend on the dimension also remains to be addressed.

Conclusion

We have used the kinetic equations (2.72) and (2.74) to describe the dynamics of a two-dimensional Bose gas after an interaction quench. We have applied this framework to the calculation of two commonly measured observables, the quantum structure factor and the coherence function of the superfluid following an interaction quench.

Furthermore, we have employed the self-consistent Born approximation to compute generalized (nonperturbative) relaxation time scales for the quasiparticles. Our analysis reveals that, while these corrections are small for large q, they cannot be neglected in the infrared regime, where we anticipate a Landau damping rate $\sim q^{3/2}$ significantly different from the perturbative result $\sim q$.

Chapter 4

Periodically kicked one-dimensional Bose gases

In the previous chapters, we discussed the nonequilibrium behavior of an interacting 2D gas of bosons. A key assumption was the *isolated* nature of the system, excluding any contact with the environment or any external driving forces. The total energy was thus conserved throughout the evolution. To illustrate this conservation law, one can consider the kinetic equations (2.72) and (2.74) derived in Sec. 2.3, which, from the initial state to the final thermal distribution, verify $\partial_\tau \int_{\boldsymbol{q}} c|\boldsymbol{q}|n_{\boldsymbol{q},\tau} = 0$ for all τ. Here, we wish to explore another fruitful research direction of nonequilibrium quantum physics: periodically-driven systems [167–169]. These models are characterized by Hamiltonians of the form

$$\hat{H}(t) = \hat{H}_\alpha + F(t)\hat{H}_\beta, \tag{4.1}$$

where, typically, $[\hat{H}_\alpha, \hat{H}_\beta] \neq 0$ and F is a periodic function of time t. The time dependence of $\hat{H}$ implies that the energy is not a conserved quantity anymore. In fact, such systems are generally expected to "heat" to an infinite-temperature state [170–172]. In the following, our focus will be on the interplay between external forcing and interactions, where F is a periodic sequence of "kicks" and a mean-field, self-interaction term is present in either $\hat{H}_\alpha$ or $\hat{H}_\beta$. This study is, in particular, motivated by the growing interest in driven quantum systems involving temporally-modulated interactions [173–176], used for instance to design synthetic gauge fields or to modify many-body quantum transport.

Furthermore, in contrast to the three previous chapters, from now on we will turn our attention to Bose gases in *one* dimension. Let us make several general comments with respect to this change. First, these systems have a well-established physical relevance, thanks in particular to cold atom experiments. Indeed, it is nowadays possible to achieve this geometry in laboratories by several means, for instance by trapping atoms in atom-chips [64], arrays of tubes or tori [65]. Second, from a theoretical point of view it should be pointed out that the one-dimensional (1D) version of the Hamiltonian (1.1) modeling an homogeneous system of bosons

with a contact-like repulsive potential, i.e., the Lieb-Liniger model, can be solved exactly by the Bethe Ansatz [10, 13, 18, 19]. Similarly, the 1D nonlinear Schrödinger equation, which is the mean-field limit of the Lieb-Liniger model, can be solved by means of the inverse scattering technique [11, 12]. However, the integrability of these models is in general broken by the introduction of a periodic drive (see, however, Ref. [177] for an exception).

In the opening section of this chapter on driven problems, we introduce the quantum kicked rotor, together with the phenomenon of dynamical localization and its interplay with weak nonlinear interactions. Then, in Sec. 4.2, we move to the quantum dynamics of a different system, a Bose gas subjected to periodically-kicked interactions, which was the main focus of the thesis. In stark contrast with the kicked rotor, in the case of infinitely short (delta) kicks, it was recently shown that this system exhibits an ultrafast, exponential spreading of the wave function in momentum space [61, 62]. After recovering this behavior for a random variant of the model studied in [61, 62], we elaborate on this phenomenon by computing two observables that play a crucial role in this context, the average populations of the "condensate" (i.e., the uniform mode of momentum $q = 0$) and of the first excitation. In both cases, we give a detailed analysis of the "linear" regime of very short times, as well as an extension beyond that regime.

4.1 Quantum kicked rotor

4.1.1 The model

Let us start our discussions by quickly considering the quantum kicked rotor, a paradigmatic model for quantum chaos [57, 59], for which

$$\hat{H}_\alpha = \hat{p}^2/2m, \quad \hat{H}_\beta = K\cos(\hat{x}), \tag{4.2}$$

with conjugate variables $\hat{x}, \hat{p}$ such that $[\hat{x}, \hat{p}] = i$, in units of $\hbar = 1$. In most studies, F is a train of Dirac pulses at integer times n (the "kicks"), i.e., $F(t) = \sum_n \delta(t - n)$. The stochasticity parameter K sets the strength of the kicks. The quantum kicked rotor exhibits localization in momentum space, meaning that the variance of a wave packet's momentum distribution saturates for times larger than a characteristic time scale called the "localization time". Because this phenomenon occurs in p-space, it is referred to as *dynamical* localization [58]. In contrast, the standard map, the classical counterpart of the kicked rotor, is characterized by the diffusive growth of its kinetic energy, $E(t) = \langle \hat{p}^2/2m \rangle \propto t$ [54, 178]. The suppression of classical diffusion observed in the quantum problem is reminiscent of the phenomenon of Anderson localization in disordered systems, in that it stems from quantum interferences within a random-walk problem [59, 179, 180]. The quantum kicked rotor was first experimentally realized in Raizen's group about thirty years ago [181, 182] and has since received considerable attention [183–190].

In particular, dynamical localization was first demonstrated within an ultracold sodium setup, as illustrated in Fig. 4.1(a). The authors of Ref. [182] also verified the exponential localization of the momentum distribution of the Bose gas as $|\psi(p)|^2 \sim \exp(-|p|/\xi)$, where ξ is the localization length.

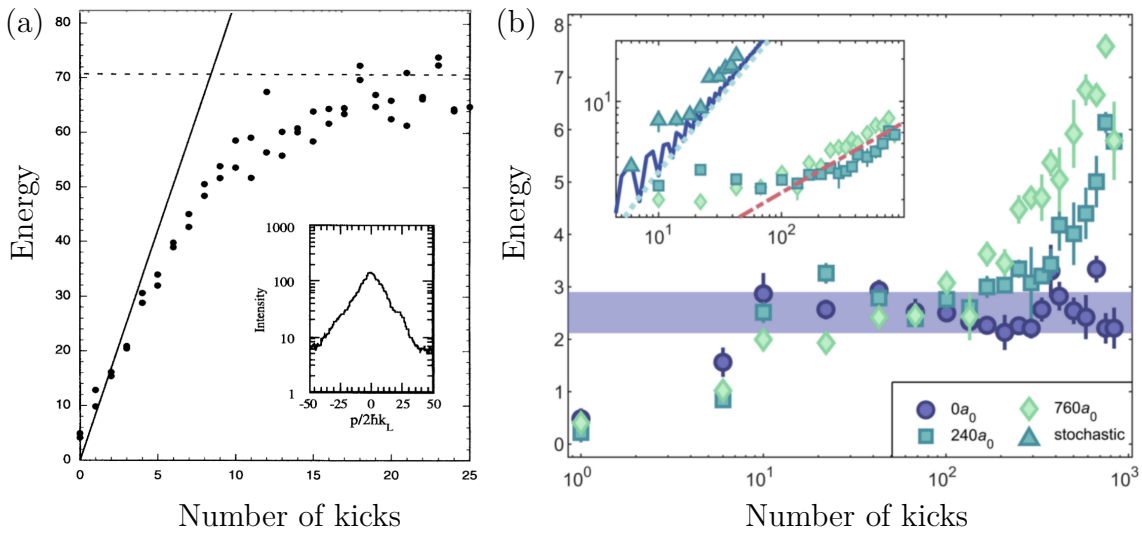

Figure 4.1: (a) Kinetic energy $E(t)$ of the kicked rotor as a function of the stroboscopic time (number of kicks), as measured in Ref. [182]. $E(t)$ is in units of the recoil energy $E_R = \hbar^2 k_L^2/2m$, where k_L is the wave number of the laser used to kick the atoms of mass m. At short times, the wave packet spreads according to the diffusive law $E(t) \sim t$ (plain line). Diffusion is suppressed after a sufficient number of kicks, a phenomenon known as dynamical localization. Inset: profile of the wave function in momentum space once dynamical localization is established (i.e., after a few tens of kicks). The results show that the momentum density, measured by means of a time-of-flight technique, decays exponentially. (b) The same experiment was carried in a more recent cold atom setup [189]. Here the authors could probe the effect of atomic interactions well beyond the localization time, using a Feshbach resonance to tune the interaction strength g between particles (here, g is proportional to the scattering length a expressed in units of the Bohr radius a_0). The horizontal shaded region corresponds to the localization energy scale. Inset: at late times, localization breaks down and is replaced by a sub-diffusive behavior where the energy grows as $\sqrt{t}$ (dashed line). The "stochastic" data refer to a case where the period of the kicks fluctuates randomly, which leads to classical diffusive behavior (dotted line).

4.1.2 Effect of finite pulses

Historically, the specific role of the driving function $F(t)$ was one of the first object of study in the quantum kicked rotor. More precisely, the broadening of pulses with respect to the idealization of δ-kicks was first investigated theoretically in Ref. [191] and later experimentally in the second generation of Raizen's experiment [192–194]. Importantly, it was understood that dynamical localization subsists for kicks of finite duration, such as square pulses [193] or Gaussian pulses [191, 194], although requiring a number of adjustments in the theory. For instance, for square pulses of height $\sim f$ and duration $\sim 1/f$, momentum transport is limited to a band $|p| < f$, leading to bimodal momentum distributions after the localization time (cf. Fig. 7 in Ref. [193]). Furthermore, the localization length was found to be reduced compared to the δ-kicks limit [189]. Nevertheless, the finite duration of the kicks was not deemed a significant limitation for the phenomenon of dynamical localization itself. For the problem of periodically-kicked interactions introduced in Sec. 4.2 below, we will see in the next chapter that the conclusion is dramatically different.

4.1.3 Effect of atomic interactions

In the bosonic quantum kicked rotor, the role of weak interactions was studied theoretically in [195–200]. To this aim, these works simply added to $\hat{H}_\alpha$ a mean-field term representing interactions between bosonic particles:

$$\hat{H}_\alpha = \hat{p}^2/2m + g|\psi(x,t)|^2, \quad \hat{H}_\beta = K\cos(\hat{x}). \tag{4.3}$$

Due to the time dependence of the wave function in $\hat{H}_\alpha$, the Hamiltonian (4.1) with H_α given by (4.3) is no longer periodic in time. As a consequence, the standard tools of Floquet theory [6] cannot be used, which represents a significant complication. It has been found that even a weak nonlinearity may have a dramatic impact on the dynamics, by breaking the localization of wave packets, leading instead to a sub-diffusive spreading. Such algebraic law $\langle \hat{p}^2/2m \rangle \sim t^\nu$ was observed very recently in two cold-atom experiments [189, 190], and the rough estimate $\nu \simeq 1/2$ was found [189] [see Fig. 4.1(b)]. It should be noted that a similar phenomenon was also pointed out in nonlinear, spatially disordered chains [197, 201–206]. In the next chapter, we will observe and analyze a closely related sub-diffusion mechanism, with similar sub-diffusive exponent, in a different system involving kicked interactions. Let us finally mention that a many-body version of the quantum kicked rotor was studied in Ref. [207, 208], in a regime of strong interactions where dynamical localization may survive.

4.2 Gross-Pitaevskii map

Recently, a model presenting some resemblance with the interacting kicked rotor (4.3) was introduced and studied theoretically in Ref. [61] (see also [60] for an early discussion of a closely related problem). It addresses the mean-field, dynamical evolution of a one-dimensional Bose gas with a time-dependent interaction coupling parameter. More precisely, the "Gross-Pitaevskii map" (we borrow Guarneri's terminology [62]) is defined by the Hamiltonian (4.1), where the δ-kicks are no longer made up of a $K\cos(\hat{x})$ potential but of the self-interacting term $g|\psi|^2$, i.e.,

$$\hat{H} = \hat{p}^2/2m + g|\psi(x,t)|^2 \times \sum_n \delta(t-n), \tag{4.4}$$

with normalization $\int dx|\psi(x,t)|^2 = 1$ and where periodic boundary conditions on the wave packet are assumed. Like in the kicked rotor, the relevant dynamics is here observed in momentum space, i.e., by probing the time evolution of the Fourier transform of $\psi(x,t)$, defined as

$$\psi_q(t) = \frac{1}{\sqrt{2\pi}} \int_0^{2\pi} dx\, e^{iqx}\psi(x,t). \tag{4.5}$$

Recalling that permissible reduced momenta $q \in \mathbb{Z}$, this relation can be inverted as

$$\psi(x,t) = \frac{1}{\sqrt{2\pi}} \sum_q e^{-iqx}\psi_q(t), \tag{4.6}$$

with the normalization $\sum_q |\psi_q(t)|^2 = 1$. Using the model (4.4), the authors of [61, 62] observed a strongly chaotic dynamics characterized by an *exponential spreading* of the wave function in momentum space, which we review below in Sec. 4.2.2. In [63], this model was also shown to support stroboscopic solitonic solutions in position space.

4.2.1 Numerical implementation

Random Gross-Pitaevskii map The time evolution of the wave function ψ during one period (free evolution and kick) can be accurately described by the evolution operator

$$\hat{\mathcal{U}}(n) = \exp(-ig|\psi(x,t=n-1)|^2)\exp(-i\phi_q), \tag{4.7}$$

where we have replaced the deterministic phase induced by the free evolution term $\hat{p}^2/2m$ by a random variable ϕ_q distributed over $[0,2\pi]$. To ensure the validity of the latter approximation, it is possible to introduce a period T in the time modulation F and impose $T \gg 2m$. In Eq. (4.4), we have set $T = 1$ for simplicity, but an extension to a more generic drive is straightforward, as will be discussed in Sec. 5.2 of the next chapter. Quantities of interest of the Gross-Pitaevskii map (dispersion,

condensate fraction, etc) are typically not self-averaging and, therefore, a benefit of the *random* variant (4.7) is to facilitate the process of averaging. Conveniently, such averaging procedure also excludes a number of phenomena, like quantum resonances [209–211], which are not the primary focus of our study.

Initial state To numerically describe the dynamics entailed by Eq. (4.4), one needs to evolve a given initial state with the evolution operator (4.7). To this aim, in the following we take as an initial state the wave function

$$\psi_q(t=0) \propto \exp(-\lambda^2 q^2), \tag{4.8}$$

of momentum width λ^{-1} typically smaller than 1. In practice, this state is a good model for the narrow momentum distribution of a Bose-Einstein condensate. Note that the corresponding spatial distribution is broad, nearly uniform at the scale of the system size, and it remains uniform on average during the time evolution (this was also the configuration of [62]).

In order to numerically describe the evolution of the wave packet $\psi_q(t)$, we successively apply the evolution operator (4.7) to the initial state (4.8), using a split-step method to evaluate the wave function at each stroboscopic time. In the simulations we discretize the spatial interval $[0, 2\pi]$ into N_s spatial steps, where $N_s \gg 1$. All our results, finally, are averaged over typically $N_r \sim 10^4$ realizations of the random phase ϕ_q. Some observables of interest, like $|\psi_0|^2$, are however very sensitive to the numerical instability inherent to the nonlinear Schrödinger equation [212, 213]. These instabilities are discussed in more detail in Appendix C. In order to circumvent them, we have worked with a high-precision arithmetic whenever exponential sensitivity to initial conditions was the limiting factor. Typically, our algorithm ensured $N_d = 100$ significant decimal digits. We have systematically checked that increasing N_s or N_d does not alter our numerical calculations.

4.2.2 Wave-packet spreading

To characterize the temporal spreading of the wave packet (4.8) subjected to the interaction kicks, we examine the temporal evolution of its mean-square width in momentum space,

$$\sigma^2(t) = \sum_q q^2 \, \overline{|\psi_q(t)|^2}. \tag{4.9}$$

Here, the overbar refers to averaging over the random phase ϕ_q accumulated between the kicks. The corresponding time evolution of $\sigma^2(t)$ is shown in Fig. 4.2. It is exponential, and characterized by two distinct dynamical regimes separated by a certain characteristic time t_E. $\sigma^2(t)$ first grows exponentially up to t_E, then, for $t > t_E$, the increase slows down albeit it remains exponential. Such an exponential spreading was confirmed by methods of classical chaos based on the calculation of Lyapunov exponents [62] and on a mapping with a generalized kicked rotor [61].

At weak interaction strength $g/2\pi \ll 1$ and in the short-time regime, the mean-square width (4.9) is dominated by the contribution of the first mode, i.e., $\sigma^2(t) \simeq 2|\overline{\psi_1(t)}|^2$. Therefore, in Sec. 4.2.3, we study of the growth of the average population of the first Fourier mode. Our main result [cf. Eq. (4.21)] which was not discussed in the previous work [61, 62], is displayed in Fig. 4.2 (dashed curve), and matches very well the numerical simulations.

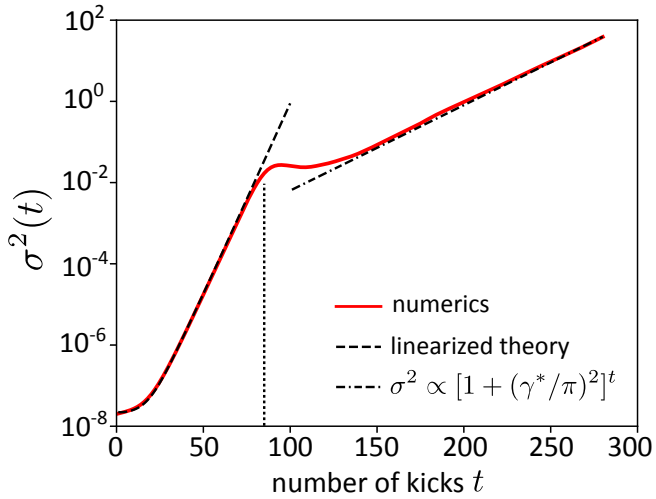

Figure 4.2: Mean-square width of the wave packet as a function of the number of kicks t, for the Gross-Pitaevskii map. Here $g = 0.7$, $\lambda = 3.03$. The dashed curve is the theoretical prediction for short times, Eq. (4.21), and the dashed-dotted curve is the prediction of [61, 62] for long times, Eq. (4.10). The vertical dotted line indicates the position of the characteristic time t_E separating the two regimes of exponential growth, given by Eq. (4.22).

At $t \sim t_E$, the modes $|q| > 1$ start to significantly impact the dynamics (see also Sec. 4.2.4). For this reason, t_E has the physical meaning of the typical time needed for the wave function to spread over a significant portion of phase space, the so-called Ehrenfest time [6]. We will use this terminology from now on.

The momentum dispersion in the regime $t > t_E$ was studied in the previous works [61, 62], where it was found that

$$\sigma^2(t) \sim \exp[t \ln(1 + (g/\pi)^2)]. \tag{4.10}$$

In [62], in particular, the authors derived this exponential growth by rewriting Eq. (4.4) in the form of a generalized kicked-rotor model and by studying the evolution of $\sigma^2(t)$ in the corresponding classical map. A similar exponential growth was also found in [60], in a slightly different model involving a linear kicking potential on top of the nonlinear sequence of kicks. The exponential law (4.10) is shown in Fig. 4.2, and well captures the numerical results at long time.

In the next subsection, we present a theoretical perturbative description allowing us to provide an analytical expression for the growth rate at short time (corresponding to the first dashed curve in Fig. 4.2). Then we further elaborate on the random Gross-Pitaevskii map, by examining the time evolution of the condensate fraction under the interactions kicks. All these results serve as a benchmark for the regime of kicks of finite duration that will be addressed in the next chapter and for which a novel physics, different from that of Fig. 4.2, emerges.

4.2.3 Growth and saturation of the first Fourier mode

In this section, we compute the average population of the first Fourier mode that governs the early stage of the dynamics. This calculation is, in particular, useful to explain the first exponential slope in Fig. 4.2. Indeed, if the initial state (4.8) is sufficiently peaked, $\lambda \gg 1$, the momentum dispersion is approximately $\sigma^2(t) \simeq 2\overline{|\psi_1(t)|^2}$ until the Ehrenfest time is reached.

Before proceeding with the calculation of $\overline{|\psi_1(t)|^2}$, we mention an alternative representation of our model. The (random) Gross-Pitaevskii map characterized by Eq. (4.7) can also be represented by the Hamiltonian

$$\hat{H} = g|\psi(x,t)|^2 + \hat{A}_q \times \sum_n \delta(t-n), \tag{4.11}$$

where $\hat{A}_q$ is the operator that multiplies the Fourier modes by the random phase $\exp(-i\phi_q)$. In between the kicks, which are now composed of the random phases, the system evolves according to the equation of motion

$$i\partial_t \psi(x,t) = g|\psi(x,t)|^2 \psi(x,t). \tag{4.12}$$

Therefore, over one period, the evolution operator related to the Hamiltonian (4.11) can be written as

$$\hat{\mathcal{U}}(n) = \exp\left[-i\int_{n-1}^{n} dt\, g|\psi(x,t)|^2\right] \exp(-i\phi_q), \tag{4.13}$$

which is equal to Eq. (4.7) due to the conservation of $|\psi(x,t)|^2$ under the dynamics governed by Eq. (4.12). Indeed, in the density-phase formalism $\psi = \sqrt{n}e^{i\theta}$, one immediately obtains $\partial_t n = 0$. While Eq. (4.7) is easily evolved numerically, the propagator (4.13) is more convenient do deal with analytically [see Eq. (4.14)].

We now have all the necessary tools to compute the average population of the first Fourier mode $\overline{|\psi_1|^2}(t)$ under the evolution operator (4.13).

Short times The growth of $|\psi_1|^2$ corresponds to a fast initial depletion of the condensate from $q = 0$ to the neighboring momentum sites $q \neq 0$. To describe it quantitatively, we start from the evolution equation of the Fourier modes during a given kick n:

$$i\partial_t \psi_q = \frac{g}{2\pi} \sum_{q_1,q_2} \psi^*_{q_1} \psi_{q_2} \psi_{q+q_1-q_2}. \tag{4.14}$$

This equation corresponds to the first exponential term in the evolution operator $\hat{\mathcal{U}}(n)$, and is the Fourier transform of Eq. (4.12) mentioned above.

At short time, mostly modes $q = -1, 0, 1$ are populated. Neglecting the other modes and assuming $|\psi_j|^2 \ll |\psi_0|^2$ $(j = \pm 1)$, we can linearize Eq. (4.14), which leads to $\psi_0(t) \simeq \psi_0(n-1)\exp[-ig(t-n+1)/2\pi]$ and

$$i\partial_t \psi_j \simeq \frac{g}{\pi}\psi_j + \frac{g}{2\pi}\psi_0^2 \psi_{-j}^*. \tag{4.15}$$

These equations still contain nonlinear factors that are conveniently removed with the gauge transformation $\tilde{\psi}_j = \psi_j/\psi_0$. Then we introduce the circular state vector for the first Fourier mode after the kick n, $\Gamma(n) = (\Re\,\tilde{\psi}_1(n), \Im\,\tilde{\psi}_1(n))^\intercal$, and assume for simplicity[1] $\tilde{\psi}_1 = \tilde{\psi}_{-1}$. The propagation of this state vector over one period obeys $\Gamma(n) = U\ \Gamma(n-1)$, where the transfer matrix U is given by

$$U \simeq \begin{pmatrix} 1 & 0 \\ -g/\pi & 1 \end{pmatrix} \begin{pmatrix} \cos\phi_1 & -\sin\phi_1 \\ \sin\phi_1 & \cos\phi_1 \end{pmatrix}. \tag{4.16}$$

The second matrix in the right-hand side describes the free-space propagation between two interacting pulses, which involves the uniformly distributed kinetic phase ϕ_1, see Eq. (5.8). The first matrix, on the other hand, describes the propagation during the kick n, and is inferred from Eq. (4.15) and its complex-conjugated version. The average population of the first Fourier mode after n kicks, finally, follows from:

$$\overline{|\psi_1(t=n)|^2} = \frac{1}{2\pi}\int_{-\pi}^{\pi} d\phi_1\, \|U^n \Gamma(0)\|^2, \tag{4.17}$$

where the transfer matrix U is given by Eq. (4.16), and the initial state vector is $\Gamma(0) = (e^{-\lambda^2}, 0)^\intercal$. By symmetry, the contribution of negative ϕ_1 equals the one of positive ϕ_1, so that the integral average in Eq. (4.17) can be replaced by $1/\pi \int_0^\pi d\phi_1$. Explicitly, the matrix U reads

$$U = \begin{pmatrix} \cos\phi_1 & -\sin\phi_1 \\ -\frac{g}{\pi}\cos\phi_1 + \sin\phi_1 & \cos\phi_1 + \frac{g}{\pi}\sin\phi_1 \end{pmatrix}, \tag{4.18}$$

whose eigenvalues are of the form $\mu \pm \sqrt{\mu^2 - 1}$, with $\mu = \cos\phi_1 + (g/2\pi)\sin\phi_1$. For values of ϕ_1 such that $\mu^2 - 1 < 0$, the spectrum of U is unimodular. The exponential growth of the first Fourier mode observed in the numerical simulations, on the other hand, stems from the contributions of ϕ_1 such that $\mu^2 - 1 > 0$. Indeed, in this case one of the two (distinct) eigenvalues is of modulus strictly larger than

[1] This assumption amounts to imposing $\phi_1 = \phi_{-1}$. Although this condition is not strictly verified for a given realization of the random phase, we have verified that the final result is unchanged when one considers $\phi_1 \neq \phi_{-1}$. Indeed, in this case the eigenvalues of U, which is now a 4×4 matrix, are given by $e^{-i(\phi_1 - \phi_{-1})/2}(\mu \pm \sqrt{\mu^2 - 1})$. This is the same form as in the case $\phi_1 = \phi_{-1}$, except for the additional phase factor $e^{-i(\phi_1 - \phi_{-1})/2}$, which nevertheless has no impact on the final result, Eq. (4.21).

one, eventually leading to an exponential growth of $\overline{|\psi_1(t)|^2}$. For weak interactions $g/2\pi \ll 1$, $\mu^2 - 1 \simeq \phi_1(g/\pi - \phi_1)$ such that the values of ϕ_1 leading to $\mu^2 - 1 > 0$ lie in the interval $[0, g/\pi]$. Note that this upper bound also defines the probability $\mathcal{P} = g/\pi^2$ that the first excitation grows exponentially when one "draws" a value of ϕ_1.

The diagonalization of U provides

$$U^n \Gamma(0) = -\exp(-\lambda^2) \begin{pmatrix} \frac{\eta}{x} \sinh xn - \cosh xn \\ \frac{\nu}{x} \sinh xn \end{pmatrix}, \tag{4.19}$$

for $g \ll 1$, where $\eta = \phi_1 g/2\pi$, $x = \sqrt{\phi_1(g/\pi - \phi_1)}$ and $\nu = g/\pi - \phi_1$. At leading order in g, this leads to

$$\overline{|\psi_1(t = n)|^2} \simeq e^{-2\lambda^2} + \frac{g e^{-2\lambda^2}}{\pi^2} \int_0^{g/\pi} \frac{d\phi_1}{\phi_1} \sinh^2[t\sqrt{\phi_1(g/\pi - \phi_1)}]. \tag{4.20}$$

The integral over ϕ_1 can be calculated by a saddle point approximation, the saddle point being $\phi_1 = g/2\pi$. This gives

$$\overline{|\psi_1(t)|^2} \simeq e^{-2\lambda^2} \left[1 + \frac{1}{2\pi}\sqrt{\frac{g}{2t}} e^{gt/\pi}\right]. \tag{4.21}$$

This analytical result is displayed in Fig. 4.3(a), on top of the exact numerical resolution of the random Gross-Pitaevskii map. As announced, the agreement is very good up to the vicinity of the Ehrenfest time.

Intermediate times The above approach can also be used to access the Ehrenfest time, by noting that at $t \sim t_E$ the linearization breaks down. Precisely, we find t_E from the condition $\max_{\phi_1} \|U^{t_E}\Gamma(0)\|^2 = 1/2$, i.e., from the specific configuration where $|\psi_1|^2$ is maximal and becomes of the order of $|\psi_0|^2$ (recall that, as long as only two modes are considered, $|\psi_0|^2 + 2|\psi_1|^2 = 1$ due to the normalization). This criterion leads to

$$t_E \simeq \frac{2\pi\lambda^2}{g}. \tag{4.22}$$

The Ehrenfest time t_E thus represents the limit between linear and nonlinear dynamics. To provide a better and complementary understanding of the latter, in Appendix D we elaborate on the above two-modes approximation, by proposing a slightly more involved approach where the equations are *not* linearized as was done in Eq. (4.15). Those calculations rely on the density-phase formalism and take advantage of the exact solution of a Bernoulli differential equation. They provide (see Appendix D) the more accurate result:

$$\overline{|\psi_1(t)|^2} \simeq e^{-2\lambda^2} + \frac{g}{\pi^2} \int_0^1 \frac{d\alpha}{2 + \frac{|\alpha - 1/8|}{\alpha(1-\alpha)} \cosh\left[2g\sqrt{\alpha(1-\alpha)}(t - 2t_h)/\pi\right]}, \tag{4.23}$$

which is shown in Fig. 4.3(a) and is in good agreement with the numerical simulations even slightly beyond the Ehrenfest time. Here, t_h is given by Eq. (D.6).

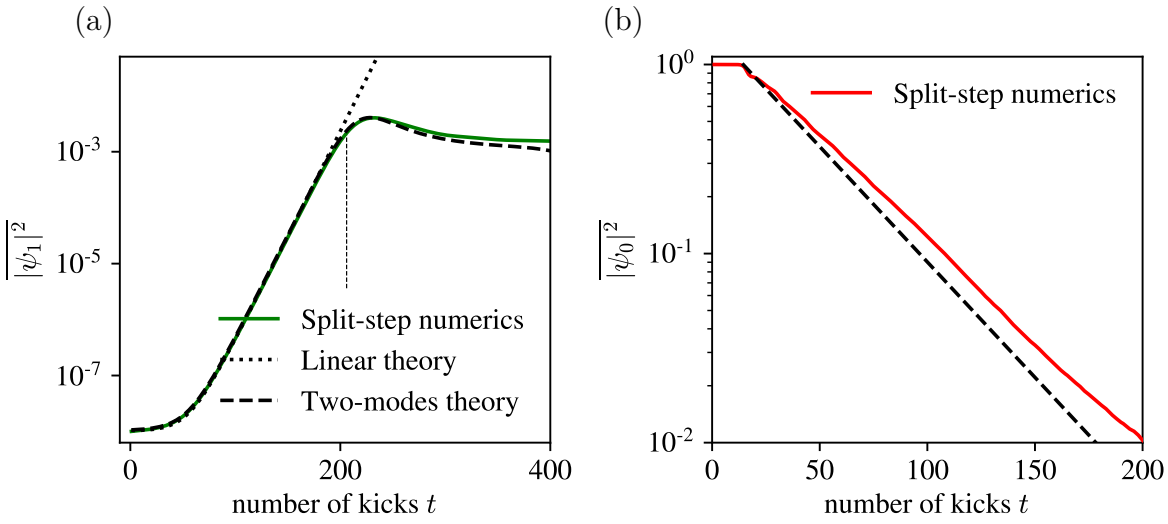

Figure 4.3: (a) Time evolution of the average population of the first Fourier mode of the wave packet with the initial condition (4.8). The growth is at first exponential, a behavior which is well described by Eq. (4.21). At times later than $t_E \simeq 210$ (vertical line), which marks the end of the validity of the linear theory, this growth saturates and $\overline{|\psi_1(t)|^2}$ slightly decreases. This saturation is well predicted by the two-modes theory represented by Eq. (D.8) of Appendix D. The parameters are $\lambda = 3.03$ and $g = 0.28$. (b) Condensate fraction versus time for $g = 4$. After t_E, the condensate is depleted exponentially by the growth of q-modes with $q \geq 1$. The dashed line is the estimate (4.31).

4.2.4 Exponential depletion of the condensate

The increase of the first Fourier mode, in turn, contributes to the depletion of the condensate population. Numerically, we find that the condensate fraction decays exponentially from t_E:

$$\overline{|\psi_0(t)|^2} \simeq \exp[-(t - t_E)/\tau]. \tag{4.24}$$

To understand this behavior and access the time scale τ, we note that $\overline{|\psi_0(t)|^2}$ is essentially the probability for the condensate mode to remain populated at time t. This probability is governed by specific realizations of the random phases $(\phi_1, \phi_2, \dots)$ for which the small-q modes have not grown exponentially at a time t larger than t_E. Below we show that for such realizations the time at which the mode q grows exponentially while the first $q - 1$ modes do not is $t_q = qt_E$, and that the probability for a given mode population $|\psi_q|^2$ to grow exponentially is

$\mathcal{P} = g/\pi^2 \ll 1$. Together, these two parameters yield the exponential decay mentioned above.

To this aim, we start by considering realizations of ϕ_1 and ϕ_2 for which the population $|\psi_2|^2$ grows exponentially but the population $|\psi_1|^2$ does not. According to the analysis of Sec. 4.2.3, $|\psi_1|^2$ does not grow exponentially when $\phi_1 \in I = [g/\pi, \pi]$ and, for weak interactions, this event occurs with the probability $1-\mathcal{P} \simeq 1$. In that case, the spectrum of the transfer matrix U is unimodular, so that ψ_1 rotates in time in the complex plane. The depletion of $|\psi_0|^2$ is then mainly controlled by the behavior of the second excitation. Our aim is then to find the new time scale t_2 at which the linearization breaks down due to the exponential growth of $|\psi_2|^2$. Similarly to Sec. 4.2.3, this can be achieved by linearizing the Gross-Pitaevskii equation (4.14) keeping the modes $q = 0, 1, 2$ only, and identifying t_2 as the time where the linearization procedure breaks down. Let us call Γ_2 the state vector of the second mode, $\Gamma_2 = (\Re\,\tilde{\psi}_2, \Im\,\tilde{\psi}_2)^\intercal$, where $\tilde{\psi}_2 = \psi_2/\psi_0$. Linearization of the equation of motion (4.14) during a pulse gives

$$d_t\Gamma_2 = \begin{pmatrix} 0 & 0 \\ -g/\pi & 0 \end{pmatrix}\Gamma_2 + \frac{g}{2\pi}\begin{pmatrix} \Im\,\tilde{\psi}_1^2 \\ -2|\tilde{\psi}_1|^2 - \Re\,\tilde{\psi}_1^2 \end{pmatrix}. \tag{4.25}$$

Over one period, this can be written as

$$\Gamma_2(n) = U\Gamma_2(n-1) + \Sigma(n), \tag{4.26}$$

where $\Sigma(n)$ refers to the rightmost term of Eq. (4.25), which implicitly depends on ϕ_1. U now denotes the transfer matrix (4.16) where ϕ_1 has been replaced by ϕ_2. Using that $\|U\Gamma_2(0)\| \sim e^{-4\lambda^2} \ll \|\Sigma(1)\| \sim e^{-2\lambda^2}$, we obtain

$$\Gamma_2(n) = \sum_{m=0}^{n-1} U^m\Sigma(n-m), \tag{4.27}$$

for times $n \geq 1$. Since $\tilde{\psi}_1$ rotates in the complex plane, we also infer $\|\Sigma(m)\| \sim e^{-2\lambda^2}$. Therefore, the same argument as in Sec. 4.2.3 shows that the exponential grows of $\langle|\psi_2(t)|^2\rangle_{\phi_1\in I}$ arises for realizations $\phi_2 \in \bar{I} = [0, g/\pi]$, occurring with probability $\mathcal{P} = g/\pi^2$. The average population of the second mode is then mainly governed by the integral $\int d\phi_2\|U^{n-1}\Sigma(1)\|^2$, which can evaluated by a saddle point approximation similar to the procedure employed in Eq. (4.20). We find:

$$\langle|\psi_2(t=n)|^2\rangle_{\phi_1\in I} \propto \exp(-4\lambda^2)\exp\left[g(t-1)/\pi\right]. \tag{4.28}$$

Up to logarithmic corrections, the only difference with the second term in the r.h.s. of Eq. (4.21) stems from the different prefactor $e^{-4\lambda^2}$ instead of $e^{-2\lambda^2}$. Accordingly, the time scale t_2 at which the linearization hypothesis breaks down is given by

$$t_2 \simeq \frac{4\pi\lambda^2}{g} = 2t_E. \tag{4.29}$$

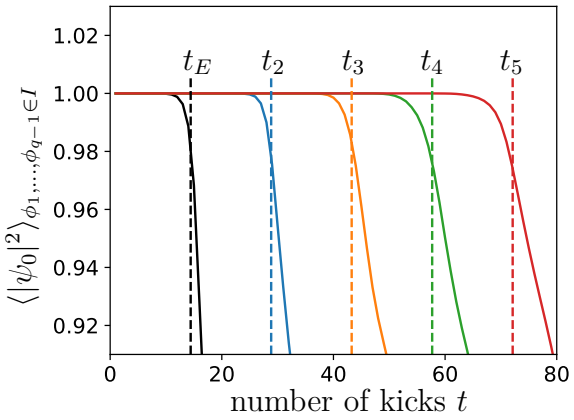

Figure 4.4: Condensed fraction $\langle|\psi_0|^2\rangle_{\phi_1,\ldots,\phi_{q-1}\in I}$ for $q = 1, \ldots, 5$ from left to right. These curves are numerically obtained by averaging the population $|\psi_0|^2$ over the random vector $(\phi_1, \phi_2 \ldots)$ under the constraint $\phi_1, \ldots, \phi_{q-1} \in I$. The case $q = 1$ (black curve) coincides with the unrestricted average $\overline{|\psi_0|^2}$. Here $\lambda = 3.03$ and $g = 4$. Vertical dashed lines indicate the positions of the theoretical predictions (4.30) for t_q.

This analysis can be extended to higher $q > 2$: we consider events of probability $(1 - \mathcal{P})^{q-1}$ for which $\phi_1, \ldots, \phi_{q-1} \in I$. Then, the depletion of the condensate is mostly controlled by the q-th mode, and the typical time scale at which linearization breaks down is

$$t_q \simeq q t_E. \tag{4.30}$$

We have corroborated this prediction numerically by computing the average population $\langle|\psi_0|^2\rangle$ under the constraint $\phi_1, \ldots, \phi_{q-1} \in I$, see Fig. (4.4).

Finally, we infer

$$\begin{aligned} \overline{|\psi_0(t_q)|^2} &\simeq (1 - \mathcal{P})^{q-1} \simeq \exp[-(q-1)\mathcal{P}] \\ &= \exp[-g(t_q - t_E)/(\pi^2 t_E)]. \end{aligned} \tag{4.31}$$

This argument confirms the numerical observation, and identifies the characteristic time τ to deplete the condensate as

$$\tau \simeq \frac{\pi^2 t_E}{g} = \frac{2\pi^3 \lambda^2}{g^2}. \tag{4.32}$$

We have also studied this time scale numerically as a function of g and λ, as shown by the two plots in Fig. 4.5, and the results agree with the prediction (4.32).

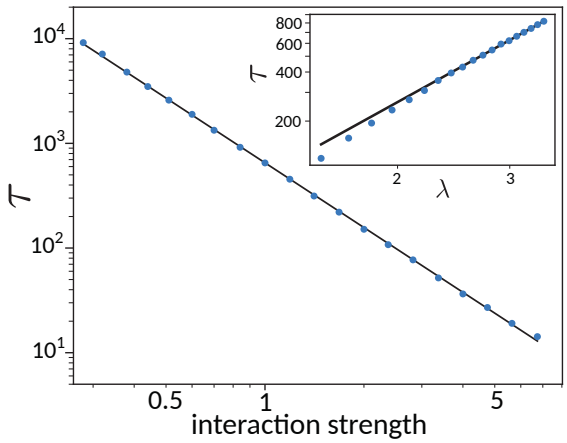

Figure 4.5: Characteristic time governing the exponential decay $\overline{|\psi_0(t)|^2} \sim \exp(-(t-t_E)/\tau)$ of the average condensate fraction in the Gross-Pitaevskii map, extracted from numerical simulations. The main panel shows τ as a function of the interaction strength g, at fixed $\lambda = 3.03$. Dots are numerical data and the solid curve is a linear fit providing $\tau \propto 1/g^{2.05}$. The inset shows τ as a function of λ, at fixed $g = 1$. The solid curve is a linear fit giving $\tau \propto \lambda^{2.16}$. Together, the plots provide $\tau \simeq 70.8\lambda^{2.16}/g^{2.05}$, in very good agreement with the theoretical prediction (4.32).

Conclusion

In this chapter, we have first introduced the quantum kicked rotor (4.2) and dynamical localization, emphasizing how this phenomenon is modified when interactions are taken into account at the mean-field level, and when kicks of finite duration are considered. We then studied more quantitatively various properties of the less known Gross-Pitaevskii map (4.4), a model that also displays remarkable transport properties, in particular an (ultrafast) exponential spreading of wave packets. We have complemented existing results in the literature on the wave packets dispersion by investigating the evolution of the average population of the first excitation [Eqs. (4.21) and (4.23)], as well as the exponential depletion of the "condensate" mode beyond the Ehrenfest time, Eq. (4.24).

Chapter 5

Sub-diffusion of wave packets with periodically kicked interactions

In the previous chapter, we presented two models of periodically driven 1D Bose gases exhibiting dramatically different dynamics. In the first one, the quantum kicked rotor, diffusion is completely suppressed in momentum space after a few tens of kicks. In contrast, for the Gross-Pitaevskii map, wave packets spread exponentially fast at all times in Fourier space. In this chapter, we revisit the Gross-Pitaevskii map by considering interaction kicks of arbitrary duration. While we recover the exponential spreading in the limit of delta kicks, we find that, as soon as the kicks are finite, the spreading is no longer exponential but rather sub-diffusive at long time. This phenomenon stems from the competition between the kinetic and interaction energies within the kicks, which is absent in the limit of delta kicks. At the microscopic level, we interpret this sub-diffusive spreading in terms of a mechanism of incoherent coupling of the momentum sites, a phenomenon that also occurs in the interacting version of the kicked rotor. Regarding the shape of the momentum distribution, we find that the periodically kicked interactions first give rise to an early-time exponential depletion of the condensate mode, quickly followed by the emergence of a "thermal" background of particles spreading sub-diffusively. Our analysis finally shows that the time scale where exponential spreading breaks down scales logarithmically with the kick duration. This indicates that, as soon as the kicks are finite, the sub-diffusive motion tends to take over the exponential spreading at relatively short times, even if extremely short kicks are considered.

5.1 The model

As in the previous chapter, we consider the mean-field, dynamical evolution of a one-dimensional Bose gas described by the Gross-Pitaevskii equation

$$i\hbar\partial_{\mathsf{t}}\Psi(\mathsf{x},\mathsf{t}) = \frac{\hat{\mathsf{p}}^2}{2m}\Psi(\mathsf{x},\mathsf{t}) + g(\mathsf{t})|\Psi(\mathsf{x},\mathsf{t})|^2\Psi(\mathsf{x},\mathsf{t}), \tag{5.1}$$

with normalization $\int d\mathsf{x}|\Psi(\mathsf{x},\mathsf{t})|^2 = 1$ for the wave function $\Psi(\mathsf{x},\mathsf{t})$. The momentum operator is $\hat{\mathsf{p}} = -i\hbar\partial_{\mathsf{x}}$. Instead of a periodic sequence of Dirac delta peaks, we now assume that the time dependent interaction strength takes the form of a more realistic sequence of square pulses of period T, width δt and amplitude gN, with g the interaction parameter and N the total number of particles:

$$g(\mathsf{t}) = \begin{cases} 0 & \text{if } \mathsf{t} \in [nT, (n+1)T - \delta t], \;\; n \in \mathbb{Z}, \\ gN & \text{otherwise.} \end{cases} \tag{5.2}$$

In practice, such a sequence can be realized by applying a periodic magnetic field modulation to the atomic cloud, exploiting a Feshbach resonance. From now on, we denote by L the system size and assume periodic boundary conditions, thus describing a ring geometry. This implies that the eigenstates p of the momentum operator are quantized in units of $2\pi\hbar q/L$, where $q \in \mathbb{Z}$ is an integer.

5.2 Dimensionless formulation

To study the time evolution entailed by the sequence (5.2), it is convenient to work with a dimensionless version of Eq. (5.1). To this aim, we first rescale position, time and wave function according to

$$t = \mathsf{t}/T, \quad x = 2\pi\mathsf{x}/L, \quad |\psi|^2 = |\Psi|^2 L/2\pi, \tag{5.3}$$

and introduce the effective Planck constant

$$\hbar_{\text{eff}} = \frac{\hbar T}{m}\left(\frac{2\pi}{L}\right)^2. \tag{5.4}$$

This leads to the dimensionless Gross-Pitaevskii equation

$$i\hbar_{\text{eff}}\partial_t\psi(x,t) = \frac{\hbar_{\text{eff}}^2\hat{q}^2}{2}\psi(x,t) + \gamma(t)|\psi(x,t)|^2\psi(x,t), \tag{5.5}$$

where the reduced momentum operator is $\hat{q} = -i\partial_x$. The dimensionless position x lies in the interval $[0, 2\pi)$, and the new wave function still obeys $\int dx|\psi(x,t)|^2 = 1$. The dimensionless, self-interaction modulation is now given by

$$\gamma(t) = \begin{cases} 0 & \text{if } t \in [n, n+1-\delta t/T], \;\; n \in \mathbb{Z}, \\ \gamma & \text{otherwise,} \end{cases} \tag{5.6}$$

where $\gamma = 2\pi gN\hbar_{\text{eff}}T/L\hbar$.

In the previous chapter, Eqs. (5.5) and (5.6) were investigated in the limit of Dirac delta kicks, i.e., for $\delta t/T \to 0$, $\gamma \to \infty$ with the product $\gamma\delta t/T$ constant: $\gamma(t) = \gamma\delta t/T\sum_n \delta(t-n)$. A particular consequence of taking the limit of pure delta kicks is that the kinetic energy is irrelevant at the specific times where the kicks are

nonzero. This is no longer the case as soon as the kick duration is finite: during the kicks, the kinetic energy cannot be neglected and competes with the interaction term. This is precisely the situation we explore in the following, where we will show that this competition dramatically modifies the spreading of wave packets.

The time evolution of the state vector during one period (free evolution and kick) is governed by the evolution operator

$$\hat{\mathcal{U}}(n) = \mathcal{T} \exp\left[-i\int_{n-\delta t/T}^{n} dt' \left(\frac{\hbar_{\text{eff}}\hat{q}^2}{2} + \frac{\gamma|\psi|^2}{\hbar_{\text{eff}}}\right)\right] \times \exp\left[-i\int_{n-1}^{n-\delta t/T} dt' \frac{\hbar_{\text{eff}}\hat{q}^2}{2}\right], \tag{5.7}$$

where $\mathcal{T}$ is the time-ordering operator. In this expression, the first exponential refers to the evolution during kick n, while the second one describes the free evolution stage before it. To study the system's dynamics, from now on we focus for simplicity on the limit $\hbar_{\text{eff}} \gg 1$, excluding quantum resonances where $\hbar_{\text{eff}}$ is a rational multiple of 4π [214]. Therefore, the phase $\sim \hbar_{\text{eff}}$ accumulated during the free evolution stage is very large, such that it can be accurately replaced by a random variable ϕ_q uniformly distributed over $[0, 2\pi]$. This approximation was already introduced in the previous chapter in Eq. (4.7), and finds here a simple justification in terms of $\hbar_{\text{eff}}$ which can be tuned at will, e.g. by adjusting the period T. Note that we cannot apply the same random phase approximation for the kinetic phase in the first exponential of Eq. (5.7), which is of the order of the product $\hbar_{\text{eff}}\delta t/T$, not necessarily large. To deal with the latter, it is convenient to introduce the change of variables $s\,(n) = (T/\delta t)t' + n(1 - T/\delta t)$, so that

$$\hat{\mathcal{U}}(n) = \mathcal{T} \exp\left[-i\int_{n-1}^{n} ds \left(\frac{\hat{q}^2}{2f^2} + \gamma^*|\psi|^2\right)\right] \exp(-i\phi_q), \tag{5.8}$$

where

$$\gamma^* = \frac{\gamma\delta t}{T\hbar_{\text{eff}}} = \frac{2\pi g N \delta t}{L\hbar} \tag{5.9}$$

is the effective interaction strength, and

$$f = \sqrt{\frac{T}{\delta t \hbar_{\text{eff}}}} = \frac{L}{2\pi}\sqrt{\frac{m}{\delta t \hbar}} \tag{5.10}$$

controls the amplitude of the kinetic energy during the kicks. Information about the finite duration of the kicks is entirely contained in this parameter. In particular, when $f = \infty$ the kinetic term in Eq. (5.8) vanishes and one effectively recovers the delta-kick limit of [61, 62] studied in Sec. 4.2 [the effective interaction strength γ^* was simply denoted by g in the previous chapter, cf. Eq. (4.7)].

5.3 Long-time sub-diffusion

5.3.1 Numerical simulations

The evolution of the wave-packet mean-square width for finite values of f is displayed in Fig. 5.1. The limit $f = \infty$ is also shown for comparison (black curve).

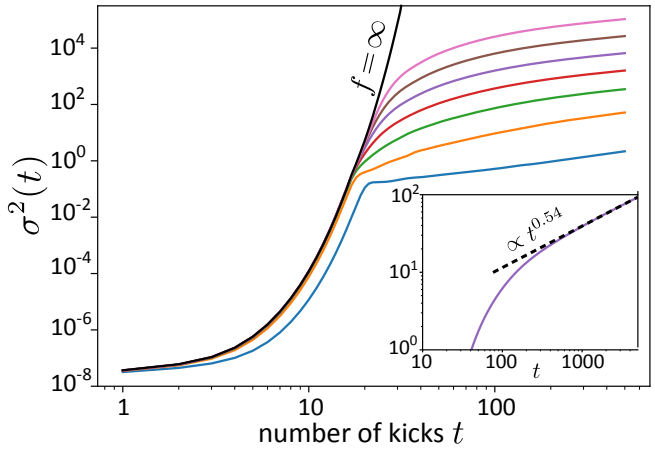

Figure 5.1: Main panel: mean-square width of the wave packet as a function of the number of kicks t up to $t = 600$, for finite, increasing values of f. Solid curves from bottom to top correspond to $f = 1, 2, 4, 8, 16, 32, 64$. Here $\gamma^* = 4$, $\lambda = 3.03$, so that the Ehrenfest time predicted by Eq. (4.22) occurs around $t_E \simeq 14$. The black curve corresponds to numerical results in the limit $f = \infty$ (delta kicks). In contrast to Fig. 4.2, the exponential growth of σ^2 in this plot does not exhibit a visible change in slope. This can be attributed to the use of a log-log scale and to the larger value of γ^* employed here, which makes it more challenging to observe the two exponential regimes shown in Fig. 4.2. Inset: mean-square width up to $t = 5000$ at $f = 16$, emphasizing the sub-diffusive behavior at finite f for $t > t_E$.

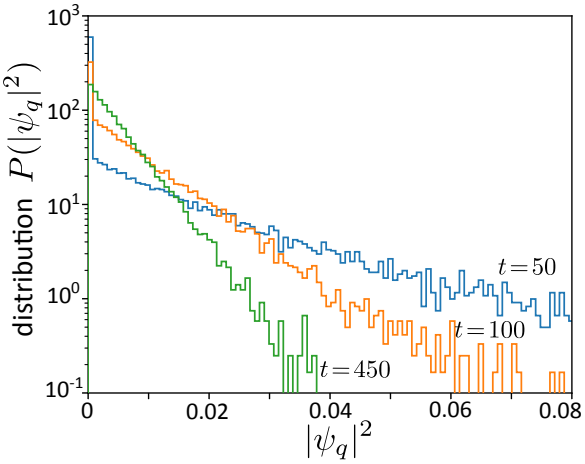

Figure 5.2: Distribution of the momentum density, $P(|\psi_q(t)|^2)$, at different times and fixed $f = 16$ and $\gamma^* = 4$. Here we choose $q = 2$ as an example, the distributions at other q-values behaving similarly. At long time, the distribution becomes exponential, suggesting that the ψ_q are complex random Gaussian variables.

The figure shows that when f is finite, the behavior of $\sigma^2(t)$ at times $t < t_E$ remains well captured by the δ-kicks theory detailed in Sec. 4.2, except, perhaps, for small values of f. On the other hand, a dramatically different evolution emerges beyond t_E: the growth of $\sigma^2(t)$ is no longer exponential but rather algebraic, with a prefactor increasing with f. An analysis up to $t \simeq 5 \times 10^3$ is shown in the inset, and suggests the following algebraic scaling at long time:

$$\sigma^2(t) \propto t^{1/2}. \tag{5.11}$$

5.3.2 Mode-coupling model

The sub-diffusive behavior observed in the numerical simulations can be understood in terms of a mechanism of "heating" where the spreading wave packet is incoherently coupled to its neighboring sites via the nonlinearity. A similar mechanism was shown to also take place in the context of the nonlinear Schrödinger equation in the presence of disorder [195, 196]. To clarify this idea, we start from the evolution equation during a kick at finite f:

$$i\partial_s \psi_q = \frac{q^2}{2f^2}\psi_q + \frac{\gamma^*}{2\pi}\sum_{q_1,q_2} \psi^*_{q_1}\psi_{q_2}\psi_{q+q_1-q_2}. \tag{5.12}$$

Let us now consider a certain momentum-site q located at the border of the spreading wave packet. At the contact with the wave packet, the amplitude of this site evolves according to Eq. (5.12). We then make the hypothesis that the coupling between this site and the spreading wave packet consists in an incoherent heating

mechanism where the second term in the right-hand side of Eq. (5.12) is replaced by a random noise. This assumption is motivated by the fact that the complex amplitudes ψ_q become Gaussian random variables at long enough time, as is confirmed by the numerical simulations in Fig. 5.2. We thus replace Eq. (5.12) by the Langevin equation:

$$i\partial_s \psi_q \simeq \frac{q^2}{2f^2}\psi_q + \frac{\gamma^*}{2\pi} f^2 \rho(s)^{3/2} \eta(s), \tag{5.13}$$

where $\rho(s)$ is the momentum density of the spreading wave packet, which for the simplicity of the argument we here take uniform, and $\eta(s)$ is an uncorrelated random noise, satisfying $\overline{\eta(s)\eta(s')} = \delta(s-s')$. The prefactor $f^2 = \mathcal{N}^2$ stems from the number $\mathcal{N}$ of terms effectively involved in each sum in the right-hand side of Eq. (5.12). At long time, this number must be related to the strength of the kinetic term in Eq. (5.12), which is precisely responsible for the existence of sub-diffusion. As a rough estimate, we identify $\mathcal{N}$ with the typical value of q for which the kinetic term in Eq. (5.12) is of the order of 1, i.e., $q \sim \mathcal{N} \sim f$. This scaling is also in good agreement with a more quantitative analysis of the inverse participation ratio discussed in Appendix E.

For late stroboscopic time $t \gg t_E$, the solution of the Langevin equation for the average squared amplitude at the site q is $\overline{|\psi_q(t)|^2} \sim f^4 \gamma^{*2} \rho^3 t$. From this, we infer that the typical time t_s it takes for the wave packet to "heat" the site q is such that $\rho \sim f^4 \gamma^{*2} \rho^3 t_s$, giving $t_s^{-1} \sim f^4 \gamma^{*2} \rho^2$. Finally, we assume that the wave-packet spreading can be described by a nonlinear diffusion equation of the type $d\sigma^2(t)/dt = D(t)$, with a diffusion coefficient $D(t)$ proportional to the heating rate t_s^{-1}. This leads to

$$\sigma^2(t) \sim f^4 \gamma^{*2} \rho^2 t. \tag{5.14}$$

For a uniform wave packet, $\rho(t) = 1/\sigma(t)$ due to norm conservation. The solution of Eq. (5.14) for $\sigma^2(t)$ then immediately yields

$$\sigma^2(t) \sim f^2 \gamma^* t^{1/2}, \tag{5.15}$$

which reproduces the time evolution in Fig. 5.1. We have also verified that the scaling of the prefactor in $f^2\gamma^*$ is well reproduced by the numerical simulations at long time, see Fig. 5.3.

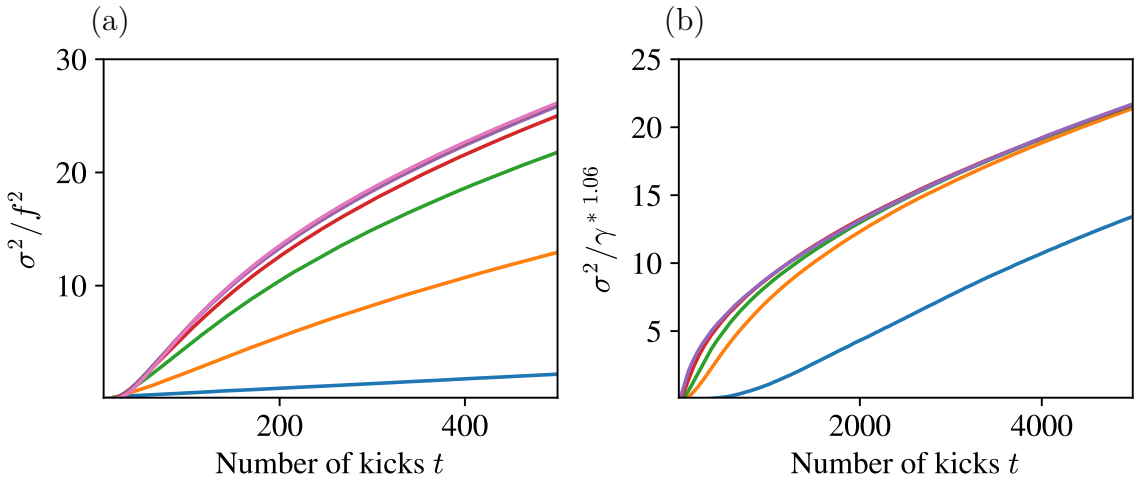

Figure 5.3: (a) Time evolution of the rescaled dispersion σ^2/f^2 for $\gamma^* = 4$ and $f = 1, 2, 4, 8, 16, 32, 64$ (from bottom to top). It confirms the scaling $\sigma^2 \propto f^2$ [Eq. (5.15)] at large enough f. (b) The dispersion also scales like $\sim (\gamma^*)^{1.06}$ at late times. Here $f = 16$, and $\gamma^* = 0.7, 1.68, 2.37, 3.37, 4.75$ (from bottom to top).

5.4 Condensate fraction and crossover to the delta-kick limit

5.4.1 Condensate fraction

Another relevant quantity for probing the difference between finite and delta kicks is the average Bose condensate fraction, defined as $\overline{|\psi_0(t)|^2}$. This quantity is shown in the main panel of Fig. 5.4 for several values of f, as well as in the $f = \infty$ limit of delta kicks. In the latter case, we recall that the decay is exponential, see Eq. (4.24) of the previous chapter.

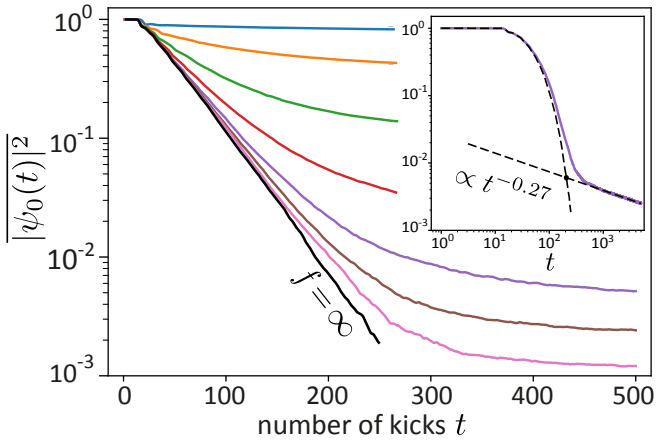

Figure 5.4: Average condensate fraction $\overline{|\psi_0(t)|^2}$ versus time for increasing values of f. Solid curves from top to bottom correspond to $f = 1, 2, 4, 8, 16, 32, 64$, and the black line is the $f = \infty$ limit. Here $\gamma^* = 4$ and $\lambda = 3.03$. The inset shows $\overline{|\psi_0(t)|^2}$ in double logarithmic scale for $f = 16$. Interpolating between the short-time (exponential) and long-time (algebraic) decays provides an estimate of the time scale t_f beyond which the description in terms of delta kicks becomes incorrect.

Like for the momentum dispersion σ^2, however, as soon as f is finite we observe a clear deviation from the exponential scaling, $\overline{|\psi_0(t)|^2}$ decreasing much more slowly. An analysis of the condensate fraction over longer times, shown in the inset of Fig. 5.4, again points toward a sub-diffusive behavior at finite f. We find $\overline{|\psi_0(t)|^2} \sim 1/t^{1/4}$, which is fully consistent with the sub-diffusive law (5.11) for the mean-square width (see also Sec. 5.5).

5.4.2 Cross-over to the delta-kick limit

The time evolutions of the condensate fraction at finite and infinite f discussed above can be used to estimate the characteristic time t_f beyond which the model $f = \infty$ of delta kicks can no longer be reliably utilized to describe the dynamics. This question is crucial from a practical point of view, since in a real experiment the duration of the kicks cannot be made arbitrarily small, especially if the bosonic interactions are modulated using Feshbach resonances. To find t_f, we interpolate the temporal scalings of the condensate fraction at finite and infinite f, where $\overline{|\psi_0(t)|^2} \sim 1/ft^{1/4}$ and $\overline{|\psi_0(t)|^2} \sim \exp[-(t - t_E)/\tau]$, respectively. This method, illustrated in the inset of Fig. 5.4, yields

$$t_f \sim \tau \ln f \sim \frac{2\pi^3\lambda^2}{\gamma^{*2}} \ln f. \tag{5.16}$$

The logarithmic dependence of t_f on f has a remarkable consequence: even for extremely large values of f, i.e., for extremely short kick durations, the breakdown

of the exponential decay of the condensate fraction [or the exponential growth of $\sigma^2(t)$] occurs at relatively short times (this phenomenon is, in fact, visible by eye in Fig. 5.1). This implies that, in a real experiment that unavoidably involves finite kicks, the sub-diffusive behavior described in the present work should be more the rule than the exception.

5.5 Momentum distribution

All the above findings can be summarized by looking at the average momentum distribution of the Bose gas at different times. Such distributions are displayed in the upper panel of Fig. 5.5. The distributions first exhibit an exponential decay of the condensate mode, $\overline{|\psi_0(t)|^2}$, at the scale of τ, quickly accompanied by a slow growth of the "thermal" modes $q \neq 0$. The latter control the subsequent sub-diffusive evolution of the wave-packet mean-square width according to Eq. (5.11). The lower panel of the figure is a zoom on the central part of the distribution at $t = 200$ and $t = 500$. As soon as the condensate fraction is negligible, i.e., at times of the order of a few τ, we numerically find that this central part is always very well approximated by the (normalized) Gaussian profile

$$\overline{|\psi_q(t)|^2} \simeq \frac{1}{\sqrt{2\pi\sigma^2(t)}} \exp\left[-\frac{q^2}{2\sigma^2(t)}\right], \tag{5.17}$$

where $\sigma^2(t)$ is the mean-square width of the *whole* distribution [satisfying Eq. (5.11)]. Note that this law, in particular, implies $\overline{|\psi_0(t)|^2} \sim 1/t^{1/4}$, in accordance with the results of the previous section. This Gaussian shape is another marked difference with the behavior observed in the $f = \infty$ limit, for which the profile is known to be exponential at all momenta [60–62].

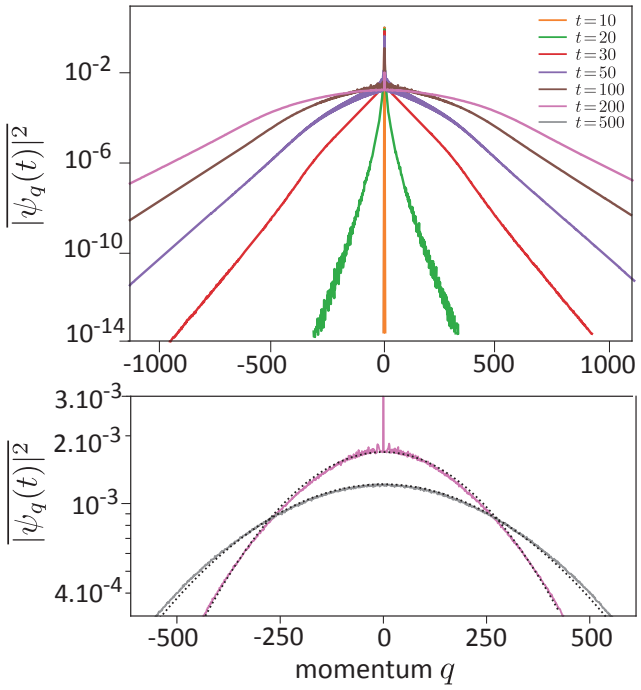

Figure 5.5: Upper panel: average momentum distribution of the wave packet at increasing times, at fixed $f = 64$, $\gamma^* = 4$ and $\lambda = 3.03$. At short time, the condensate mode $\overline{|\psi_0(t)|^2}$ decays exponentially at the scale of τ. This decay is accompanied by a slow growth of the thermal modes $q \neq 0$. The latter control the sub-diffusive evolution of the wave-packet mean-square width according to Eq. (5.11). The lower panel is a zoom on the central part of the distribution at $t = 200$ and $t = 500$. These profiles are very well described by the Gaussian distribution (5.17), without any fit parameter.

When f is finite, nevertheless, our numerics suggests that the far q-tails of the momentum distribution also decay exponentially, see Fig. 5.5. At variance with the $f = \infty$ limit, however, here the exponential decay length $\xi(t)$ does not grow exponentially in time, but rather sub-diffusively. The numerical results of Fig. 5.6, indeed, suggest $\overline{|\psi_q(t)|^2} \sim \exp[-|q|/\xi(t)]$ with $\xi(t) \sim t^\alpha$ and α close to $1/3$. Although the degree of universality of this value is not yet clear to us, this sub-diffusive law is apparently different from the one governing $\sigma^2(t)$, see Fig. 5.6. There is, of course, no contradiction at this stage, since the exponential tails provide a negligible contribution to the variance of the whole distribution. While we have not been able to find an analytical basis for the scaling of the far tails, it could stem from a mechanism different from the incoherent heating discussed in Sec. 5.3, involving, for example, resonant coherent coupling between the modes of the spreading wave packet [215].

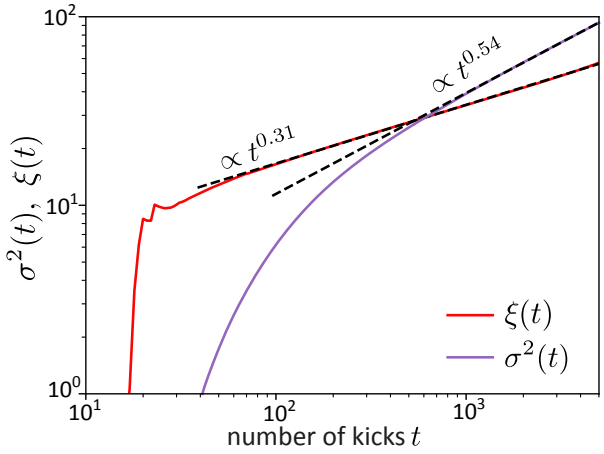

Figure 5.6: Time evolution of the exponential decay length $\xi(t)$ governing the far tails of the momentum distribution. A linear fit (dashed line) suggests an algebraic scaling close to $\xi(t) \sim t^{1/3}$. The time evolution of the mean square width $\sigma^2(t)$ is also shown for comparison. Here $f = 16$, $\gamma^* = 4$ and $\lambda = 3.03$.

Conclusion

By considering a Bose gas subjected to a periodic modulation of the interactions taking the form of finite kicks, we have found evidence for the emergence of a mechanism of sub-diffusive spreading of the wave function beyond a characteristic Ehrenfest time. This result has to be contrasted with the case of delta kicks, where the spreading is always exponential. We have interpreted the sub-diffusive motion in terms of an incoherent heating process for the nonlinear coupling of momentum sites. Beyond this analysis, however, one may ask what fundamental mechanism could explain the different dynamics observed for finite and delta kicks. A possible explanation could be the different nature of the quantities conserved within a given kick in the two scenarios. Indeed, when $f = \infty$, the evolution equation during one kick can be immediately integrated to yield

$$\psi(x, n+1) = e^{-i\gamma^*|\psi(x,n)|^2}\psi(x, n). \tag{5.18}$$

The norm of the wave function is thus conserved for all point x in that case. This local constraint in position space suggests that, conversely, the coupling between modes is weakly constrained in momentum space, resulting in a very fast spreading of the wave packet. In contrast, when f is finite, such a local solution no longer exists and, instead, the nonlinear Schödinger equation involves only *global* integrals of motions of the form $\int dx\, \psi^*(x,t)Q_j(x,t)$ with the $Q_j(x,t)$ defined via recursion relations [216]. We expect this global character to translate into a much weaker coupling between the modes in reciprocal space.

Our analysis has also revealed that, for finite kicks, the sub-diffusive motion takes over the exponential spreading at a characteristic time that scales logarithmically with the kick duration. This characteristic time is thus always relatively short, even in the limit of the extremely short kicks. This suggests that, in practice, sub-diffusion rather than exponential spreading of wave packets should be more naturally observed in this system.

Conclusion

In this thesis, we have first addressed the question of thermalization in *isolated* many-body quantum systems. Our case study was the uniform, low-temperature 2D Bose gas with weak contact interactions, for which we have specifically analyzed the effects of a quench of the coupling constant. This system is, indeed, particularly interesting due to its recent realization in several groups of ultracold atoms [44, 50], as well as for its relevance in quantum fluids of light platforms [68, 112, 147] (which emulate the classical, mean-field limit of Bose superfluids). While the experiments we have described are, for the time being, mainly capable of describing coherent phenomena for which a Bogoliubov approach is valid, recent measurements of relaxation time scales in a 2D Bose superfluid carried out in [50] show that a complete theory capturing both short and long time scales in quench protocols has become a pressing matter. On the theoretical side, precisely, most theoretical works developed so far on this particular issue have focused on the dimensions one and three. To describe the process of thermalization in ultracold 2D Bose gases, we used a Keldysh field theory, allowing us to derive quantum Boltzmann equations for both the normal and anomalous quasiparticles correlators. This enabled us to recover the 2D perturbative relaxation rates that were previously obtained in an equilibrium Matsubara formalism [88], and which correspond to Landau-Beliaev damping. The approach also provided us with explicit expressions for time-dependent observables measured experimentally, the coherence function and the structure factor, which we characterized from the short-time coherent dynamics to the final thermalization. In Sec. 3.2, finally, we extended our Keldysh formalism to the self-consistent Born approximation, which predicts the breakdown of a perturbation theory at very low energies. In this case, we obtained a novel expression for the Landau damping rate $\sim q^{3/2}T^{3/2}$, instead of $\sim qT^2$ within the perturbative approach.

In the second part of this thesis, we have also tackled the problem of the wave packet spreading of a 1D Bose gas subject to periodic interaction kicks (the Gross-Pitaevskii map). This system was recently shown to exhibit an unbounded exponential growth of the momentum dispersion in the case of δ-kicks [60–62]. By using a standard transfer matrix technique, we elaborated on these results by analyzing specifically the average population of the condensate fraction and of the first excitation. In the last chapter, finally, we considered a realistic implementation of the Gross-Pitaevskii map, for which interaction kicks take the form of square pulses

of *finite* width. Instead of the exponential transport scenario, we found that this model displays sub-diffusion at late times, due to the competition between kinetic and interaction energies during the nonlinear pulses. We proposed a mechanism of incoherent heating of the Fourier modes to explain this novel transport behavior. Strikingly, we found that, even for extremely short kicks, the crossover from exponential to sub-diffusive spreading occurs at very short times, suggesting that any future experimental realization of the Gross-Pitaevskii map would result in the observation of sub-diffusion.

There are several possible research directions for extending the results of this thesis. First, it would be interesting to compute numerically the Landau-Beliaev relaxation rates by means of the 2D Gross-Pitaevskii equation with stochastic initial conditions (also known as the truncated Wigner approximation [217, 218]). The latter technique is expected to give a correct description of Bose superfluids in the limit of very small energies. To our knowledge, such a numerical study has never been completed, even in the case of perturbative Landau damping. These simulations, in particular, should have the ability to probe the existence of a non-perturbative regime for relaxation rates, such as the one predicted in this thesis for momenta smaller than Eq. (3.42). In addition, the Landau relaxation rates could be calculated within the functional renormalization group formalism [163, 164], which is tailored to provide results in nonperturbative contexts. Previously, the $\sim q^{3/2}$ law was also predicted in 1D; a natural question is thus whether this anomalous scaling also holds in 3D. A positive answer might signal a universal mechanism behind it. In the previous works [140, 219], it was suggested that in 1D such mechanism is associated with a Kardar-Parisi-Zhang (KPZ) dynamics, although more investigations would be required to clarify this point. Finally, our self-consistent theory could be easily extended to the computation of the Keldysh self-energy, which would give access to generalized (nonperturbative) kinetic equations describing the deep infrared regime. In 1D, such theory led to the observation of algebraic relaxation of quasiparticles [96], and the question of whether similar equations yield comparable behavior in higher dimensions remains unanswered.

On the other hand, the generalized Gross-Pitaevskii map introduced in Chapter 5 could also benefit from further investigations. First all, for small values of f (nonlinear pulses of large width), we have noticed numerically the trace of nonergodic behavior, i.e., the late onset of sub-diffusion (results not shown in this thesis). In this case, we have also found evidence for the existence of quantum resonances that persist even *after* the average of random phases. One of these resonances significantly postpones the Thouless time: $t_H \sim (1/\gamma^*)^2$, instead of the law (4.22). Furthermore, the Gross-Pitaevskii map with attractive interactions was also shown to support solitonic solutions [63], a remarkable feature which is essentially the opposite of the exponential spreading scenario found for repulsive interactions. In line with the results of Chapter 5, it would be interesting to find out whether this property holds true for realistic non-linear pulses of finite width.

Appendix A

Wigner transformation

By definition, the direct Wigner transform of a two-point function $\theta(t,t')$ is

$$\tilde{\theta}(\tau,\omega) = \int d\Delta t\, e^{i\Delta t\omega}\theta(\tau+\Delta t/2, \tau-\Delta t/2). \tag{A.1}$$

Identification of variables leads to $\tau = (t+t')/2$ and $\Delta t = t - t'$. Therefore, τ is often called "forward" time, or "central" time, while Δt is the "relative" time. Eq. (A.1) states that $\tilde{\theta}$ is the Fourier transform of θ with respect to the relative time. The inverse Wigner transform reads

$$\theta(t,t') = \int \frac{d\omega}{2\pi} e^{-i(t-t')\omega}\tilde{\theta}(\tau,\omega). \tag{A.2}$$

For example, some useful Wigner transformations used in the main text are

$$\theta(t,t') = A(t,t')B(t,t') \quad \rightarrow \quad \tilde{\theta}(\tau,\omega) = \int \frac{d\nu}{2\pi}\tilde{A}(\tau,\nu)\tilde{B}(\tau,\omega-\nu), \tag{A.3}$$

$$\theta(t,t') = A(t,t')B(t',t) \quad \rightarrow \quad \tilde{\theta}(\tau,\omega) = \int \frac{d\nu}{2\pi}\tilde{A}(\tau,\nu)\tilde{B}(\tau,\nu-\omega), \tag{A.4}$$

$$\theta(t,t') = A(t',t)B(t,t') \quad \rightarrow \quad \tilde{\theta}(\tau,\omega) = \int \frac{d\nu}{2\pi}\tilde{A}(\tau,\nu-\omega)\tilde{B}(\tau,\nu), \tag{A.5}$$

$$\theta(t,t') = A^*(t,t')B(t,t') \quad \rightarrow \quad \tilde{\theta}(\tau,\omega) = \int \frac{d\nu}{2\pi}\tilde{A}^*(\tau,\nu)\tilde{B}(\tau,\nu+\omega), \tag{A.6}$$

$$\theta(t,t') = e^{i\tau\lambda},\ \lambda\in\mathbb{R} \quad \rightarrow \quad \tilde{\theta}(\tau,\omega) = e^{i\tau\lambda}\,\delta(\omega)\times 2\pi. \tag{A.7}$$

As one can see from these examples, the Wigner transform of a product is a convolution product of the Wigner transforms. Sometimes, one wishes to perform the reverse operations, i.e., compute the Wigner transform of a convolution product such as

$$\theta(t,t') = [A\circ B](t,t') = \int dt_1 A(t,t_1)B(t_1,t'). \tag{A.8}$$

Unfortunately, there are no simple results for the latter expression. Instead, the expansion

$$\begin{aligned}\tilde{\theta}(\tau,\omega) &= e^{-\frac{i}{2}\left[\partial_\tau^A\partial_\omega^B-\partial_\omega^A\partial_\tau^B\right]}\tilde{A}(\tau,\omega)\tilde{B}(\tau,\omega)\\ &= \tilde{A}\tilde{B}-\frac{i}{2}\left[\partial_\tau\tilde{A}\partial_\omega\tilde{B}-\partial_\omega\tilde{A}\partial_\tau\tilde{B}\right]+\cdots\end{aligned} \tag{A.9}$$

holds true [139]. Here, ∂_x^Y indicates differentiation with respect to the variable $x=\omega,\tau$ applied to the function $Y=A,B$. Computing all the terms in this expansion is *a priori* hopeless. Yet, we can often assume that the functions of interest $Y(t,t')=Y(\tau+\Delta t/2,\tau-\Delta t/2)$ vary much more slowly with τ than with Δt [90, 135]. Indeed, τ is related to macroscopic, external degrees of freedom (typically classical driving mechanism), while Δt represents microscopic, intrinsic processes (e.g. quantum scattering events) [139]. Therefore, we can often assume

$$\left|\frac{\partial_x Y}{Y}\right|\ll 1, \tag{A.10}$$

i.e., ω and τ are both slow variables of A and B. This separation of time scales is the main motivation for using the Wigner representation. It means that the expansion (A.9) can be truncated to its first terms. At first non-zero order, we recover the Fourier analysis result

$$\tilde{\theta}\simeq\tilde{A}\tilde{B}, \tag{A.11}$$

which is used extensively in the main text, see, e.g., Eqs. (2.47, 2.48).

As an additional illustration of the Wigner representation, let us mention here that the expansion (A.9) immediately gives the result

$$(F\circ\left[G^{0,A}\right]^{-1}-\left[G^{0,R}\right]^{-1}\circ F)_{\boldsymbol{q},\omega,\tau}=-i\partial_\tau F_{\boldsymbol{q},\omega,\tau}, \tag{A.12}$$

without resorting to the real time representation. Indeed, we recall that $[G^{0,R}_{\boldsymbol{q},\omega,\tau}]^{-1}=[G^{0,A}_{\boldsymbol{q},\omega,\tau}]^{-1}=\omega-\epsilon_{\boldsymbol{q}}$ [cf Eqs. (2.36, 2.37)], which shows that $\partial_\omega[G^{0,R/A}_{\boldsymbol{q},\omega,\tau}]^{-1}=1$, while all other possible partial derivatives vanish. Using twice Eq. (A.9), one exactly obtains Eq. (A.12).

Appendix B

Angular integration in Landau-Beliaev scattering

In Sec. 2.2.3, we have used Keldysh's formalism to derive a quantum kinetic theory of an isolated, low-temperature, two-dimensional interacting Bose gas. A byproduct of our approach was the nonequilibrium damping rate $\gamma_q = -\mathrm{Im}\,\Sigma^R_q$ [cf. Eq. (2.59)], which quantifies the lifetime of phononic quasiparticles characterized by a generic distribution function F_q. In equilibrium, the latter can be explicitly evaluated as $F_q = \coth[\epsilon_q/(2T)]$, so that γ_q reduces to the Landau-Beliaev damping rates $\gamma_q^{L/B}$ [cf. Eq. (2.76) and Eq. (2.77)] that were previously obtained within Matsubara's framework [88], but could also be derived from a simple Fermi golden rule. At the heart of all these techniques is the calculation of integrals of the form

$$I = \int_0^q p dp \int_{-\pi}^{\pi} d\theta\, f_{p,\theta}\, \delta(g_{p,\theta}).$$

As we will see, in such equations, the Dirac delta typically states the energy conservation $g_{p,\theta} = 0$ of the considered interaction process, and the function $f_{p,\theta}$ represents the scattering amplitude. The aim of this appendix is to explain how to estimate these integrals in practice.

As a reminder, the excitation spectrum of the hydrodynamical Hamiltonian (1.6) is $\epsilon_{\boldsymbol{p}} = c|\boldsymbol{p}|\sqrt{1+\xi^2\boldsymbol{p}^2}$. The low-energy regime of interest is phononic, i.e. typical momenta verify $|\boldsymbol{p}| \ll 1/\xi$, or equivalently $T \ll mc^2$. Under this assumption, it is often useful to expand $\epsilon_{\boldsymbol{p}}$ in the small parameter $\xi|\boldsymbol{p}|$, as $\epsilon_{\boldsymbol{p}} = c|\boldsymbol{p}| + \frac{1}{2}c\xi^2|\boldsymbol{p}|^3 + \cdots$.

Beliaev damping The disintegration of a phonon of energy $\epsilon_{\boldsymbol{q}}$ into two phonons $\epsilon_{\boldsymbol{p}}$, $\epsilon_{\boldsymbol{q}-\boldsymbol{p}}$ of smaller energies is referred as Beliaev damping. The energy conservation condition $g^B_{\boldsymbol{p},\theta} = \epsilon_{\boldsymbol{p}} + \epsilon_{\boldsymbol{q}-\boldsymbol{p}} - \epsilon_{\boldsymbol{q}} = 0$ shows that $|\boldsymbol{p}| < |\boldsymbol{q}|$. $g_B = 0$ can also be readily transformed into a quadratic equation on the variable $|\boldsymbol{p}-\boldsymbol{q}|$, whose angular solutions are

$$\theta^B_{\pm} = \pm \arccos\left[\frac{1}{2pq}\left(p^2+q^2+\frac{1-\sqrt{1+4\xi^2(\epsilon_p-\epsilon_q)^2/c^2}}{2\xi^2}\right)\right], \tag{B.1}$$

where we have used the shorthand notation $p \equiv |\boldsymbol{p}|$, and θ^B denotes the angle between $\boldsymbol{p}$ and $\boldsymbol{q}$. As Eq. (B.1) demonstrates, two-dimensional Beliaev scattering is composed of two channels (or "branches") in the (p, θ) plane, with reflection symmetry around the $\theta = 0$ axis. This result was derived, e.g., in Ref. [220], and reduces to $\theta^B_\pm = 0$ (respectively, $\theta^B_\pm = \pm\sqrt{3}|p-q|/2mc$) if the dispersion is linearized (respectively, rendered cubic). Furthermore,

$$\partial_\theta g^B_{p,\theta} = \frac{2pqc \sin\theta \left[2\xi^2 \left(p^2 + q^2 - 2pq\cos\theta\right) + 1\right]}{2\sqrt{\xi^2(p^2 + q^2 - 2pq\cos\theta)^2 + p^2 + q^2 - 2pq\cos\theta}}, \tag{B.2}$$

so that in principle we could also derive $|\partial_\theta g^B_{p,\theta}|_{\theta^B_+}$ exactly, by injecting Eq. (B.1) into Eq. (B.2). In practice, however, it is sufficient to observe that $|\partial_\theta g^B_{p,\theta}|_{\theta^B_+} = 0$, if the spectrum is linearized, and that

$$|\partial_\theta g^B_{p,\theta}|_{\theta^B_+} = \frac{\sqrt{3}}{2m} pq, \tag{B.3}$$

at cubic order. These results are helpful when integrating a delta distribution evaluated at $g^B_{p,\theta}$ over $d\boldsymbol{p} = pdpd\theta$:

$$\int_0^q pdp \int_{-\pi}^{\pi} d\theta f_{p,\theta}\, \delta(g^B_{p,\theta}) \simeq \int_0^q pdp \int_{-\infty}^{\infty} d\theta\, f_{p,\theta}\, \delta(g^B_{p,\theta}) = \int_0^q pdp \frac{2f_{p,\theta^B_+}}{|\partial_\theta g^B_{p,\theta}|_{\theta^B_+}}. \tag{B.4}$$

The first approximation is excellent provided the dispersion relation is well estimated by one of its low-order truncations, i.e., if $T \ll g\rho_0$. Furthermore, the factor of two in the last equality relates to the two branches of Beliaev scattering, as found in Eq. (B.1). Importantly, a purely linear spectrum renders the integral (B.4) divergent. However, keeping the cubic correction of the Bogoliubov dispersion relation regularizes the calculation. We note that the integral can also be made convergent by taking into account the correction from high-order diagrammatic terms, as evidenced by the self-consistent Born approximation presented in 3.2. Finally, at lowest order,

$$\int_0^q pdp \int_{-\pi}^{\pi} d\theta f_{p,\theta}\, \delta(g^B_{p,\theta}) \simeq \int_0^q pdp\, \frac{4mf_{p,0}}{\sqrt{3}pq}, \tag{B.5}$$

which is used to obtain Eq. (2.59).

Landau damping Let us conclude this Appendix by mentioning how to modify the previous calculation to describe Landau damping, for which two phonons $\epsilon_{\boldsymbol{p}}$, $\epsilon_{\boldsymbol{q}}$ coalesce into a quasiparticle of energy $\epsilon_{\boldsymbol{p}+\boldsymbol{q}}$. The energy conservation is now stated as $g^L_{\boldsymbol{p},\theta} = \epsilon_{\boldsymbol{p}} + \epsilon_{\boldsymbol{q}} - \epsilon_{\boldsymbol{q}+\boldsymbol{p}} = 0$. Unlike Beliaev process, there is no constraint here on the scattered momentum's modulus, i.e. $|\boldsymbol{p}| > 0$. The two scattering channels

verify

$$\theta_{\pm}^{L} = \pm \arccos\left[\frac{-1}{2pq}\left(p^2+q^2+\frac{1-\sqrt{1+4\xi^2(\epsilon_p+\epsilon_q)^2/c^2}}{2\xi^2}\right)\right]$$
$$\simeq \pm\frac{\sqrt{3}(p+q)}{2mc}, \tag{B.6}$$

which leads to $|\partial_\theta g^L_{p,\theta}|_{\theta^L_+} = \sqrt{3}pq/(2m)$, and therefore the result (B.5) is left unchanged when substituting $g^B_{p,\theta}$ for $g^L_{p,\theta}$.

Appendix C

Numerical instabilities

The numerical calculations performed in Chapters 4 and 5 are based on a second-order split-step method [221]. In practice, however, the specificities of the system of periodically kicked interactions make certain observables very sensitive to instabilities of this numerical scheme. A typical example is provided by the average condensate fraction, $\overline{|\psi_0(t)|^2}$, which decays exponentially in time. Indeed, as explained in Sec. 5.4 and in Appendix 4.2.4, at long time this quantity is governed by realizations of the random phases for which the populations $|\psi_q(t)|^2$ of other modes remain exponentially small up to large q values.

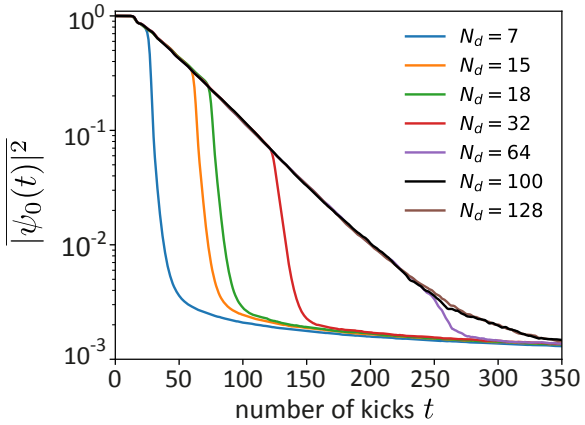

Figure C.1: Benchmarking of high-precision calculations using $N_d = 32, 64, 100, 128$ against results of standard fixed-precision formats (i.e. "single", "double" and "extended double" precisions, respectively 7, 15 and 18 significant decimal digits). Here $f = 64$, $\lambda = 3.03$ and $\gamma^* = 4$, and numerical parameters are $1/\Delta s = 500$, $N_r \sim 10^4$, $N_s = 2^{12}$.

An accurate estimation of $\overline{|\psi_0(t)|^2}$ thus requires an accurate computation of many exponentially small $|\psi_q(t)|^2$, typically limited by the round-off error threshold that depends on the finite number of significant decimal digits N_d representing

floating-point data. This issue is illustrated in Fig. C.1, which shows the average condensate fraction computed for increasing values of N_d. At too low N_d, the results exhibit a non-physical temporal collapse. In practice, for our typical choices of $\{f, \lambda, \gamma^*\}$, we have found that $N_d = 100$ allows to faithfully estimate the condensate fraction up to a several hundreds kicks at all time scales.

Appendix D

Two-modes problem beyond linearization

In Sec. 4.2.3, we studied the Gross-Pitaevskii map (4.4) in the short time regime where the equations of motion can be linearized. More precisely, by restricting the system to only two Fourier modes (the ones relevant at short times, i.e., the condensate $q = 0$ and the first excitation $q = 1$), we wrote the average population of the first mode in terms of a transfer matrix [cf. Eq. (4.17)], hence mapping the time evolution of the Gross-Pitaevskii map on a simple spectral problem. In this Appendix, we extend this calculation beyond the linear theory, thanks, in particular, to a reduction of the number of dynamical variables reminiscent of the two-body gravitational problem.

We consider the Gross-Pitaevskii map in the idealized situation where all modes of momenta $|q| > 1$ can be neglected. This assumption is correct for the initial state (4.8) at sufficiently short times. Furthermore, we assume that random phases are even in p-space so that $\psi_1 = \psi_{-1}$. During nonlinear pulses, the nonlinear equations of motion are

$$\begin{cases} id_t\tilde{\psi}_0 = 2u|\tilde{\psi}_1|^2\tilde{\psi}_0 + 2u\tilde{\psi}_1^2\tilde{\psi}_0^*, \\ id_t\tilde{\psi}_1 = u(1 - |\tilde{\psi}_1|^2)\tilde{\psi}_1 + u\tilde{\psi}_0^2\tilde{\psi}_1^*, \end{cases} \tag{D.1}$$

where the notations $u = g/2\pi$ and $\tilde{\psi}_j(t) = \psi_j(t)e^{iut}$ have been introduced. In the density-phase formalism $\tilde{\psi}_j = \sqrt{n_j}e^{i\theta_j}$, the differential system (D.1) can be expressed by means of only two real variables. Indeed, denoting by n_1 the population of the first excitation and $\Delta\theta(t) = \theta_1(t) - \theta_0(t)$ the relative phase, we obtain

$$\begin{cases} d_t n_1 = 2un_1(2n_1 - 1)\sin(2\Delta\theta), \\ d_t\Delta\theta = -un_1 + u(4n_1 - 1)[1 + \cos(2\Delta\theta)], \end{cases} \tag{D.2}$$

by means of the conservation of the norm $n_0 + 2n_1 = 1$. The first equation of this system is a Bernoulli equation, which, despite its nonlinearity, admits the solution

$$n_1(t) = \frac{1}{2 + \eta^{-2}\exp\left(\int_0^t 2u\sin[2\Delta\theta(s)]\,ds\right)}. \tag{D.3}$$

Here, $\eta^2 \equiv e^{-2\lambda^2} \ll 1$ is the initial value of n_1.

To make progress, we rely on a numerical observation: For small coupling constants $u \ll 1$, the relative phase $\Delta\theta$ is quasi-periodic in time of period $4t_h$. More precisely, the relative phase first decreases from its initial value $\Delta\theta(0) = 0$, quickly approaching the lower bound $\Delta\theta_l < 0$. From $t = t_h$ to $t = 2t_h$, the relative phase increases until $\Delta\theta \simeq 0$. Moreover, for $t < t_h$, $\Delta\theta(t_h - t) \simeq \Delta\theta(t_h + t)$. A similar property holds after $2t_h$, i.e., $\Delta\theta(2t_h - t) \simeq -\Delta\theta(2t_h + t)$. As the value of u decreases, the quasi-periodicity holds with higher precision.

Eq. (D.3) can be now improved by using the above properties of $\Delta\theta(t)$. The linearity of the integral gives $\int_0^t \cdots = 2\int_0^{t_h} \cdots - \int_0^{2t_h - t} \ldots$ for $t_h \leq t \leq 2t_h$, which leads to:

$$n_1(t_h \leq t \leq 2t_h) = \frac{1}{2 + \frac{n_1(2t_h - t)}{[n_1(t_h)]^2}}. \tag{D.4}$$

In other words, the dynamics between t_h and $2t_h$ is merely a re-writing of the dynamics before t_h, which is known from the linear theory. A similar equation can be obtained after $2t_h$. Therefore, for $t \leq 3t_h$, the quasi-periodicity of the relative phase leads to

$$n_1(t) = \frac{1}{2 + \frac{4a}{u\eta^2} e^{-4\sqrt{a(2u-a)}t_h} \cosh\left(2\sqrt{a(2u-a)}(t - 2t_h)\right)}. \tag{D.5}$$

Here, a is the random angle due to the free evolution in between nonlinear pulses. We have assumed that $0 \leq a \leq 2u$.

In order to compute t_h, we solve perturbatively the differential equation on $\Delta\theta$ in (D.2), by using the linear solution n_1^{lin} instead of n_1. The quantity $1 + \cos[2\Delta\theta(t)]$ can be eliminated by using the conservation of the energy during a nonlinear pulse. We find

$$t_h = \frac{1}{4\sqrt{a(2u-a)}} \ln\left[8\,\eta^{-2}\left(\frac{a}{u}\right)^2 \frac{2u-a}{|4a-u|}\right], \tag{D.6}$$

in excellent agreement with numerical simulations. The final solution is then

$$n_1(t) = \frac{1}{2 + \frac{u}{2a}\frac{|4a-u|}{2u-a} \cosh\left(2\sqrt{a(2u-a)}(t - 2t_h)\right)}. \tag{D.7}$$

Finally, for $t \leq 3t_h$, the average population of the first Fourier mode reads

$$\overline{n_1(t)} \simeq \eta^2 + \frac{2u}{\pi}\int_0^1 \frac{d\alpha}{2 + \frac{|\alpha - 1/8|}{\alpha(1-\alpha)} \cosh\left(4u\sqrt{\alpha(1-\alpha)}(t - 2t_h)\right)}, \tag{D.8}$$

which is represented in Fig. (4.3). The linear solution (4.21) is just a particular case of this equation, for $t \leq t_h$.

Appendix E

Statistics of fluctuations

In addition to the dispersion $\sigma^2(t) = \sum_q q^2 \overline{|\psi_q(t)|^2}$, the spreading of the wave packet can be characterized by the inverse participation ratio (IPR) $1/\sum_q \overline{|\psi_q(t)|^4}$, which measures the average number of excited modes at a given time t. The IPR is shown in Fig. (E.1) as a function of time.

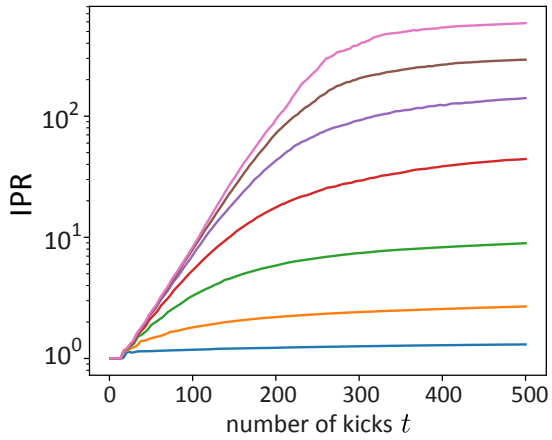

Figure E.1: Inverse participation ratio versus time. Solid curves from bottom to top correspond to $f = 1, 2, 4, 8, 16, 32, 64$. Here $\gamma^* = 4$ and $\lambda = 3.03$.

At very short times, $1/\sum_q \overline{|\psi_q|^4} \simeq 1$ since only one mode is appreciably populated. This is the regime discussed in Sec. 4.2.2. When $t \geq t_E$, many q modes start to be populated and the IPR rapidly increases. At late times, finally, the increase is slowed down as the system enters the sub-diffusive regime described in Sec. 5.3. We also note that for sufficiently large f, IPR $\propto f$ at a given time. This result validates the estimation of Sec. 5.3 for the number of modes effectively participating in the second term in the right-hand side of Eq. (5.12) in the sub-diffusive regime.

We finally comment on the fluctuations of the momentum dispersion $\sigma^2(t) =$

$\sum_q q^2 \, |\psi_q(t)|^2$ from one realization of the random phases to the other. These fluctuations are illustrated in Fig. E.2, which shows the behavior of $\sigma^2(t)$ for many realizations. The fluctuations are typically large in the vicinity of the Ehrenfest time, while the dispersion becomes self-averaging in the long-time, sub-diffusive regime. The standard deviation of the dispersion, defined as

$$\mathrm{sd}(\sigma) = \left[\overline{\left(\sum_q q^2 \, |\psi_q(t)|^2 \right)^2} - \left(\sum_q q^2 \, \overline{|\psi_q(t)|^2} \right)^2 \right]^{1/2}, \tag{E.1}$$

is shown in the inset of Fig. E.2 and confirms this behavior.

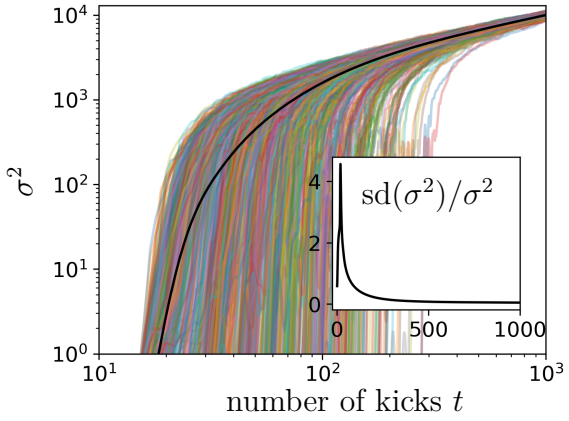

Figure E.2: Wave-packet momentum dispersion $\sigma^2(t)$ for $\sim 10^3$ realizations of the random phases (colored curves), and its average (thick black curve). Here $f = 16$, $\lambda = 3.03$ and $\gamma^* = 4$. The inset shows the standard deviation of the dispersion relative to its average.

Bibliography

[1] J. M. Deutsch, "Eigenstate thermalization hypothesis," *Reports on Progress in Physics*, vol. 81, no. 8, p. 082001, 2018.

[2] M. Srednicki, "The approach to thermal equilibrium in quantized chaotic systems," *Journal of Physics A: Mathematical and General*, vol. 32, no. 7, p. 1163, 1999.

[3] A. Polkovnikov, K. Sengupta, A. Silva, and M. Vengalattore, "Colloquium: Nonequilibrium dynamics of closed interacting quantum systems," *Reviews of Modern Physics*, vol. 83, no. 3, p. 863, 2011.

[4] J. Eisert, M. Friesdorf, and C. Gogolin, "Quantum many-body systems out of equilibrium," *Nature Physics*, vol. 11, no. 2, pp. 124–130, 2015.

[5] R. Nandkishore and D. A. Huse, "Many-body localization and thermalization in quantum statistical mechanics," *Annu. Rev. Condens. Matter Phys.*, vol. 6, no. 1, pp. 15–38, 2015.

[6] F. Haake, *Quantum signatures of chaos*. Springer, 1991.

[7] M. L. Mehta, *Random matrices*. Elsevier, 2004.

[8] L. D'Alessio, Y. Kafri, A. Polkovnikov, and M. Rigol, "From quantum chaos and eigenstate thermalization to statistical mechanics and thermodynamics," *Advances in Physics*, vol. 65, no. 3, pp. 239–362, 2016.

[9] E. Lieb, T. Schultz, and D. Mattis, "Two soluble models of an antiferromagnetic chain," *Annals of Physics*, vol. 16, no. 3, pp. 407–466, 1961.

[10] E. H. Lieb and W. Liniger, "Exact analysis of an interacting Bose gas. I. the general solution and the ground state," *Physical Review*, vol. 130, no. 4, p. 1605, 1963.

[11] A. Shabat and V. Zakharov, "Exact theory of two-dimensional self-focusing and one-dimensional self-modulation of waves in nonlinear media," *Sov. Phys. JETP*, vol. 34, no. 1, p. 62, 1972.

[12] M. J. Ablowitz and H. Segur, *Solitons and the inverse scattering transform*. SIAM, 1981.

[13] T. Giamarchi, *Quantum physics in one dimension*, vol. 121. Clarendon press, 2003.

[14] J.-S. Caux and F. H. Essler, "Time evolution of local observables after quenching to an integrable model," *Physical review letters*, vol. 110, no. 25, p. 257203, 2013.

[15] E. Ilievski, M. Medenjak, T. Prosen, and L. Zadnik, "Quasilocal charges in integrable lattice systems," *Journal of Statistical Mechanics: Theory and Experiment*, vol. 2016, no. 6, p. 064008, 2016.

[16] O. A. Castro-Alvaredo, B. Doyon, and T. Yoshimura, "Emergent hydrodynamics in integrable quantum systems out of equilibrium," *Phys. Rev. X*, vol. 6, p. 041065, Dec 2016.

[17] E. Ilievski and J. De Nardis, "Ballistic transport in the one-dimensional hubbard model: The hydrodynamic approach," *Phys. Rev. B*, vol. 96, p. 081118, Aug 2017.

[18] A. Minguzzi and P. Vignolo, "Strongly interacting trapped one-dimensional quantum gases: Exact solution," *AVS Quantum Science*, vol. 4, no. 2, 2022.

[19] I. Bouchoule, J. Dubail, L. Dubois, and D. M. Gangardt, "Relaxation of phonons in the Lieb-Liniger gas by dynamical refermionization," *Physical Review Letters*, vol. 130, no. 14, p. 140401, 2023.

[20] N. Linden, S. Popescu, A. J. Short, and A. Winter, "Quantum mechanical evolution towards thermal equilibrium," *Physical Review E*, vol. 79, no. 6, p. 061103, 2009.

[21] M. Rigol, V. Dunjko, V. Yurovsky, and M. Olshanii, "Relaxation in a completely integrable many-body quantum system: an ab initio study of the dynamics of the highly excited states of 1d lattice hard-core bosons," *Physical review letters*, vol. 98, no. 5, p. 050405, 2007.

[22] L. Vidmar and M. Rigol, "Generalized Gibbs ensemble in integrable lattice models," *Journal of Statistical Mechanics: Theory and Experiment*, vol. 2016, no. 6, p. 064007, 2016.

[23] T. Kinoshita, T. Wenger, and D. S. Weiss, "A quantum Newton's cradle," *Nature*, vol. 440, no. 7086, pp. 900–903, 2006.

[24] F. Alet and N. Laflorencie, "Many-body localization: An introduction and selected topics," *Comptes Rendus Physique*, vol. 19, no. 6, pp. 498–525, 2018.

[25] D. A. Abanin, E. Altman, I. Bloch, and M. Serbyn, "Colloquium: Many-body localization, thermalization, and entanglement," *Reviews of Modern Physics*, vol. 91, no. 2, p. 021001, 2019.

[26] C. Turner, A. Michailidis, D. Abanin, M. Serbyn, and Z. Papić, "Quantum scarred eigenstates in a Rydberg atom chain: Entanglement, breakdown of thermalization, and stability to perturbations," *Physical Review B*, vol. 98, no. 15, p. 155134, 2018.

[27] S. Moudgalya, B. A. Bernevig, and N. Regnault, "Quantum many-body scars and hilbert space fragmentation: a review of exact results," *Reports on Progress in Physics*, vol. 85, no. 8, p. 086501, 2022.

[28] S. Choi, C. J. Turner, H. Pichler, W. W. Ho, A. A. Michailidis, Z. Papić, M. Serbyn, M. D. Lukin, and D. A. Abanin, "Emergent SU (2) dynamics and perfect quantum many-body scars," *Physical review letters*, vol. 122, no. 22, p. 220603, 2019.

[29] N. O'Dea, F. Burnell, A. Chandran, and V. Khemani, "From tunnels to towers: Quantum scars from Lie algebras and q-deformed Lie algebras," *Physical Review Research*, vol. 2, no. 4, p. 043305, 2020.

[30] H. Bernien, S. Schwartz, A. Keesling, H. Levine, A. Omran, H. Pichler, S. Choi, A. S. Zibrov, M. Endres, M. Greiner, *et al.*, "Probing many-body dynamics on a 51-atom quantum simulator," *Nature*, vol. 551, no. 7682, pp. 579–584, 2017.

[31] I. Bloch, J. Dalibard, and W. Zwerger, "Many-body physics with ultracold gases," *Rev. Mod. Phys.*, vol. 80, pp. 885–964, Jul 2008.

[32] L. Sanchez-Palencia and M. Lewenstein, "Disordered quantum gases under control," *Nature Physics*, vol. 6, no. 2, pp. 87–95, 2010.

[33] M. Gring, M. Kuhnert, T. Langen, T. Kitagawa, B. Rauer, M. Schreitl, I. Mazets, D. A. Smith, E. Demler, and J. Schmiedmayer, "Relaxation and prethermalization in an isolated quantum system," *Science*, vol. 337, no. 6100, pp. 1318–1322, 2012.

[34] S. Trotzky, Y.-A. Chen, A. Flesch, I. P. McCulloch, U. Schollwöck, J. Eisert, and I. Bloch, "Probing the relaxation towards equilibrium in an isolated strongly correlated one-dimensional Bose gas," *Nature physics*, vol. 8, no. 4, pp. 325–330, 2012.

[35] T. Langen, R. Geiger, M. Kuhnert, B. Rauer, and J. Schmiedmayer, "Local emergence of thermal correlations in an isolated quantum many-body system," *Nature Physics*, vol. 9, no. 10, pp. 640–643, 2013.

[36] C. Eigen, J. A. Glidden, R. Lopes, N. Navon, Z. Hadzibabic, and R. P. Smith, "Universal scaling laws in the dynamics of a homogeneous unitary Bose gas," *Physical Review Letters*, vol. 119, no. 25, p. 250404, 2017.

[37] C. Eigen, J. A. Glidden, R. Lopes, E. A. Cornell, R. P. Smith, and Z. Hadzibabic, "Universal prethermal dynamics of Bose gases quenched to unitarity," *Nature*, vol. 563, no. 7730, pp. 221–224, 2018.

[38] S. Erne, R. Bücker, T. Gasenzer, J. Berges, and J. Schmiedmayer, "Universal dynamics in an isolated one-dimensional Bose gas far from equilibrium," *Nature*, vol. 563, no. 7730, pp. 225–229, 2018.

[39] J. A. Glidden, C. Eigen, L. H. Dogra, T. A. Hilker, R. P. Smith, and Z. Hadzibabic, "Bidirectional dynamic scaling in an isolated Bose gas far from equilibrium," *Nature Physics*, vol. 17, no. 4, pp. 457–461, 2021.

[40] A. Griffin, T. Nikuni, and E. Zaremba, *Bose-condensed gases at finite temperatures*. Cambridge University Press, 2009.

[41] M. Van Regemortel, H. Kurkjian, M. Wouters, and I. Carusotto, "Prethermalization to thermalization crossover in a dilute Bose gas following an interaction ramp," *Physical Review A*, vol. 98, no. 5, p. 053612, 2018.

[42] I. Chantesana, A. P. Orioli, and T. Gasenzer, "Kinetic theory of nonthermal fixed points in a Bose gas," *Physical Review A*, vol. 99, no. 4, p. 043620, 2019.

[43] A. N. Mikheev, C.-M. Schmied, and T. Gasenzer, "Low-energy effective theory of nonthermal fixed points in a multicomponent Bose gas," *Physical Review A*, vol. 99, no. 6, p. 063622, 2019.

[44] C.-L. Hung, V. Gurarie, and C. Chin, "From cosmology to cold atoms: observation of Sakharov oscillations in a quenched atomic superfluid," *Science*, vol. 341, no. 6151, pp. 1213–1215, 2013.

[45] S. Sunami, V. P. Singh, D. Garrick, A. Beregi, A. J. Barker, K. Luksch, E. Bentine, L. Mathey, and C. J. Foot, "Universal scaling of the dynamic BKT transition in quenched 2D Bose gases," *arXiv preprint arXiv:2209.13587*, 2022.

[46] M. Gałka, P. Christodoulou, M. Gazo, A. Karailiev, N. Dogra, J. Schmitt, and Z. Hadzibabic, "Emergence of isotropy and dynamic scaling in 2D wave turbulence in a homogeneous Bose gas," *Physical Review Letters*, vol. 129, no. 19, p. 190402, 2022.

[47] V. N. Popov, "On the theory of the superfluidity of two-and one-dimensional Bose systems," *Teoreticheskaya i Matematicheskaya Fizika*, vol. 11, no. 3, pp. 354–365, 1972.

[48] V. N. Popov, *Functional integrals in quantum field theory and statistical physics*, vol. 8. Springer Science & Business Media, 2001.

[49] C. Mora and Y. Castin, "Extension of Bogoliubov theory to quasicondensates," *Physical Review A*, vol. 67, no. 5, p. 053615, 2003.

[50] J. Beugnon and N. Navon, "Exploring the Kibble–Zurek mechanism with homogeneous Bose gases," *Journal of Physics B: Atomic, Molecular and Optical Physics*, vol. 50, no. 2, p. 022002, 2017.

[51] P. Comaron, F. Larcher, F. Dalfovo, and N. P. Proukakis, "Quench dynamics of an ultracold two-dimensional Bose gas," *Physical Review A*, vol. 100, no. 3, p. 033618, 2019.

[52] P. Kos, M. Ljubotina, and T. Prosen, "Many-body quantum chaos: Analytic connection to random matrix theory," *Physical Review X*, vol. 8, no. 2, p. 021062, 2018.

[53] B. Bertini, P. Kos, and T. Prosen, "Exact spectral form factor in a minimal model of many-body quantum chaos," *Physical review letters*, vol. 121, no. 26, p. 264101, 2018.

[54] B. V. Chirikov, "Research concerning the theory of non-linear resonance and stochasticity," 10 1969.

[55] G. M. Zaslavsky, *The physics of chaos in Hamiltonian systems*. world scientific, 2007.

[56] M. Santhanam, S. Paul, and J. B. Kannan, "Quantum kicked rotor and its variants: Chaos, localization and beyond," *Physics Reports*, vol. 956, pp. 1–87, 2022.

[57] G. Casati, B. Chirikov, F. Izraelev, and J. Ford, "Stochastic behavior of a quantum pendulum under a periodic perturbation," in *Stochastic Behavior in Classical and Quantum Hamiltonian Systems: Volta Memorial Conference, Como, 1977*, pp. 334–352, Springer, 1979.

[58] S. Fishman, D. Grempel, and R. Prange, "Chaos, quantum recurrences, and Anderson localization," *Physical Review Letters*, vol. 49, no. 8, p. 509, 1982.

[59] D. Grempel, R. Prange, and S. Fishman, "Quantum dynamics of a nonintegrable system," *Physical Review A*, vol. 29, no. 4, p. 1639, 1984.

[60] B. Mieck and R. Graham, "Bose–Einstein condensate of kicked rotators with time-dependent interaction," *Journal of Physics A: Mathematical and General*, vol. 38, no. 7, p. L139, 2005.

[61] W.-L. Zhao, J. Gong, W.-G. Wang, G. Casati, J. Liu, and L.-B. Fu, "Exponential wave-packet spreading via self-interaction time modulation," *Physical Review A*, vol. 94, no. 5, p. 053631, 2016.

[62] I. Guarneri, "Gross-Pitaevski map as a chaotic dynamical system," *Physical Review E*, vol. 95, no. 3, p. 032206, 2017.

[63] A. Goussev, P. Reck, F. Moser, A. Moro, C. Gorini, and K. Richter, "Overcoming dispersive spreading of quantum wave packets via periodic nonlinear kicking," *Physical Review A*, vol. 98, no. 1, p. 013620, 2018.

[64] I. Bouchoule, N. Van Druten, and C. I. Westbrook, "Atom chips and one-dimensional Bose gases," *Atom chips*, pp. 331–363, 2011.

[65] A. Griffin, D. W. Snoke, and S. Stringari, *Bose-Einstein condensation*. Cambridge University Press, 1996.

[66] V. Berezinskii, "Destruction of long-range order in one-dimensional and two-dimensional systems possessing a continuous symmetry group. II. Quantum systems," *Sov. Phys. JETP*, vol. 34, no. 3, pp. 610–616, 1972.

[67] J. M. Kosterlitz and D. J. Thouless, "Ordering, metastability and phase transitions in two-dimensional systems," *Journal of Physics C: Solid State Physics*, vol. 6, no. 7, p. 1181, 1973.

[68] M. Abuzarli, N. Cherroret, T. Bienaimé, and Q. Glorieux, "Nonequilibrium prethermal states in a two-dimensional photon fluid," *Physical Review Letters*, vol. 129, no. 10, p. 100602, 2022.

[69] J. Ville, R. Saint-Jalm, É. Le Cerf, M. Aidelsburger, S. Nascimbène, J. Dalibard, and J. Beugnon, "Sound propagation in a uniform superfluid two-dimensional Bose gas," *Physical review letters*, vol. 121, no. 14, p. 145301, 2018.

[70] S. Matveenko and G. Shlyapnikov, "Tkachenko modes and their damping in the vortex lattice regime of rapidly rotating bosons," *Physical Review A*, vol. 83, no. 3, p. 033604, 2011.

[71] H. Shen and W. Zheng, "Landau damping in a mixture of Bose and Fermi superfluids," *Physical Review A*, vol. 92, no. 3, p. 033620, 2015.

[72] P. Fedichev, G. Shlyapnikov, and J. Walraven, "Damping of low-energy excitations of a trapped Bose-Einstein condensate at finite temperatures," *Physical review letters*, vol. 80, no. 11, p. 2269, 1998.

[73] S. Matveenko, M. Bahovadinov, M. Baranov, and G. Shlyapnikov, "Rotons and their damping in elongated dipolar Bose-Einstein condensates," *Physical Review A*, vol. 106, no. 1, p. 013319, 2022.

[74] S. Tsuchiya and A. Griffin, "Damping of Bogoliubov excitations in optical lattices," *Physical Review A*, vol. 70, no. 2, p. 023611, 2004.

[75] G. Shchedrin, D. Jaschke, and L. D. Carr, "Damping-free collective oscillations of a driven two-component Bose gas in optical lattices," *Physical Review A*, vol. 97, no. 4, p. 043601, 2018.

[76] D. Santamore and E. Timmermans, "Collective excitations of low-density fermion-boson quantum-liquid mixtures," *Physical Review A*, vol. 72, no. 5, p. 053601, 2005.

[77] M. Bonitz, *Quantum kinetic theory*, vol. 412. Springer, 2016.

[78] M. Schick, "Two-dimensional system of hard-core bosons," *Physical Review A*, vol. 3, no. 3, p. 1067, 1971.

[79] D. Petrov and G. Shlyapnikov, "Interatomic collisions in a tightly confined Bose gas," *Physical Review A*, vol. 64, no. 1, p. 012706, 2001.

[80] S. Pilati, J. Boronat, J. Casulleras, and S. Giorgini, "Quantum Monte Carlo simulation of a two-dimensional Bose gas," *Physical Review A*, vol. 71, no. 2, p. 023605, 2005.

[81] A. Rançon and N. Dupuis, "Nonperturbative renormalization group approach to strongly correlated lattice bosons," *Phys. Rev. B*, vol. 84, p. 174513, Nov 2011.

[82] A. Rançon and N. Dupuis, "Universal thermodynamics of a two-dimensional bose gas," *Phys. Rev. A*, vol. 85, p. 063607, Jun 2012.

[83] N. D. Mermin and H. Wagner, "Absence of ferromagnetism or antiferromagnetism in one-or two-dimensional isotropic Heisenberg models," *Physical Review Letters*, vol. 17, no. 22, p. 1133, 1966.

[84] P. C. Hohenberg, "Existence of long-range order in one and two dimensions," *Physical Review*, vol. 158, no. 2, p. 383, 1967.

[85] D. R. Nelson and J. Kosterlitz, "Universal jump in the superfluid density of two-dimensional superfluids," *Physical Review Letters*, vol. 39, no. 19, p. 1201, 1977.

[86] N. Bogoliubov, "On the theory of superfluidity," *J. Phys*, vol. 11, no. 1, p. 23, 1947.

[87] N. Dupuis, "Infrared behavior and spectral function of a Bose superfluid at zero temperature," *Physical Review A*, vol. 80, no. 4, p. 043627, 2009.

[88] M.-C. Chung and A. B. Bhattacherjee, "Damping in 2D and 3D dilute Bose gases," *New Journal of Physics*, vol. 11, no. 12, p. 123012, 2009.

[89] G. Bighin, L. Salasnich, P. Marchetti, and F. Toigo, "Beliaev damping of the Goldstone mode in atomic Fermi superfluids," *Physical Review A*, vol. 92, no. 2, p. 023638, 2015.

[90] A. Altland and B. D. Simons, *Condensed matter field theory*. Cambridge university press, 2010.

[91] J. Dalibard, "Fluides quantiques de basse dimension et transition de Kosterlitz-Thouless," *Cours du Collège de France*, 2017.

[92] S. Beliaev, "Energy spectrum of a non-ideal Bose gas," *Sov. Phys. JETP*, vol. 7, no. 2, pp. 299–307, 1958.

[93] L. P. Pitaevskii and S. Stringari, "Landau damping in dilute Bose gases," *Physics Letters A*, vol. 235, p. 398, 1997.

[94] C. J. Pethick and H. Smith, *Bose–Einstein condensation in dilute gases*. Cambridge university press, 2008.

[95] A. F. Andreev, "The hydrodynamics of two- and one-dimensional liquids," *Sov. Physics JETP*, vol. 51, p. 1038, 1980.

[96] M. Buchhold and S. Diehl, "Kinetic theory for interacting Luttinger liquids," *The European Physical Journal D*, vol. 69, pp. 1–20, 2015.

[97] J. L. Roberts, N. R. Claussen, S. L. Cornish, E. A. Donley, E. A. Cornell, and C. E. Wieman, "Controlled collapse of a bose-einstein condensate," *Phys. Rev. Lett.*, vol. 86, pp. 4211–4214, May 2001.

[98] M. Greiner, C. A. Regal, and D. S. Jin, "Probing the excitation spectrum of a fermi gas in the bcs-bec crossover regime," *Phys. Rev. Lett.*, vol. 94, p. 070403, Feb 2005.

[99] R. P. Smith, S. Beattie, S. Moulder, R. L. D. Campbell, and Z. Hadzibabic, "Condensation dynamics in a quantum-quenched bose gas," *Phys. Rev. Lett.*, vol. 109, p. 105301, Sep 2012.

[100] F. H. Essler, S. Evangelisti, and M. Fagotti, "Dynamical correlations after a quantum quench," *Physical Review Letters*, vol. 109, no. 24, p. 247206, 2012.

[101] S. S. Natu and E. J. Mueller, "Dynamics of correlations in a dilute Bose gas following an interaction quench," *Physical Review A*, vol. 87, p. 053607, 2012.

[102] A. Rançon, C.-L. Hung, C. Chin, and K. Levin, "Quench dynamics in Bose-Einstein condensates in the presence of a bath: Theory and experiment," *Phys. Rev. A*, vol. 88, no. 3, p. 031601, 2013.

[103] P. Makotyn, C. E. Klauss, D. L. Goldberger, E. Cornell, and D. S. Jin, "Universal dynamics of a degenerate unitary bose gas," *Nature Physics*, vol. 10, no. 2, pp. 116–119, 2014.

[104] A. G. Sykes, J. P. Corson, J. P. D'Incao, A. P. Koller, C. H. Greene, A. M. Rey, K. R. A. Hazzard, and J. L. Bohn, "Quenching to unitarity: Quantum dynamics in a three-dimensional bose gas," *Phys. Rev. A*, vol. 89, p. 021601, Feb 2014.

[105] A. Mitra, "Quantum quench dynamics," *Annual Review of Condensed Matter Physics*, vol. 9, pp. 245–259, 2018.

[106] C. Chin, R. Grimm, P. Julienne, and E. Tiesinga, "Feshbach resonances in ultracold gases," *Reviews of Modern Physics*, vol. 82, no. 2, p. 1225, 2010.

[107] D. J. Eisenstein and C. L. Bennet, "Cosmic sound waves rule," *Physics Today*, vol. 61, no. 11, p. 44, 2008.

[108] C.-L. Hung, X. Zhang, L.-C. Ha, S.-K. Tung, N. Gemelke, and C. Chin, "Extracting density–density correlations from in situ images of atomic quantum gases," *New Journal of Physics*, vol. 13, no. 7, p. 075019, 2011.

[109] I. Carusotto and C. Ciuti, "Quantum fluids of light," *Reviews of Modern Physics*, vol. 85, no. 1, p. 299, 2013.

[110] C. Michel, O. Boughdad, M. Albert, P.-É. Larré, and M. Bellec, "Superfluid motion and drag-force cancellation in a fluid of light," *Nature communications*, vol. 9, no. 1, p. 2108, 2018.

[111] W. Wan, S. Jia, and J. W. Fleischer, "Dispersive superfluid-like shock waves in nonlinear optics," *Nature Physics*, vol. 3, no. 1, pp. 46–51, 2007.

[112] M. Abuzarli, T. Bienaimé, E. Giacobino, A. Bramati, and Q. Glorieux, "Blast waves in a paraxial fluid of light (a)," *Europhysics Letters*, vol. 134, no. 2, p. 24001, 2021.

[113] T. Bardon-brun, S. Pigeon, and N. Cherroret, "Classical Casimir force from a quasi-condensate of light," *Physical Review Research*, vol. 2, 03 2020.

[114] Q. Fontaine, P.-É. Larré, G. Lerario, T. Bienaimé, S. Pigeon, D. Faccio, I. Carusotto, É. Giacobino, A. Bramati, and Q. Glorieux, "Interferences between Bogoliubov excitations in superfluids of light," *Physical Review Research*, vol. 2, no. 4, p. 043297, 2020.

[115] M. Ota, F. Larcher, F. Dalfovo, L. Pitaevskii, N. P. Proukakis, and S. Stringari, "Collisionless sound in a uniform two-dimensional Bose gas," *Physical review letters*, vol. 121, no. 14, p. 145302, 2018.

[116] J. L. Ville, T. Bienaimé, R. Saint-Jalm, L. Corman, M. Aidelsburger, L. Chomaz, K. Kleinlein, D. Perconte, S. Nascimbène, J. Dalibard, and J. Beugnon, "Loading and compression of a single two-dimensional Bose gas in an optical accordion," *Physical Review A*, vol. 95, no. 1, p. 013632, 2017.

[117] M. Aidelsburger, J. Ville, R. Saint-Jalm, S. Nascimbène, J. Dalibard, and J. Beugnon, "Relaxation dynamics in the merging of n independent condensates," *Physical Review Letters*, vol. 119, no. 19, p. 190403, 2017.

[118] M. Cheneau, P. Barmettler, D. Poletti, M. Endres, P. Schauß, T. Fukuhara, C. Gross, I. Bloch, C. Kollath, and S. Kuhr, "Light-cone-like spreading of correlations in a quantum many-body system," *Nature*, vol. 481, no. 7382, pp. 484–487, 2012.

[119] J. Berges, S. Borsányi, and C. Wetterich, "Prethermalization," *Physical review letters*, vol. 93, no. 14, p. 142002, 2004.

[120] E. H. Lieb and D. W. Robinson, "The finite group velocity of quantum spin systems," *Communications in Mathematical Physics*, vol. 28, no. 3, pp. 251 – 257, 1972.

[121] B. Nachtergaele, Y. Ogata, and R. Sims, "Propagation of correlations in quantum lattice systems," *Journal of statistical physics*, vol. 124, pp. 1–13, 2006.

[122] B. Diu, C. Guthmann, D. Lederer, and B. Roulet, *Eléments de physique statistique*, vol. 37. Editions Hermann, 1989.

[123] N. Nessi and A. Iucci, "Equations of motion for the out-of-equilibrium dynamics of isolated quantum systems from the projection operator technique," in *Journal of Physics: Conference Series*, vol. 568, p. 012013, IOP Publishing, 2014.

[124] M. Kira, "Hyperbolic Bloch equations: atom-cluster kinetics of an interacting Bose gas," *Annals of Physics*, vol. 356, pp. 185–243, 2015.

[125] M. Moeckel and S. Kehrein, "Real-time evolution for weak interaction quenches in quantum systems," *Annals of Physics*, vol. 324, no. 10, pp. 2146–2178, 2009.

[126] M. Eckstein, A. Hackl, S. Kehrein, M. Kollar, M. Moeckel, P. Werner, and F. A. Wolf, "New theoretical approaches for correlated systems in nonequilibrium," *The European Physical Journal Special Topics*, vol. 180, pp. 217–235, 2009.

[127] W. Casteels, S. Finazzi, A. Le Boité, F. Storme, and C. Ciuti, "Truncated correlation hierarchy schemes for driven-dissipative multimode quantum systems," *New Journal of Physics*, vol. 18, no. 9, p. 093007, 2016.

[128] M. Van Regemortel, W. Casteels, I. Carusotto, and M. Wouters, "Spontaneous Beliaev-Landau scattering out of equilibrium," *Physical Review A*, vol. 96, no. 5, p. 053854, 2017.

[129] R. P. Feynman, "Space-time approach to non-relativistic quantum mechanics," *Reviews of modern physics*, vol. 20, no. 2, p. 367, 1948.

[130] J. Zinn-Justin, *Path integrals in quantum mechanics*. OUP Oxford, 2004.

[131] H. Bruus and K. Flensberg, *Many-body quantum theory in condensed matter physics: an introduction*. OUP Oxford, 2004.

[132] P. Danielewicz, "Quantum theory of nonequilibrium processes, i," *Annals of Physics*, vol. 152, no. 2, pp. 239–304, 1984.

[133] M. Garny and M. M. Müller, "Kadanoff-Baym equations with non-Gaussian initial conditions: The equilibrium limit," *Physical Review D*, vol. 80, no. 8, p. 085011, 2009.

[134] J. Berges, "Introduction to nonequilibrium quantum field theory," in *AIP Conference Proceedings*, vol. 739, pp. 3–62, American Institute of Physics, 2004.

[135] A. Kamenev, *Field theory of non-equilibrium systems*. Cambridge University Press, 2011.

[136] P. Lange, P. Kopietz, and A. Kreisel, "Damping of phase fluctuations in superfluid Bose gases," *The European Physical Journal B*, vol. 85, pp. 1–6, 2012.

[137] V. Pastukhov, "Damping of Bogoliubov excitations at finite temperatures," *Journal of Physics A: Mathematical and Theoretical*, vol. 48, no. 40, p. 405002, 2015.

[138] L. M. Sieberer, M. Buchhold, and S. Diehl, "Keldysh field theory for driven open quantum systems," *Rep. Prog. Phys.*, vol. 79, p. 096001, 2016.

[139] T. D. Honeychurch and D. S. Kosov, "Timescale separation solution of the Kadanoff-Baym equations for quantum transport in time-dependent fields," *Phys. Rev. B*, vol. 100, no. 24, p. 245423, 2019.

[140] M. Kulkarni and A. Lamacraft, "Finite-temperature dynamical structure factor of the one-dimensional Bose gas: From the Gross-Pitaevskii equation to the Kardar-Parisi-Zhang universality class of dynamical critical phenomena," *Physical Review A*, vol. 88, no. 2, p. 021603, 2013.

[141] M. Buchhold, M. Heyl, and S. Diehl, "Prethermalization and thermalization of a quenched interacting Luttinger liquid," *Physical Review A*, vol. 94, no. 1, p. 013601, 2016.

[142] A. Kreisel, F. Sauli, N. Hasselmann, and P. Kopietz, "Quantum Heisenberg antiferromagnets in a uniform magnetic field: Nonanalytic magnetic field dependence of the magnon spectrum," *Physical Review B*, vol. 78, no. 3, p. 035127, 2008.

[143] Q. Glorieux, T. Aladjidi, P. D. Lett, and R. Kaiser, "Hot atomic vapors for nonlinear and quantum optics," *New Journal of Physics*, vol. 25, no. 5, p. 051201, 2023.

[144] D. Vocke, T. Roger, F. Marino, E. M. Wright, I. Carusotto, M. Clerici, and D. Faccio, "Experimental characterization of nonlocal photon fluids," *Optica*, vol. 2, no. 5, pp. 484–490, 2015.

[145] Q. Fontaine, T. Bienaimé, S. Pigeon, E. Giacobino, A. Bramati, and Q. Glorieux, "Observation of the Bogoliubov dispersion in a fluid of light," *Physical review letters*, vol. 121, no. 18, p. 183604, 2018.

[146] N. Šantić, A. Fusaro, S. Salem, J. Garnier, A. Picozzi, and R. Kaiser, "Nonequilibrium precondensation of classical waves in two dimensions propagating through atomic vapors," *Physical review letters*, vol. 120, no. 5, p. 055301, 2018.

[147] J. Steinhauer, M. Abuzarli, T. Aladjidi, T. Bienaimé, C. Piekarski, W. Liu, E. Giacobino, A. Bramati, and Q. Glorieux, "Analogue cosmological particle creation in an ultracold quantum fluid of light," *Nature Communications*, vol. 13, p. 2890, 2022.

[148] E. Gozzi, E. Cattaruzza, and C. Pagani, *Path integrals for pedestrians*. World Scientific Publishing Company, 2015.

[149] S. Jeon, "Boltzmann equation in classical and quantum field theory," *Physical Review C*, vol. 72, no. 1, p. 014907, 2005.

[150] J. Berges, "Nonequilibrium quantum fields: from cold atoms to cosmology," *arXiv preprint arXiv:1503.02907*, 2015.

[151] P. C. Martin, E. Siggia, and H. Rose, "Statistical dynamics of classical systems," *Physical Review A*, vol. 8, no. 1, p. 423, 1973.

[152] R. V. Jensen, "Functional integral approach to classical statistical dynamics," *Journal of Statistical Physics*, vol. 25, pp. 183–210, 1981.

[153] N. Berti, K. Baudin, A. Fusaro, G. Millot, A. Picozzi, and J. Garnier, "Interplay of thermalization and strong disorder: Wave turbulence theory, numerical simulations, and experiments in multimode optical fibers," *Physical Review Letters*, vol. 129, no. 6, p. 063901, 2022.

[154] G. I. Martone, P.-E. Larr'e, A. Fabbri, and N. Pavloff, "Momentum distribution and coherence of a weakly interacting Bose gas after a quench," *Physical Review A*, 2018.

[155] J. Berges, A. Rothkopf, and J. Schmidt, "Nonthermal fixed points: effective weak coupling for strongly correlated systems far from equilibrium," *Physical review letters*, vol. 101, no. 4, p. 041603, 2008.

[156] J. Berges and D. Mesterhazy, "Introduction to the nonequilibrium functional renormalization group," *Nuclear Physics B-Proceedings Supplements*, vol. 228, pp. 37–60, 2012.

[157] J. Berges and D. Sexty, "Bose-Einstein condensation in relativistic field theories far from equilibrium," *Physical Review Letters*, vol. 108, no. 16, p. 161601, 2012.

[158] J. Berges, K. Boguslavski, S. Schlichting, and R. Venugopalan, "Nonequilibrium fixed points in longitudinally expanding scalar theories: Infrared cascade, Bose condensation, and a challenge for kinetic theory," *Physical Review D*, vol. 92, no. 9, p. 096006, 2015.

[159] S. Tan, "Energetics of a strongly correlated Fermi gas," *Annals of Physics*, vol. 323, no. 12, p. 2952, 2008.

[160] L. D. Landau and E. M. Lifshitz, *Quantum mechanics: non-relativistic theory*, vol. 3. Elsevier, 2013.

[161] A. Sinner, N. Hasselmann, and P. Kopietz, "Spectral function and quasiparticle damping of interacting bosons in two dimensions," *Physical review letters*, vol. 102, no. 12, p. 120601, 2009.

[162] A. Sinner, N. Hasselmann, and P. Kopietz, "Functional renormalization-group approach to interacting bosons at zero temperature," *Physical Review A*, vol. 82, no. 6, p. 063632, 2010.

[163] L. Canet, H. Chaté, B. Delamotte, and N. Wschebor, "Nonperturbative renormalization group for the Kardar-Parisi-Zhang equation: General framework and first applications," *Phys. Rev. E*, vol. 84, p. 061128, Dec 2011.

[164] N. Dupuis, L. Canet, A. Eichhorn, W. Metzner, J. M. Pawlowski, M. Tissier, and N. Wschebor, "The nonperturbative functional renormalization group and its applications," *Physics Reports*, vol. 910, pp. 1–114, 2021.

[165] N. Dupuis, "Unified picture of superfluidity: From bogoliubov's approximation to popov's hydrodynamic theory," *Phys. Rev. Lett.*, vol. 102, p. 190401, May 2009.

[166] A. Rançon and N. Dupuis, "Tan's two-body contact in a planar bose gas: Experiment versus theory," *Phys. Rev. Lett.*, vol. 130, p. 263401, Jun 2023.

[167] A. Eckardt, "Colloquium: Atomic quantum gases in periodically driven optical lattices," *Reviews of Modern Physics*, vol. 89, no. 1, p. 011004, 2017.

[168] R. Moessner and S. L. Sondhi, "Equilibration and order in quantum Floquet matter," *Nature Physics*, vol. 13, no. 5, pp. 424–428, 2017.

[169] T. Oka and S. Kitamura, "Floquet engineering of quantum materials," *Annual Review of Condensed Matter Physics*, vol. 10, pp. 387–408, 2019.

[170] M. Reitter, J. Näger, K. Wintersperger, C. Sträter, I. Bloch, A. Eckardt, and U. Schneider, "Interaction dependent heating and atom loss in a periodically driven optical lattice," *Physical review letters*, vol. 119, no. 20, p. 200402, 2017.

[171] L. D'Alessio and M. Rigol, "Long-time behavior of isolated periodically driven interacting lattice systems," *Physical Review X*, vol. 4, no. 4, p. 041048, 2014.

[172] P. Ponte, A. Chandran, Z. Papić, and D. A. Abanin, "Periodically driven ergodic and many-body localized quantum systems," *Annals of Physics*, vol. 353, pp. 196–204, 2015.

[173] J. Wang and J. Gong, "Butterfly Floquet spectrum in driven SU (2) systems," *Physical review letters*, vol. 102, no. 24, p. 244102, 2009.

[174] J. Gong, L. Morales-Molina, and P. Hänggi, "Many-body coherent destruction of tunneling," *Physical review letters*, vol. 103, no. 13, p. 133002, 2009.

[175] S. Greschner, G. Sun, D. Poletti, and L. Santos, "Density-dependent synthetic gauge fields using periodically modulated interactions," *Physical review letters*, vol. 113, no. 21, p. 215303, 2014.

[176] F. Meinert, M. J. Mark, K. Lauber, A. J. Daley, and H.-C. Nägerl, "Floquet engineering of correlated tunneling in the Bose-Hubbard model with ultracold atoms," *Physical review letters*, vol. 116, no. 20, p. 205301, 2016.

[177] A. Colcelli, G. Mussardo, G. Sierra, and A. Trombettoni, "Integrable Floquet Hamiltonian for a periodically tilted 1d gas," *Physical Review Letters*, vol. 123, no. 13, p. 130401, 2019.

[178] B. V. Chirikov, "A universal instability of many-dimensional oscillator systems," *Physics reports*, vol. 52, no. 5, pp. 263–379, 1979.

[179] P. W. Anderson, "Absence of diffusion in certain random lattices," *Physical review*, vol. 109, no. 5, p. 1492, 1958.

[180] N. Argaman, Y. Imry, and U. Smilansky, "Semiclassical analysis of spectral correlations in mesoscopic systems," *Physical Review B*, vol. 47, no. 8, p. 4440, 1993.

[181] F. Moore, J. Robinson, C. Bharucha, P. Williams, and M. Raizen, "Observation of dynamical localization in atomic momentum transfer: A new testing ground for quantum chaos," *Physical review letters*, vol. 73, no. 22, p. 2974, 1994.

[182] F. Moore, J. Robinson, C. Bharucha, B. Sundaram, and M. Raizen, "Atom optics realization of the quantum δ-kicked rotor," *Physical Review Letters*, vol. 75, no. 25, p. 4598, 1995.

[183] J. Chabé, G. Lemarié, B. Grémaud, D. Delande, P. Szriftgiser, and J. C. Garreau, "Experimental observation of the Anderson metal-insulator transition with atomic matter waves," *Physical review letters*, vol. 101, no. 25, p. 255702, 2008.

[184] M. Lopez, J.-F. Clément, P. Szriftgiser, J. C. Garreau, and D. Delande, "Experimental test of universality of the Anderson transition," *Physical Review Letters*, vol. 108, no. 9, p. 095701, 2012.

[185] I. Manai, J.-F. Clément, R. Chicireanu, C. Hainaut, J. C. Garreau, P. Szriftgiser, and D. Delande, "Experimental observation of two-dimensional Anderson localization with the atomic kicked rotor," *Physical review letters*, vol. 115, no. 24, p. 240603, 2015.

[186] C. Hainaut, I. Manai, R. Chicireanu, J.-F. Clément, S. Zemmouri, J. C. Garreau, P. Szriftgiser, G. Lemarié, N. Cherroret, and D. Delande, "Return to the origin as a probe of atomic phase coherence," *Physical Review Letters*, vol. 118, no. 18, p. 184101, 2017.

[187] C. Hainaut, I. Manai, J.-F. Clément, J. C. Garreau, P. Szriftgiser, G. Lemarié, N. Cherroret, D. Delande, and R. Chicireanu, "Controlling symmetry and localization with an artificial gauge field in a disordered quantum system," *Nature communications*, vol. 9, no. 1, p. 1382, 2018.

[188] C. Hainaut, A. Rançon, J.-F. Clément, I. Manai, P. Szriftgiser, D. Delande, J. C. Garreau, and R. Chicireanu, "Experimental realization of an ideal Floquet disordered system," *New Journal of Physics*, vol. 21, no. 3, p. 035008, 2019.

[189] A. Cao, R. Sajjad, H. Mas, E. Q. Simmons, J. L. Tanlimco, E. Nolasco-Martinez, T. Shimasaki, H. E. Kondakci, V. Galitski, and D. M. Weld, "Interaction-driven breakdown of dynamical localization in a kicked quantum gas," *Nature Physics*, vol. 18, no. 11, pp. 1302–1306, 2022.

[190] J. H. See Toh, K. C. McCormick, X. Tang, Y. Su, X.-W. Luo, C. Zhang, and S. Gupta, "Many-body dynamical delocalization in a kicked one-dimensional ultracold gas," *Nature Physics*, vol. 18, no. 11, pp. 1297–1301, 2022.

[191] R. Blümel, S. Fishman, and U. Smilansky, "Excitation of molecular rotation by periodic microwave pulses. A testing ground for Anderson localization," *The Journal of chemical physics*, vol. 84, no. 5, pp. 2604–2614, 1986.

[192] W. Oskay, D. Steck, B. Klappauf, and M. Raizen, "Quantum chaos with cold cesium atoms," *Laser Phys.*, vol. 9, pp. 265–269, 1999.

[193] B. Klappauf, W. Oskay, D. Steck, and M. Raizen, "Quantum chaos with cesium atoms: pushing the boundaries," *Physica D: Nonlinear Phenomena*, vol. 131, no. 1-4, pp. 78–89, 1999.

[194] C. Bharucha, J. Robinson, F. Moore, B. Sundaram, Q. Niu, and M. Raizen, "Dynamical localization of ultracold sodium atoms," *Physical Review E*, vol. 60, no. 4, p. 3881, 1999.

[195] D. Shepelyansky, "Delocalization of quantum chaos by weak nonlinearity," *Physical review letters*, vol. 70, no. 12, p. 1787, 1993.

[196] G. Gligorić, J. Bodyfelt, and S. Flach, "Interactions destroy dynamical localization with strong and weak chaos," *Europhysics Letters*, vol. 96, no. 3, p. 30004, 2011.

[197] N. Cherroret, B. Vermersch, J. C. Garreau, and D. Delande, "How nonlinear interactions challenge the three-dimensional Anderson transition," *Physical Review Letters*, vol. 112, no. 17, p. 170603, 2014.

[198] S. Lellouch, A. Rançon, S. De Bièvre, D. Delande, and J. C. Garreau, "Dynamics of the mean-field-interacting quantum kicked rotor," *Physical Review A*, vol. 101, no. 4, p. 043624, 2020.

[199] P. Haldar, S. Mu, B. Georgeot, J. Gong, C. Miniatura, and G. Lemarié, "Prethermalization and wave condensation in a nonlinear disordered Floquet system," *arXiv preprint arXiv:2109.14347*, 2021.

[200] M. Martinez, P.-É. Larré, D. Delande, and N. Cherroret, "Low-energy prethermal phase and crossover to thermalization in nonlinear kicked rotors," *Physical Review A*, vol. 106, no. 4, p. 043304, 2022.

[201] A. Pikovsky and D. Shepelyansky, "Destruction of Anderson localization by a weak nonlinearity," *Physical review letters*, vol. 100, no. 9, p. 094101, 2008.

[202] G. Kopidakis, S. Komineas, S. Flach, and S. Aubry, "Absence of wave packet diffusion in disordered nonlinear systems," *Physical Review Letters*, vol. 100, no. 8, p. 084103, 2008.

[203] I. Garcia-Mata and D. L. Shepelyansky, "Delocalization induced by nonlinearity in systems with disorder," *Physical Review E*, vol. 79, no. 2, p. 026205, 2009.

[204] J. Bodyfelt, T. Laptyeva, C. Skokos, D. Krimer, and S. Flach, "Nonlinear waves in disordered chains: Probing the limits of chaos and spreading," *Physical Review E*, vol. 84, no. 1, p. 016205, 2011.

[205] C. Skokos, I. Gkolias, and S. Flach, "Nonequilibrium chaos of disordered nonlinear waves," *Physical Review Letters*, vol. 111, no. 6, p. 064101, 2013.

[206] N. Cherroret, "A self-consistent theory of localization in nonlinear random media," *Journal of Physics: Condensed Matter*, vol. 29, no. 2, p. 024002, 2016.

[207] C. Rylands, E. B. Rozenbaum, V. Galitski, and R. Konik, "Many-body dynamical localization in a kicked Lieb-Liniger gas," *Phys. Rev. Lett.*, vol. 124, p. 155302, Apr 2020.

[208] V. Vuatelet and A. Rançon, "Effective thermalization of a many-body dynamically localized Bose gas," *Physical Review A*, vol. 104, no. 4, p. 043302, 2021.

[209] F. Izrailev and D. L. Shepelyanskii, "Quantum resonance for a rotator in a nonlinear periodic field," *Theoretical and Mathematical Physics*, vol. 43, no. 3, pp. 553–561, 1980.

[210] V. Sokolov, O. Zhirov, D. Alonso, and G. Casati, "Quantum resonances of the kicked rotor and the SU (q) group," *Physical Review Letters*, vol. 84, no. 16, p. 3566, 2000.

[211] M. Lepers, V. Zehnlé, and J. C. Garreau, "Kicked-rotor quantum resonances in position space," *Physical Review A*, vol. 77, no. 4, p. 043628, 2008.

[212] T. I. Lakoba, "Instability analysis of the split-step Fourier method on the background of a soliton of the nonlinear Schrödinger equation," *Numerical Methods for Partial Differential Equations*, vol. 28, no. 2, pp. 641–669, 2012.

[213] A. Semenova, S. A. Dyachenko, A. O. Korotkevich, and P. M. Lushnikov, "Comparison of split-step and hamiltonian integration methods for simulation of the nonlinear Schrödinger type equations," *Journal of Computational Physics*, vol. 427, p. 110061, 2021.

[214] M. Lepers, V. Zehnlé, and J. C. Garreau, "Kicked-rotor quantum resonances in position space," *Physical Review A*, vol. 77, no. 4, p. 043628, 2008.

[215] S. Flach, "Spreading of waves in nonlinear disordered media," *Chemical Physics*, vol. 375, no. 2-3, pp. 548–556, 2010.

[216] F. Magri, "A simple model of the integrable Hamiltonian equation," *Journal of Mathematical Physics*, vol. 19, no. 5, pp. 1156–1162, 1978.

[217] A. Sinatra, C. Lobo, and Y. Castin, "Classical-field method for time dependent Bose-Einstein condensed gases," *Phys. Rev. Lett.*, vol. 87, p. 210404, Nov 2001.

[218] A. Sinatra, C. Lobo, and Y. Castin, "The truncated Wigner method for Bose-condensed gases: limits of validity and applications," *Journal of Physics B: Atomic, Molecular and Optical Physics*, vol. 35, no. 17, p. 3599, 2002.

[219] H. van Beijeren, "Exact results for anomalous transport in one-dimensional hamiltonian systems," *Phys. Rev. Lett.*, vol. 108, p. 180601, Apr 2012.

[220] N. Katz, J. Steinhauer, R. Ozeri, and N. Davidson, "Beliaev damping of quasiparticles in a Bose-Einstein condensate," *Physical review letters*, vol. 89, no. 22, p. 220401, 2002.

[221] J. Weideman and B. M. Herbst, "Split-step methods for the solution of the nonlinear Schrödinger equation," *SIAM Journal on Numerical Analysis*, vol. 23, no. 3, pp. 485–507, 1986.